

2

DTIC FILE COPY

REPORT

LARGE WAVES IN CHANNELS

David Divoky
Rajendra Bhat

Taylor & Divoky, Inc.
9086 Cypress Green Drive
Jacksonville, Florida 32216

June 20, 1987

Technical Report

Contract No. DNA 001-86-C-0189

This work was sponsored by the Defense Nuclear Agency
under RDT&E RMSS Code B 4662 D RW RD 00024 SPSS 3100 A H2590D

Prepared for
Director
DEFENSE NUCLEAR AGENCY
Washington, D.C. 20305-1000

DISTRIBUTION STATEMENT A

Approved for public release
Distribution Unlimited

DTIC
ELECTE
OCT 16 1990
S D & D

This copy made at U.S. Government expense

3

AD-A227 720

SECURITY CLASSIFICATION OF THIS PAGE

REPORT DOCUMENTATION PAGE				Form Approved OMB No 0704-0188 Exp. Date: Jun 30, 1986	
1. CLASSIFICATION			1b. RESTRICTIVE MARKINGS		
2. SECURITY			3. DISTRIBUTION / AVAILABILITY OF REPORT		
3. DOWNGRADING SCHEDULE					
4. PERFORMING ORGANIZATION REPORT NUMBER(S)			5. MONITORING ORGANIZATION REPORT NUMBER(S)		
6a. NAME OF PERFORMING ORGANIZATION Taylor & Divoky Inc.		6b. OFFICE SYMBOL (If applicable)	7a. NAME OF MONITORING ORGANIZATION Director Defense Nuclear Agency		
6c. ADDRESS (City, State, and ZIP Code) 9086 Cypress Green Drive Jacksonville, FL 32216-7791			7b. ADDRESS (City, State, and ZIP Code) Washington, DC 20305-1000		
8a. NAME OF FUNDING / SPONSORING ORGANIZATION		8b. OFFICE SYMBOL (If applicable)	9. PROCUREMENT INSTRUMENT IDENTIFICATION NUMBER DNA 001-86-C-0189		
8c. ADDRESS (City, State, and ZIP Code)			10. SOURCE OF FUNDING NUMBERS		
			PROGRAM ELEMENT NO. 62715H	PROJECT NO. RW	TASK NO. RD
					WORK UNIT ACCESSION NO. 000024
11. TITLE (Include Security Classification) Large Waves in Channels					
12. PERSONAL AUTHOR(S) Divoky, David J.; Bhat, Rajendra					
13a. TYPE OF REPORT Technical Report		13b. TIME COVERED FROM 860828 To 870620		14. DATE OF REPORT (Year, Month, Day) 870620	
15. PAGE COUNT 8					
16. SUPPLEMENTARY NOTATION This work was sponsored by the Defense Nuclear Agency under RDT & E RMSS Code B4662 D RW RD 0024 SPSS 3100 A H2590D					
17. COSATI CODES			18. SUBJECT TERMS (Continue on reverse if necessary and identify by block number)		
FIELD	GROUP	SUB-GROUP	Water Waves, Explosion Waves, Landslide Waves		
19. ABSTRACT (Continue on reverse if necessary and identify by block number)					
<p>In this Phase I SBIR effort, the behavior of large amplitude water waves in channels is reviewed. Wave generation may be by explosion or landslide, creating long disturbances which propagate with little attenuation. A three-dimensional solitary wave theory is described and implemented in a numerical model. Results are shown for transverse wave amplification on sloping banks. Amplifications of more than two are typical for realistic channels. Examples of explosion waves are discussed for typical sites.</p>					
20. DISTRIBUTION / AVAILABILITY OF ABSTRACT			21. SECURITY CLASSIFICATION		
<input type="checkbox"/> UNCLASSIFIED/UNLIMITED <input type="checkbox"/> SAME AS RPT <input type="checkbox"/> DTIC USERS					
22a. NAME OF RESPONSIBLE INDIVIDUAL			22b. TELEPHONE (Including Area Code)		22c. OFFICE SYMBOL
					DNA/STTI

DD FORM 1473, 84 MAR


83 APR edition may be used until exhausted
All other editions are obsolete

SECURITY CLASSIFICATION OF THIS PAGE

THIS COPY MADE AT U.S. GOVERNMENT PRINTING OFFICE

SUMMARY

This report covers Phase I of a study of Large Waves in Channels, sponsored by DNA under the SBIR Program. The first phase was intended to review the knowledge of the behavior of very large waves in natural channelized geometries. The waves considered are very long, as might be generated by submerged explosions of moderate yield. Owing to channelization, such waves may propagate considerable distances with little attenuation. On sloping banks, the waves are subject to a substantial transverse amplification, further increasing their potential effects. Breaking may occur in the bank regions, subjecting shoreline structures and facilities to large, destructive effects.



Having demonstrated the potential hazard of channel waves, it is recommended that Phase II further pursue the three-dimensional wave theory in order to better define wave transformation, to remove certain theoretical limitations, to develop expressions for water particle velocities and accelerations in the bank regions (for assessment of forces on structures), and to investigate the conditions under which the bank waves will break, forming turbulent bores.

Accession For	
NTIS GRA&I	<input checked="" type="checkbox"/>
DTIC TAB	<input type="checkbox"/>
Unannounced	<input type="checkbox"/>
Justification	
By <i>peult</i>	
Distribution	
Availability Codes	
Dist	Avail and/or Special
A-1	



Conversion factors for U.S. Customary to metric (SI) units of measurement

MULTIPLY \longrightarrow BY \longrightarrow TO GET
TO GET \longleftarrow BY \longleftarrow DIVIDE

angstrom	1.000 000 X E -10	meters (m)
atmosphere (normal)	1.013 25 X E +2	kilo pascal (kPa)
bar	1.000 000 X E +2	kilo pascal (kPa)
barn	1.000 000 X E -28	meter ² (m ²)
British thermal unit (thermochemical)	1.054 350 X E +3	joule (J)
caloric (thermochemical)	4.184 000	joule (J)
cal (thermochemical)/cm ²	4.184 000 X E -2	mega joule/m ² (MJ/m ²)
curie	3.700 000 X E +1	giga becquerel (GBq)
degree (angle)	1.745 329 X E -2	radian (rad)
degree Fahrenheit	$t_F = (t_C + 459.67)/1.8$	degree kelvin (K)
electron volt	1.602 19 X E -19	joule (J)
erg	1.000 000 X E -7	joule (J)
erg/second	1.000 000 X E -7	watt (W)
foot	3.048 000 X E -1	meter (m)
foot-pound-force	1.355 818	joule (J)
gallon (U.S. liquid)	3.785 412 X E -3	meter ³ (m ³)
inch	2.540 000 X E -2	meter (m)
jerk	1.000 000 X E +9	joule (J)
joule/kilogram (J/kg) (radiation dose absorbed)	1.000 000	Gray (Gy)
kilotons	4.183	terajoules
kip (1000 lbf)	4.448 222 X E +3	newton (N)
kip/inch ² (ksi)	6.894 757 X E +3	kilo pascal (kPa)
knap	1.000 000 X E +2	newton-second/m ² (N-s/m ²)
micron	1 000 000 X E -6	meter (m)
mil	2.540 000 X E -5	meter (m)
mile (international)	1.609 344 X E +3	meter (m)
ounce	2.834 952 X E -2	kilogram (kg)
pound-force (lbf avoirdupois)	4.448 222	newton (N)
pound-force inch	1.129 848 X E -1	newton-meter (N-m)
pound-force/inch	1.751 268 X E +2	newton/meter (N/m)
pound-force/foot ²	4.788 026 X E -2	kilo pascal (kPa)
pound-force/inch ² (psi)	6.894 757	kilo pascal (kPa)
pound-mass (lbm avoirdupois)	4.535 924 X E -1	kilogram (kg)
pound-mass-foot ² (moment of inertia)	4.214 011 X E -2	kilogram-meter ² (kg-m ²)
pound-mass/foot ³	1.601 846 X E +1	kilogram/meter ³ (kg/m ³)
rad (radiation dose absorbed)	1.000 000 X E -2	*Gray (Gy)
roentgen	2.579 760 X E -4	coulomb/kilogram (C/kg)
shake	1 000 000 X E -8	second (s)
slug	1.459 390 X E +1	kilogram (kg)
torr (mm Hg, 0° C)	1.333 22 X E -1	kilo pascal (kPa)

*The becquerel (Bq) is the SI unit of radioactivity; 1 Bq = 1 event/s.

**The Gray (Gy) is the SI unit of absorbed radiation.

A more complete listing of conversions may be found in "Metric Practice Guide E 380-21" American Society for Testing and Materials

TABLE OF CONTENTS

1.	INTRODUCTION	1
2.	REVIEW OF PRIOR WORK	11
2.1	Source Mechanisms	11
2.1.1	<u>Explosion Sources</u>	11
2.1.2	<u>Landslides</u>	13
2.2	Wave Behavior	17
2.2.1	<u>Theoretical Descriptions</u>	17
2.2.2	<u>Observations</u>	18
3.	WAVES IN A UNIFORM CHANNEL	24
3.1	Nonlinear Three-Dimensional Waves	24
3.1.1	<u>Theoretical Development</u>	24
3.1.2	<u>Analytical Solutions</u>	33
3.1.3	<u>Numerical Solutions</u>	35
3.2	Damping	38
3.2.1	<u>Frictional Damping</u>	38
3.2.2	<u>Breaking Dissipation</u>	40
3.3	Channel Branching Effects	44
4.	PREDICTIONS AND COMPARISONS WITH OBSERVATIONS	46
4.1	Parametric Presentation of Numerical Results	46
4.2	Comparisons with Observations	69
4.2.1	<u>Data of Peregrine</u>	69
4.2.2	<u>Lituya Bay Landslide Wave</u>	69
5.	EXAMPLES	71
6.	CONCLUSIONS AND RECOMMENDATIONS	78
7.	REFERENCES	81
APPENDIX A: Listing of Channel Wave Computer Program		

THIS COPY "MADE AT U.S. GOVERNMENT PRINTING OFFICE"

LIST OF ILLUSTRATIONS

Figure 1a:	Map of Lituya Bay Showing Forest Trimline	2
	(Miller, 1960)	
Figure 1b:	Photograph of Lituya Bay Before & After Landslide	3
	[REDACTED]	
	[REDACTED]	
Figure 3a:	Wave Propagation Patterns for Gentle and Steep Slopes at Moderate and Grazing Incidence	7
Figure 3b:	Wave Amplitude Variation for the Cases Shown in Figure 3a	8
Figure 4:	Summary of Experimental Data Relating Wave Properties to Explosion Parameters	12
Figure 5:	Landslide Regression Formula of Slingerland & Voight (1982)	15
Figure 6:	Wave Profiles on Three Slopes	19
	(Divoky & Lane, 1973)	
Figure 7:	Wave Profiles on Three Slopes	20
	(Divoky & Lane, 1973)	
Figure 8a:	Transverse Profiles from Peregrine, 1969 Bottom Width = 1.5, Slope = 45°	22
Figure 8b:	Transverse Profiles from Peregrine, 1969 Bottom Width = 2.0, Slope = 45°	22
Figure 9:	Sketch of Channel Coordinate System	25
Figure 10:	Sketch Illustrating Approximate Surface Boundary Condition (see text)	37
Figure 11:	Frictional Height Reduction for Initial Height of 0.2	41
Figure 12:	Frictional Height Reduction for Initial Height of 0.4	42
Figure 13:	Frictional Height Reduction for Initial Height of 0.6	43
Figure 14a:	Amplitude Variation for Indicated Condition	47
Figure 14b:	Amplitude Variation for Indicated Condition	48
Figure 14c:	Amplitude Variation for Indicated Condition	49


Figure 14d: Amplitude Variation for Indicated Condition	50
Figure 15a: Amplitude Variation for Indicated Condition	51
Figure 15b: Amplitude Variation for Indicated Condition	52
Figure 15c: Amplitude Variation for Indicated Condition	53
Figure 15d: Amplitude Variation for Indicated Condition	54
Figure 16a: Amplitude Variation for Indicated Condition	55
Figure 16b: Amplitude Variation for Indicated Condition	56
Figure 16c: Amplitude Variation for Indicated Condition	57
Figure 16d: Amplitude Variation for Indicated Condition	58
Figure 17a: Amplitude Variation for Indicated Condition	59
Figure 17b: Amplitude Variation for Indicated Condition	60
Figure 17c: Amplitude Variation for Indicated Condition	61
Figure 17d: Amplitude Variation for Indicated Condition	62
Figure 18a: Amplitude Variation for Indicated Condition	63
Figure 18b: Amplitude Variation for Indicated Condition	64
Figure 18c: Amplitude Variation for Indicated Condition	65
Figure 18d: Amplitude Variation for Indicated Condition	66
Figure 19: Variation of Amplitude at Bank with Bottom Width	67
Figure 20: Variation of Amplitude at Bank with Bank Slope	68

Figure 24: Approximate Limit of Bank Amplification as a Function of Bank Slope	79
---	----

1. INTRODUCTION

In this Phase I report we present a preliminary review of the behavior of 'Large Waves in Channels.' The waves of interest are long oscillatory or solitary waves such as might be generated by large explosions, landslides, or other impulsive mechanisms. We do not consider waves of extreme length such as tides or flood waves, nor short waves in the range of the normal oceanographic environment. The waves of interest are those that are longer than the width of the channel and long with respect to the depth, but not 'too' long.

The purpose of this small Phase I study is to assess the general nature of this problem, to review available information, and to define directions for new research to be undertaken in Phase II; Phase I, itself, is not considered a research phase. Nevertheless, we have felt it appropriate to present some new results even here, as will be shown later.

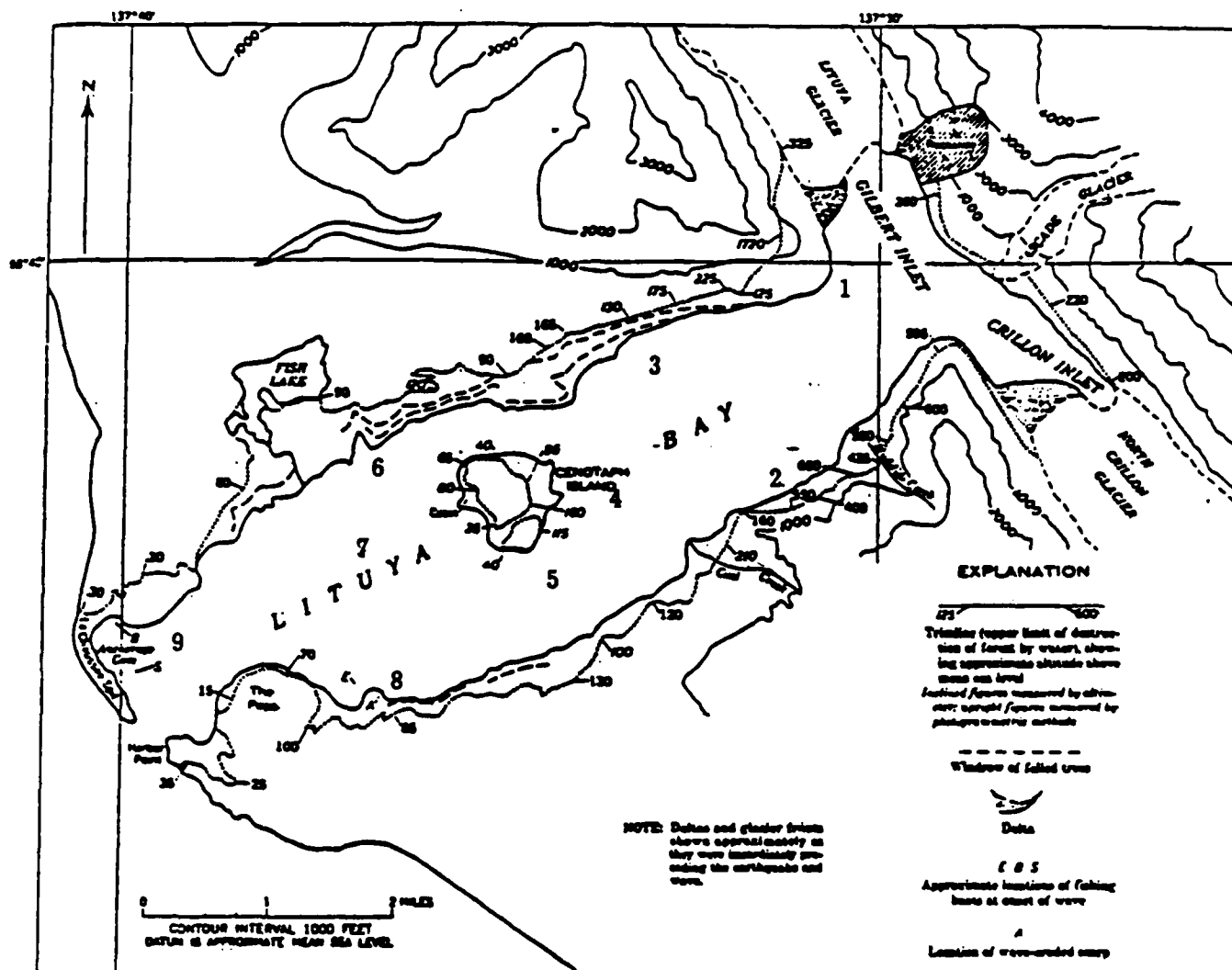


Lituya Bay is situated on the Gulf of Alaska south of Yakutat. As shown in Figure 1, it is roughly T-shaped, approximately eight miles long, and two miles wide; depths of several hundred feet are common. The landslide (documented in Miller, 1960) took place in the northeast portion of Gilbert Inlet (shown shaded in Figure 1). Approximately 40 million cubic yards of rock descended at high speed into the Bay with devastating results.

The southwest bank of Gilbert Inlet directly opposite the slide was inundated by the slide-generated water waves, to a height of over 1500 feet, completely leveling forest to that elevation (Iida, et al, 1967). This is certainly dramatic, but perhaps not unexpected considering the proximity of the landslide -- the opposite bank was in the direct path of the 'splash' generated by the intruding mass.

More interesting were the effects outside the immediate region of the slide, along the banks of the central portion of the Bay. According to Iida, et al (1967) and Wiegel (1964), a large wave progressed seaward through the Bay with heights of 200-300 feet, as estimated from the elevation to which large trees "were removed as if they were matchsticks" from the side slopes (Wiegel, 1964).

The dotted contours in Figure 1a show the elevation of destruction, the numeric labels being height in feet. On the northern bank one sees heights of about 90 to 200 feet, while on the southern bank damage elevations range from about 100 to 600 feet. The Bay both before and after the slide is shown in Figure 1b.



THIS COPY ISSUED BY U.S. GOV.

FIGURE 1a: Map of Lituya Bay Showing Forest Trimline (Miller, 1960)

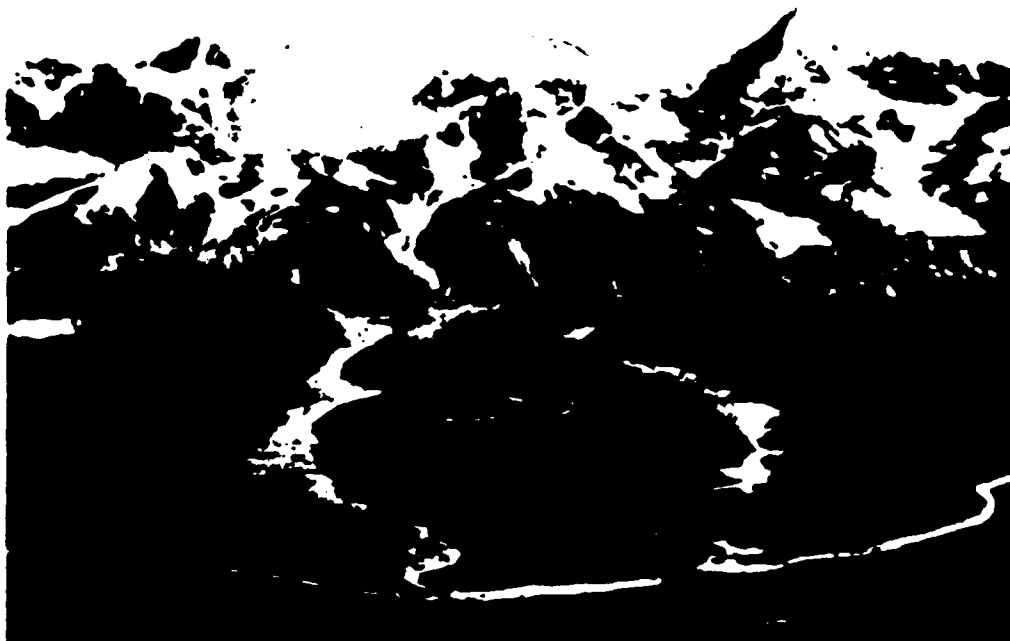
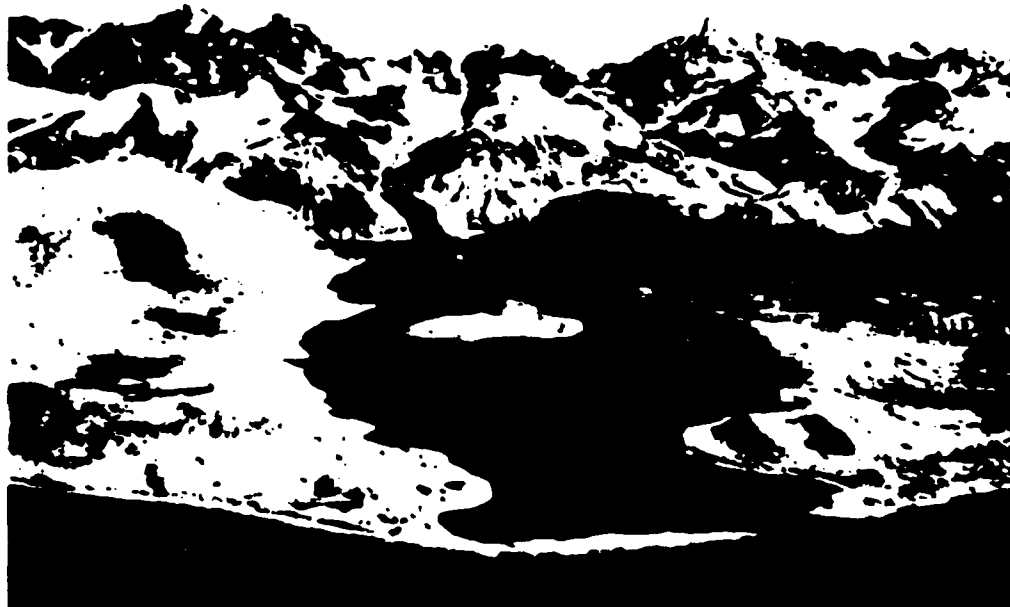



Figure 1b: Photograph of Lituya Bay Before & After
Landslide.

This copy made at U.S. Government expense.

reproduced from Wiegel (1964). These photos show the large areas of forest destroyed by the passing wave.



There are two major reasons why waves in channels pose a special problem. First, the channelized geometry conducts the wave energy from the source to a site a distance away with very little loss. This is in contrast to the usual case of explosion waves in open water. In open water, an impulsive wave system is free to expand in all directions; radial spreading causes a wave height reduction which is proportional to the square-root of distance, leading to rapid decay of height. As ordinary waves approach a slope they refract and their heights are limited by breaking. But in a channel, the causes of height reduction are limited to dispersive spreading (small for long waves) and energy loss. The major source of energy loss may be turbulent breaking in the zones of shallow flow on the banks. But these breaking zones are precisely the damage zones, so that breaking should actually be considered a damage mechanism, not a mitigating damping mechanism. The wave height in the bank zone is replenished by lateral flow. These differences are summarized in the schematic sketches of Figure 3.

The second factor contributing to a high hazard in channels is the possibility of significant amplification of wave height on the banks. As we shall show later, our Phase I work indicates that amplifications of a factor of two or more are to be expected on typical bank slopes for moderately wide channels. This amplification is found as a higher-order approximation to solitary wave theory. The three-dimensional solitary wave theory described later reveals that a large transverse variation of wave amplitude is characteristic of solitary waves in channels and that the degree of amplification at the banks depends upon both channel width and bank slope. The general nature of the transverse variation is found to be consistent with the limited available experimental data.

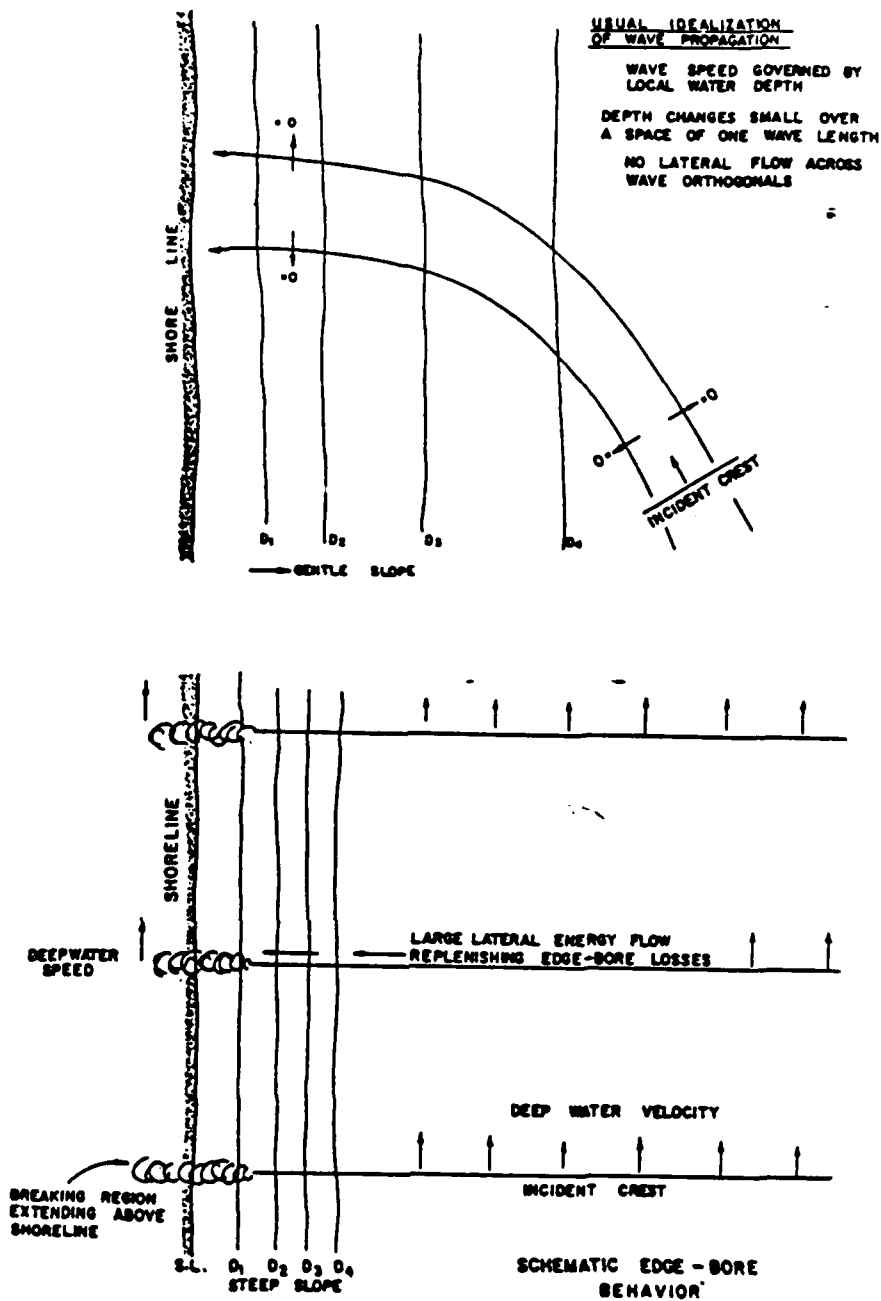
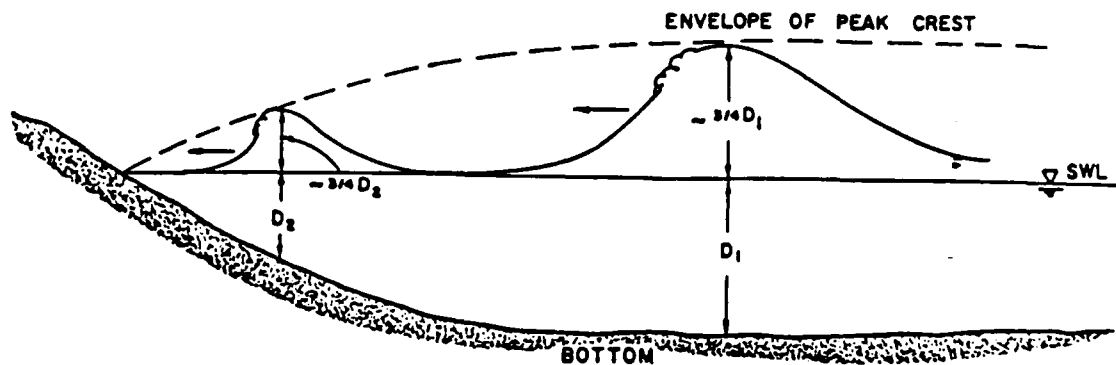
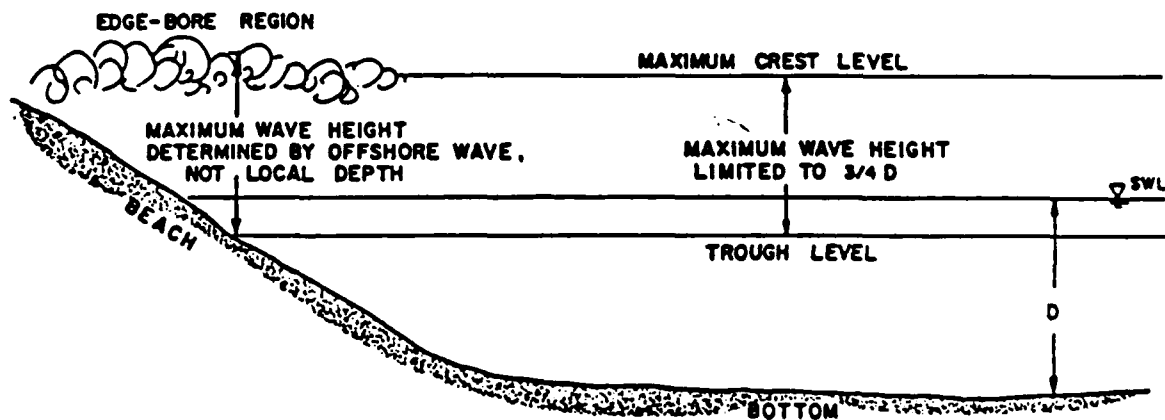


Figure 3a: Wave propagation patterns for gentle and steep slopes, at moderate and grazing incidence.



THE HEIGHT OF A NORMAL BREAKER IS
LIMITED BY LOCAL DEPTH ($H \approx 3/4 D$)



SCHEMATIC BEHAVIOR OF EDGE-BORE HEIGHT
(DIRECTION OF PROPAGATION NORMAL TO PAGE)

Figure 3b: Wave amplitude variation for the cases shown in Figure 3a.

[REDACTED]

The explosion (or landslide) waves discussed here are, in a sense, a more focused phenomenon. Under proper circumstances, they will propagate with almost no reduction in height for considerable distances. Their effects are greatest along the shorelines (the banks), rather than in deeper water. The major dissipation is the destructive near-shore breaking which, being of limited extent (concentrated right at the bank), may not attenuate the wave 'too' fast.

[REDACTED]

[REDACTED]

The major content of this report is contained in Sections 3 and 4 where we describe and implement a three-dimensional solitary wave theory to estimate the lateral enhancement of wave height. We have worked out the analytical solution for triangular channel cross-sections and have constructed a simple numerical model for the simulation of a range of trapezoidal channel geometries. It is found that amplification factors of two or more are realistic for natural channels. We also briefly describe the effects of friction and channel bifurcation as dissipative mechanisms.

Our Phase I study shows the importance of channel effects and indicates the direction of work required for a better understanding of this sort of wave behavior. In particular, no investigation of particle velocities in the bank zones has been undertaken, and no information is available describing the breaking characteristics on the banks. Both of these questions are vital for an understanding of dynamic effects. There is also almost no experimental data to guide the development of theories or to verify them. Consequently, we conclude by recommending a program of theoretical and numerical work supplemented by small scale laboratory tests for a Phase II continuation.

2. REVIEW OF PRIOR WORK

2.1. Source Mechanisms

We consider two primary source mechanisms for the sort of waves under consideration here: explosions and landslides. In both, active research is underway elsewhere and has reached a state of adequate understanding for the purposes of this study. Consequently, our concern is limited to adopting appropriate order-of-magnitude data as input.

2.1.1. Explosion Sources

Explosion wave prediction (see LeMehaute, 1971, for a general summary) is accomplished by calibration of idealized models of wave generation by an initial free-surface deformation. The source is usually assumed to be a symmetric 'crater' which collapses under gravity yielding an outgoing wave system.

The initial crater is fictitious in that its shape is chosen so that the mathematics is tractable, and its dimensions are chosen so that predicted wave heights and periods match observations reasonably well. The predicted waves are obtained by the transform methods originally introduced by Kranzer and Keller (1959).

Considerable effort has led to the establishment of reasonable shapes for the source crater as well as to empirical scaling laws relating crater dimensions to weapon yield and placement. For example, in deep water, the familiar curve shown in Figure 4 is obtained, relating the product of maximum wave amplitude, η , and range, r (this product being conserved in deep water) to explosion yield, W , and depth of burst, z . Although this data shows a narrow peak in wave height for shallow bursts (the so-called upper critical depth effect) it is adequate for our purposes to follow LeMehaute (1985) and adopt an average value given by

$$\eta_{\max} = 8W^{0.54}/r$$

in which the dimensions are feet and pounds of TNT-equivalent. Similarly, one can take for the wave period T (in seconds)

$$T = 1.7W^{0.15}$$

from which the length can be calculated.

These deepwater relationships will not generally be appropriate for waves in channels, however, owing to the relative shallowness of most real channels. The effect of shallow water is to greatly reduce the efficiency of wave generation.

Wang, et al (1977) reviewed available explosion data for shallow water (especially the data of Strange, 1955) and revised the

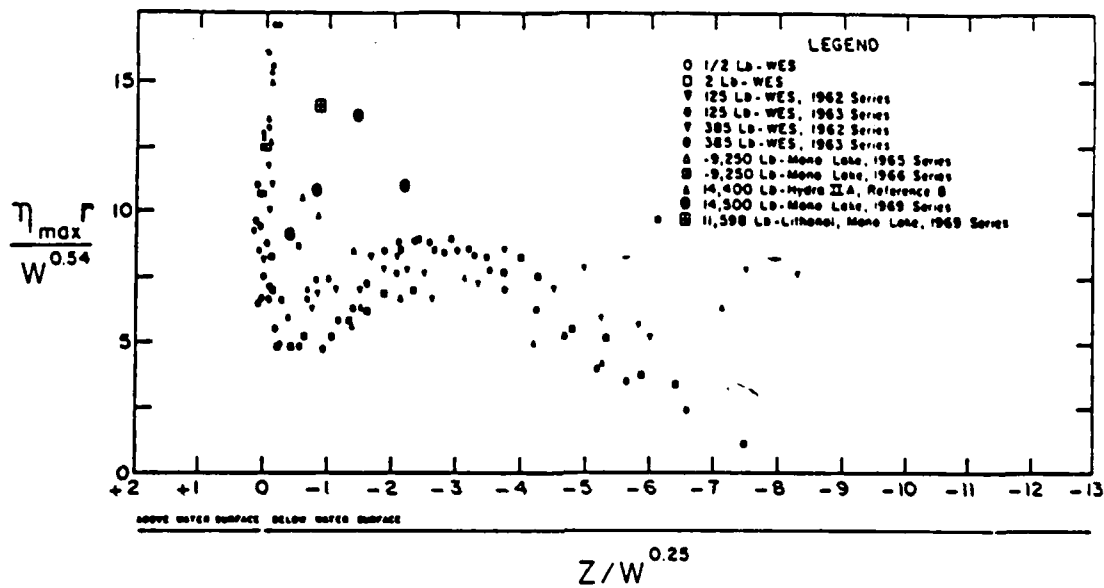


Figure 4: Summary of Experimental Data Relating Wave Properties to Explosion Parameters.

scaling laws accordingly. As given in the recent summary of LeMehaute (1985), Wang's revised expressions are

$$\eta_{\max} r / (W^{0.25 + 8/3}) = 1.44 (d / W^{1/3})^{0.93}$$
$$\beta = 0.83 (d / W^{1/3})^{0.007}$$

These expressions are appropriate for reduced depths $(d / W^{1/3})$ less than one (the original data being from 0.088 to 0.585).

The deepwater relations given above can be accepted for reduced depths greater than about six. For intermediate depths, LeMehaute (1971) suggests that heights should be reduced by half between a reduced depth of 6.0 and a depth of 1.0; a simple linear variation is suggested.

An important question for channel waves is the dependence of wave length on water depth for a given explosion yield. In order to exist and survive, these waves must be longer than both the channel depth and the channel width.

It seems reasonable on physical grounds to argue that the wave length of the highest waves generated by an explosion will be, if not independent of, at least insensitive to the water depth. The dominant length scale in the spectrum of waves generated by an initial 'crater' must be of the same order of magnitude as a characteristic horizontal measure of the crater itself. That is, we should expect energy to be concentrated at lengths near the diameter of the crater, within a small factor.

Indeed, data shows that in deep water the length of the largest waves is about three-fourths the assumed crater diameter, confirming our assumption.

Now, in shallow water it is reasonable to assume that to a first approximation the horizontal scale of the crater is unaffected by the depth. That is, the blast creates a disturbance which has about the same diameter no matter what the depth is, although the vertical crater scale might be substantially affected.

In the absence of a better simple alternative, we shall then assume that wavelengths in channels can be estimated from deepwater empirical relationships. Should it be necessary to estimate wave periods, one can simply work backward from the length and the depth.

2.1.2 Landslides

A detailed numerical model of landslide generated water waves was developed by Chiang, Divoky, Parnicky, and Wier (1981). This model incorporates a sophisticated 'box-car' model of landslide dynamics on an arbitrary slope, accounting for the interaction of the slide with the water upon entry into the basin. This coupled calculation then proceeds to follow the generation and propaga-

tion of the water waves. Other models of varying complexity have been developed by a number of authors including especially Raney and Butler (1975) and Noda (1969), the latter being an analytical development describing the intrusion of a mass of simple shape into a fluid.

It had been hoped that the model of Chiang, et al., could be converted from mainframe to PC for the present study and that simple example cases could be run for an idealized geometry. However, this proved impossible within the limited Phase I resources.

More than adequate for our purposes, however, are empirical guidelines. Slingerland and Voight (1982) present a simple regression model relating landslide induced wave height to slide kinetic energy and water depth. Their expression is

$$\log(\eta_{\max}/d) = a + b \log(E)$$

in which a and b are regression coefficients and E is a dimensionless slide kinetic energy given by

$$E = 1/2 MV^2/(\rho g d^4)$$

Here, M is the slide mass, g is the acceleration of gravity, and V is the maximum slide velocity. The wave amplitude η_{\max} is the value observed at a standard reference distance of $4d$ from the slide point of entry, and assumes that the waves spreads freely into a 180-degree half-space. Should the slide occur at a corner, Slingerland and Voight recommend the artifice of simply adjusting the assumed energy in order to account for the effects of reduced spreading area.

Figure 5 shows the regression relation along with the data points upon which it is based. It is clear that within this data base, the simple relation suggested by Slingerland and Voight is entirely adequate.

To use this formula for a first order estimate in channels (with slide intrusion assumed to occur on one side), the amplitude should be adjusted to account for channel width. It is reasonable to imagine that the height which should be considered the initial height for propagation in a channel is approximately that obtained when the expanding semi-circular wave encounters the opposite bank. At this time, complicated reflection and dissipation processes on the opposite bank truncate the wave expansion and leave two segments of the wave to propagate up- and downstream. These segments are perpendicular to the bank on the near shore but are curved toward the bank on the opposite shore, leading to additional dissipation. However, if the wave is reasonably long compared to the channel width it may be assumed that it will tend toward cross-channel uniformity with distance.

Since the regression expression of Slingerland and Voight adopts

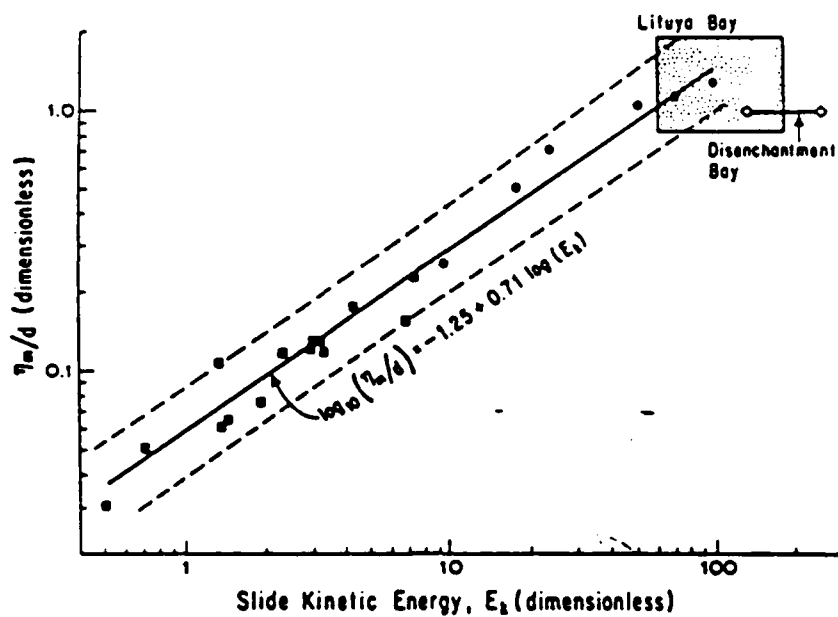


Figure 5: Landslide Regression Formula of Slingerland & Voight (1982).

a reference distance of $4d$, the height prediction must be scaled by a factor such as

$$(4d/B_0)^p$$

in which B_0 is the channel width and p is an exponent ranging between 0.5 (longwaves, no dispersion) and 1.0 (fully dispersive waves). It is recommended that p be taken as 0.5 unless the channel is quite deep; this choice will tend to slightly underestimate the wave height, helping to compensate for unconsidered dissipation.

2.2. Wave Behavior

2.2.1. Theoretical Descriptions

Very little of the literature on waves in channels is pertinent to this study, most dealing, for example, with the propagation of flood waves or dam-break waves. These are phenomena quite distinct from the explosion-scale intermediate waves of interest here.

However, a small number of papers were found which are directly applicable, developing a theory of cnoidal and solitary waves in channels of arbitrary cross-section. When taken to higher order, these theories are capable of describing major features of flow in the sloping bank regions which are the areas of primary interest in this study (up to the point of breaking, that is).

The papers of interest followed the important earlier work of Korteweg and de Vries (1895), Ursell (1953), and Benjamin and Lighthill (1954) who laid the necessary groundwork. Korteweg and de Vries and Ursell had clarified the roles played by the two fundamental dimensionless length scales involved in longwave theory. These are σ and ϵ defined by

$$\sigma = h/L \qquad \epsilon = \eta/h$$

in which h is a typical depth, L is a horizontal length scale such as wavelength, and η is a typical amplitude.

Ursell showed that the simultaneous smallness of σ and ϵ does not lead to a unique theory as was assumed (the longwave paradox), but that the relative magnitudes of these parameters is equally important. The combined parameter

$$U = \epsilon/\sigma^2$$

is called the Ursell parameter and can be interpreted as a measure of the relative importance of nonlinearity, which tends to steepen the wave with propagation distance (measured by ϵ), and frequency dispersion, which tends to broaden the wave (measured by σ). It was shown that when the parameter U is on the order of unity, these opposing tendencies may balance, permitting the existence of waves of permanent form.

Korteweg and de Vries (1895) and Benjamin and Lighthill (1954) developed the governing equations for cnoidal waves (and, in the limit, solitary waves), the latter in terms of gross flow quantities.

Peters (1966) considered solitary waves in a channel of arbitrary cross-section. His paper is of interest since he first develops the rotational case and then the irrotational case as a limit. He also gives an analytical solution for semi-circular channels which will be discussed in a later section.

The papers of most interest are those of Peregrine (1968) and Fenton (1973). The work of these authors is quite similar. Both consider long waves in arbitrary channels and derive similar expressions for flow quantities. Peregrine's development is the more standard, being in terms of particle velocities and elevation whereas Fenton's approach is really an extension of that of Benjamin and Lighthill, being defined in terms of integrated flow quantities.

Although we shall show Peregrine's development in a later section (upon which we have based a preliminary model of transverse wave amplitude variation), Fenton's derivations present certain conceptual advantages. In particular, he retains both σ and ϵ in his derivation, thereby showing precisely their relative importance. Peregrine, on the other hand, simply sets $U = 1$ and suppresses σ in favor of ϵ .

These papers do not go much beyond development of the governing equations, except to discuss the transverse amplitude variation in a general way. No pursuit of particle velocities is made, for example, such as will be necessary to define breaking criteria and dynamic effects.

2.2.2. Observations

Experimental observations of the important features of waves in channels are almost totally lacking. In particular, we are interested in the transverse wave profile and the likelihood that amplitudes on the banks may be significantly greater than at the center of the channel.

It is not clear why this has not been a topic of interest. A large quantity of experimental data for trapezoidal channels is reported in Benet and Cunge (1971) which was expected to be a good source of data for this review. Surprisingly, however, the critical data is not reported. All measurements seem to have been made on the banks and what appears to be amplification data is actually the ratio of peak bank height to the surcharge in mean water level associated with a sudden discharge.

Data for waves impinging at a small angle to a slope was obtained by Divoky and Lane (1973), but is of limited use here. Firstly, the waves were not long with respect to the depth and secondly, the test arrangement was in a 2-D basin, not a channel. Consequently, the waves in many cases were not propagating stably, the observed amplifications showing considerable scatter.

Nevertheless, it may be of interest to show the most pertinent cases. Figures 6 and 7 show the observed amplitude profiles along a crest for nominal angles of incidence of 0 and 3.5 degrees, for three nominal beach slopes: 20, 30, and 45 degrees. The water depth at the toe of the slope was 1.2 ft and the wave period was about 1.1 seconds. Amplitudes along the crests were

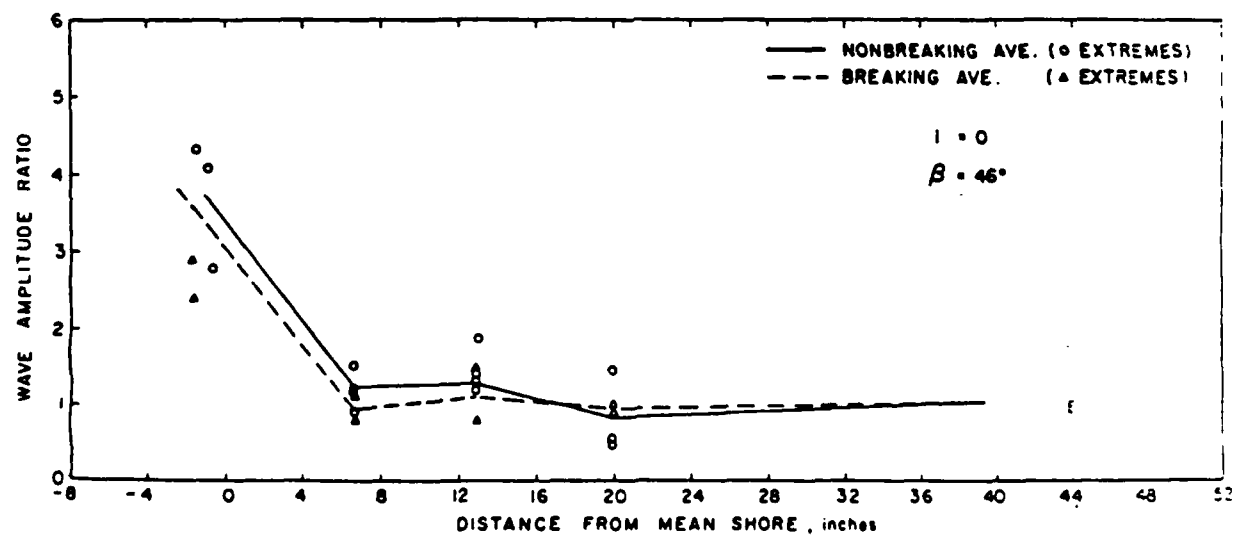
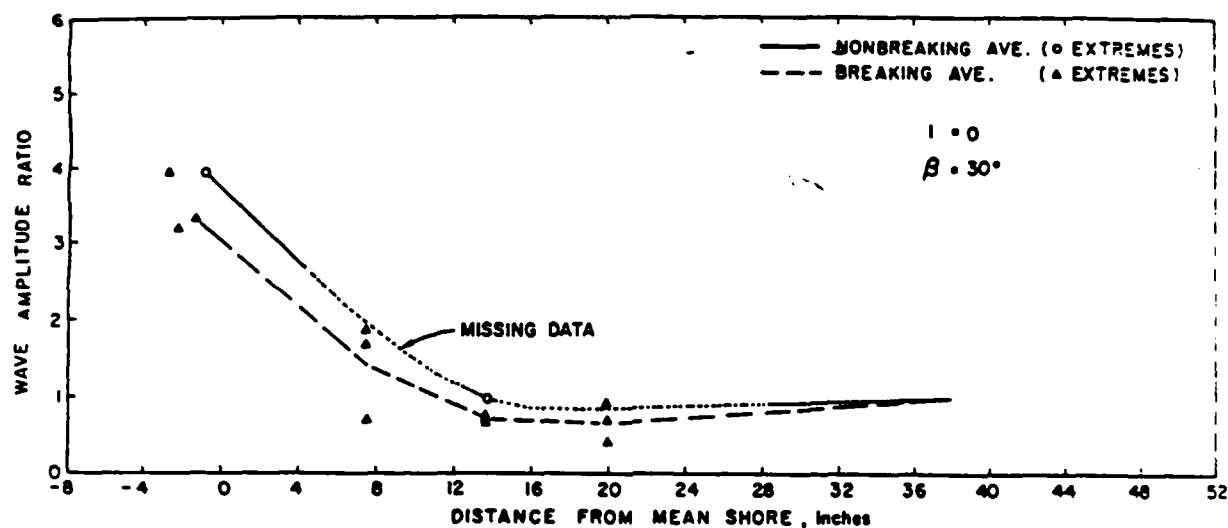
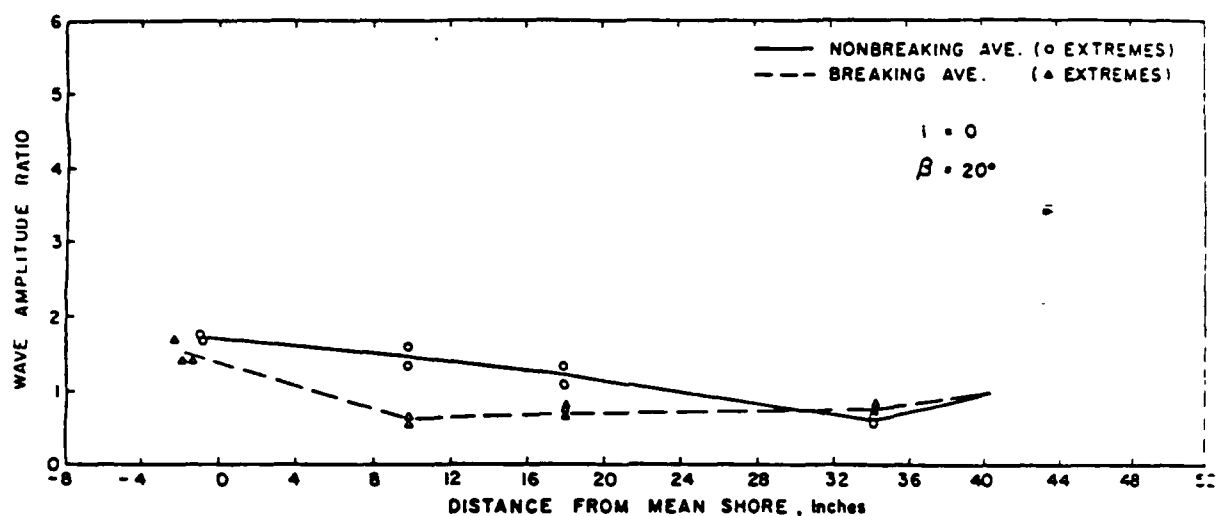


Figure 6: Wave Profiles on Three Slopes, (Divoky & Lane, 1973).

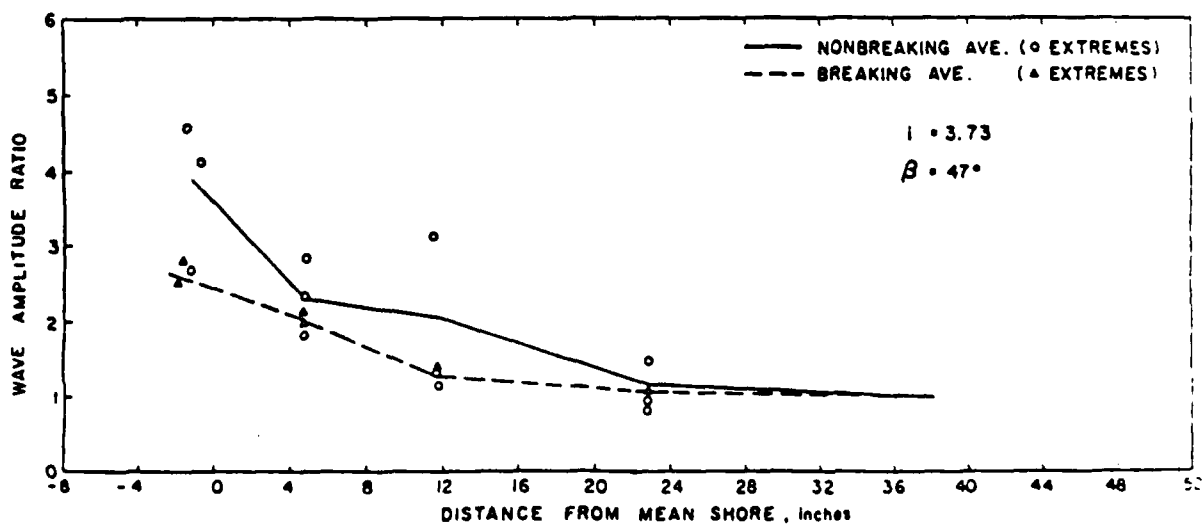
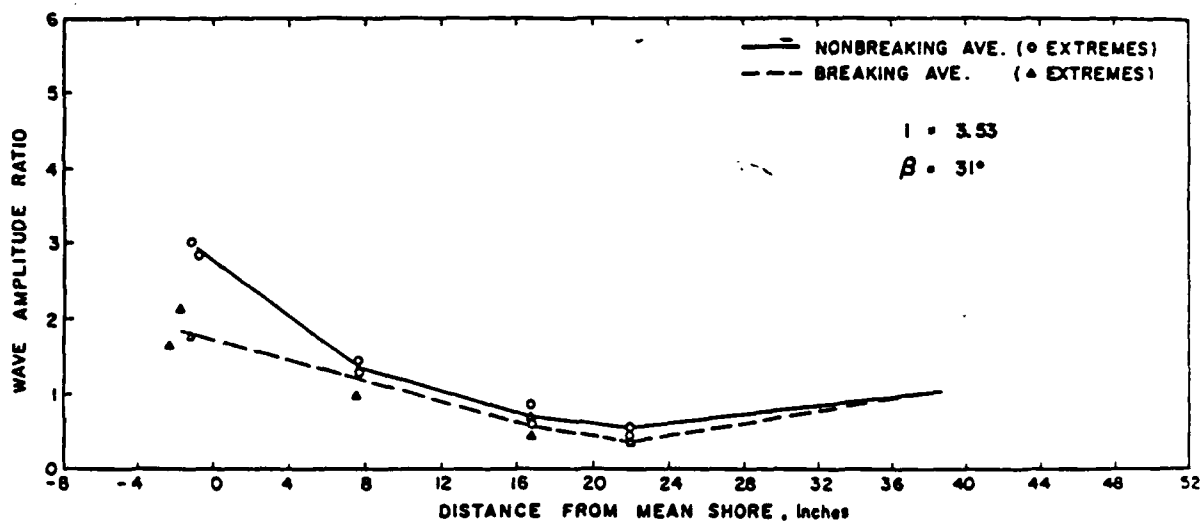
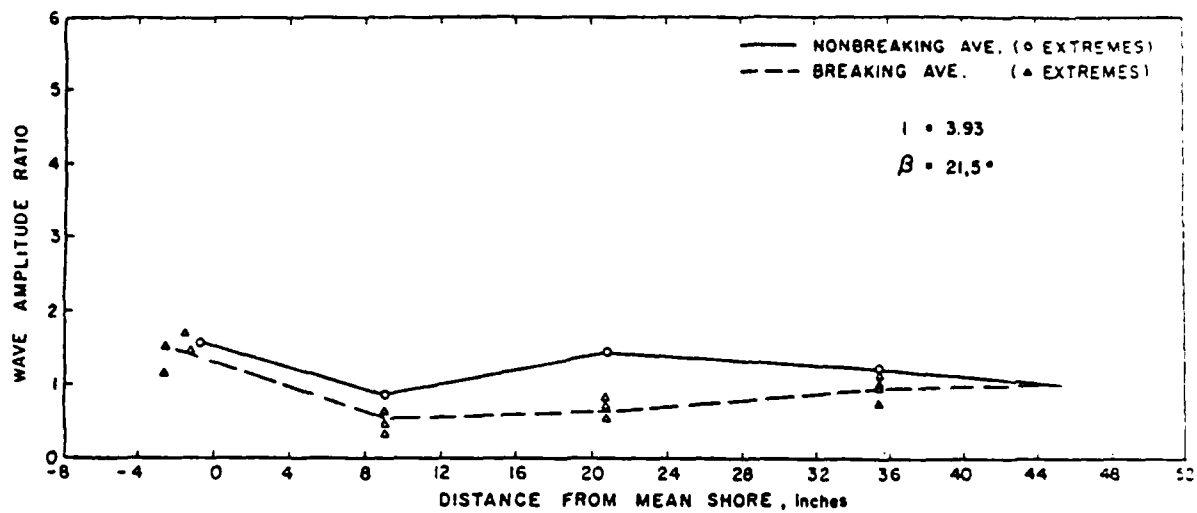


Figure 7: Wave Profiles on Three Slopes. (Divoky & Lane, 1973).

measured with a resistance gage or, on the slope, estimated from the limit of the wetted-zone. Amplitudes were arbitrarily normalized to unity at the farthest offshore points.

It can be seen from these figures that for both 30 and 45 degrees there is an amplitude enhancement of as much as a factor of four. On the 20 degree slopes, however, amplifications were only about half as large. The reasons for this were not evident, especially since the same trend is observed for both breaking and non-breaking waves, but it does seem to be a consistent feature of the data for waves of grazing incidence. Perhaps, because of the small experimental scale, scale effects became disproportionate in the shallow wedge region of the bank in the 20 degree case.

The wave generator was adjusted to produce both small waves showing no near-shore breaking, as well as larger waves revealing breaking at the tip of flow. It was found that for 0 degree incidence, wave breaking occurred for a deepwater wave steepness H_0/L_0 of 0.01, 0.013, and 0.017 for beach slopes of 20, 30, and 45 degrees, respectively. The same trend was observed for an incident angle of 3.5 degrees, with each critical steepness about 0.003 higher than for the 0 degree case. For less oblique incidence, the breaking criterion became extremely erratic reflecting the complex behavior in a Mach-stem zone.

The final -- and most pertinent -- data is that obtained by Peregrine (1969) in two small lab test series. The results are semi-quantitative, being presented only as two drawings of surface profile across half trapezoids for various center amplitudes. Both cases involved side slopes of 45 degrees, one having a bottom half-width of 1.5, the other 2.0 (normalized by depth). These are reproduced in Figure 8. The elevations shown at the left edge (full-channel center line) are normalized by depth. The solid lines represent the crest profiles, while the small x's indicate the corresponding values from Peregrine's model. In general, the agreement is seen to be very good. Surface heights at the banks appear to be about 50% greater than at the channel center for the larger amplitudes.

Note in particular that in the case of a bottom width of 2.0 and a center amplitude of 0.27, the crest at the bank is breaking, or nearly so. Despite this, the theoretical prediction appears quite good.

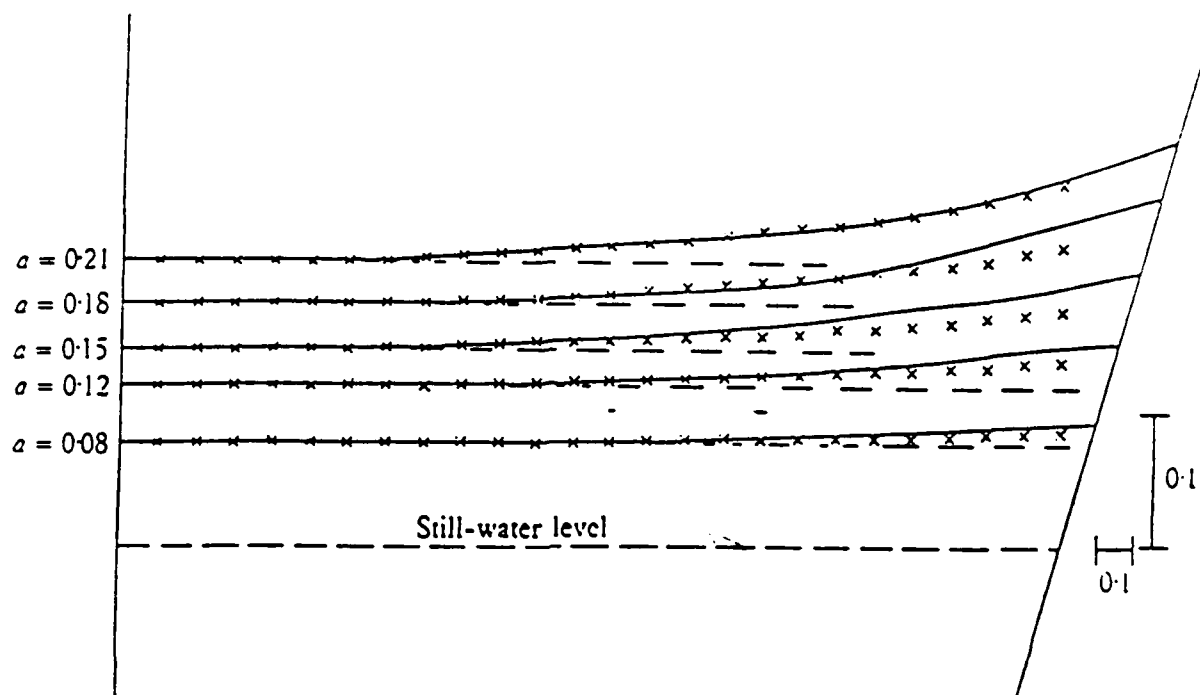


Figure 8a: Transverse Profiles from Peregrine, 1969
 Bottom Width = 1.5, Slope = 45° .

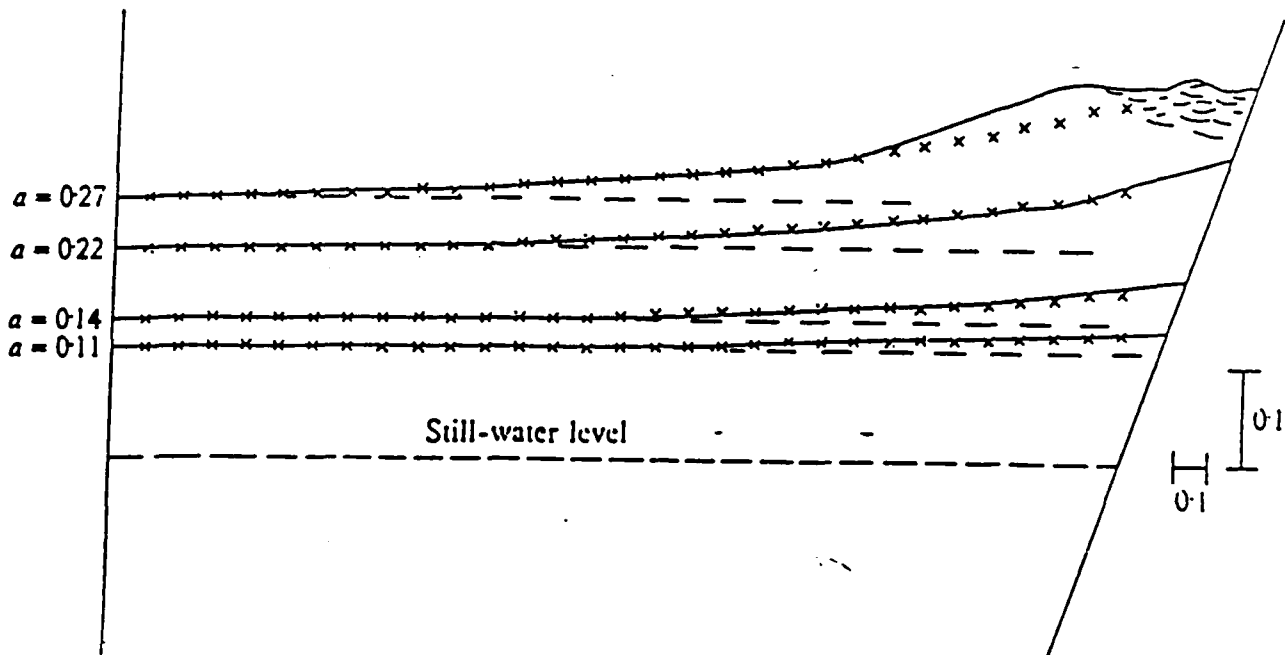


Figure 8b: Transverse Profiles From Peregrine, 1969
Bottom Width = 2.0, Slope = 45°.

3. WAVES IN A UNIFORM CHANNEL

3.1 Nonlinear Three-dimensional Waves

3.1.1 Theoretical Development

We have adopted the development given by Peregrine (1968) for use in this study. As noted earlier, Peregrine's formulation is more immediately useful in our context than is the presentation of Fenton, for example, although the essential features remain the same. Consequently, this summary follows Peregrine closely.

Consider a cartesian coordinate system embedded in the still water surface with the x-axis taken in the direction of wave propagation, the y-axis taken transverse to the channel, and the z-axis positive upward (Figure 9). The y-origin may be visualized as above the channel invert or, in our later consideration of symmetrical channels, at the midpoint of the cross-section. We consider the flow to occur in a channel of arbitrary, but uniform, cross-section; that is, the cross-section is defined by

$$z_c = z_c(y) \quad (1)$$

which is independent of x.

Introduce dimensionless variables

$$(x, y, z) = (x^*, y^*, z^*)/h_0$$

$$t = t^* \sqrt{g/h_0}$$

$$(u, v, w) = \vec{u} = \vec{u}^* / \sqrt{gh_0}$$

$$p = (p^* - p_0)/\rho gh_0 \quad (2)$$

in which the starred quantities are dimensional, g is the acceleration of gravity, h_0 is a characteristic water depth (such as the maximum undisturbed depth), (u, v, w) are the components of the fluid particle velocity \vec{u} , p is pressure, and p_0 is atmospheric pressure.

Neglecting only the shear stresses, the momentum equations become simply the Euler equations,

$$\vec{u}_t + (\vec{u} \cdot \nabla) \vec{u} + \nabla p + (0, 0, 1) = 0 \quad (3)$$

and the incompressible continuity equation is just

$$\nabla \cdot \vec{u} = 0 \quad (4)$$

This can also be written in terms of the macroscopic quantities Q and A (volume flux and instantaneous wetted cross-section) as

$$A_t + Q_x = 0 \quad (4a)$$

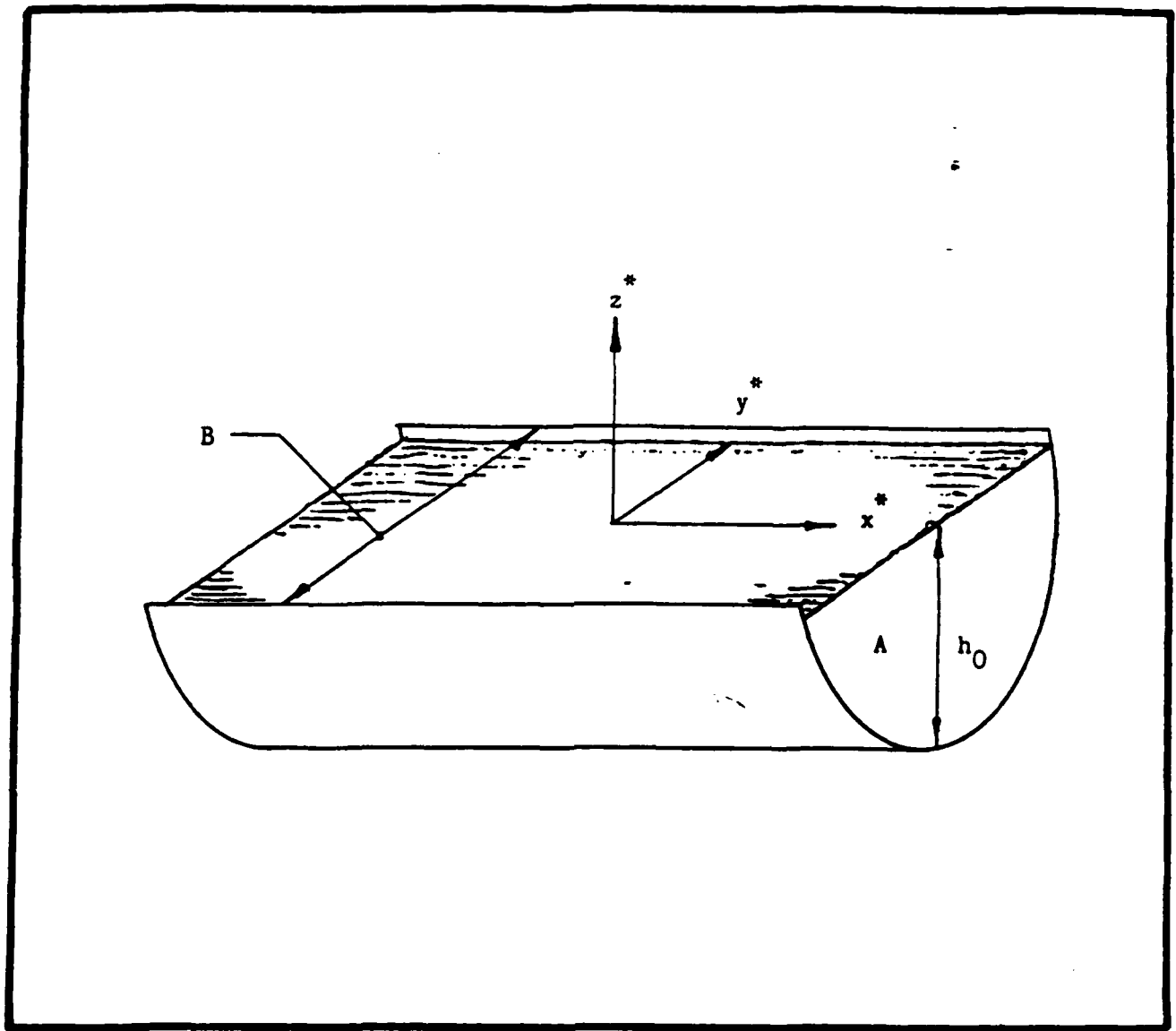


Figure 9: Sketch of Channel Coordinate System.

We obviously have

$$A = A(x,t) \quad \text{and} \quad Q = \iint_A u \, dydz$$

We assume irrotational flow so that

$$\nabla \times \vec{u} = 0 \quad (5)$$

The free surface is denoted by η ; on the surface

$$z = \eta(x,y,t)$$

where we must satisfy the boundary conditions

$$p = 0$$

$$\eta_t + u_x + v_y = w \quad (6)$$

Note that in these equations and those to follow, we adopt the subscript convention to denote partial differentiation (in the interests of notational simplicity).

Two dimensionless relative length scales are now introduced in order to proceed with an expansion of these equations. These are the relative depth, σ , and the relative amplitude, ϵ , given by

$$\sigma = h_0/L^*$$

$$\epsilon = a^*/h_0 \quad (7)$$

in which L^* is a characteristic wavelength and a^* is a measure of the peak amplitude.

In our problem, we assume that σ is very small since we are restricting attention to long waves. We will also assume that ϵ is small, although we shall be interested in waves which may be a few tenths of the depth in height.

A number of authors have shown (for constant depth or rectangular channels) that solitary waves of unchanging form are possible only if a balance exists between two processes measured by σ and ϵ . The effect of finite amplitude, measured by ϵ , is to cause a steepening of wave form with propagation distance, eventually leading to breaking. The effect of frequency dispersion, measured by σ , is the opposite, tending to reduce average steepness with distance. If these opposing influences are comparable, then a finite-amplitude wave of permanent form is possible. Not only solitary, but also periodic waves -- the cnoidal wave approximation -- are found in this case, although we shall in this preliminary review focus on the solitary case.

Ursell (1953), in particular, clarified the importance of the relative magnitudes of σ and ϵ , showing that the ratio

$$U = \epsilon / \sigma^2 = a^* L^{*2} / h_0^3 \quad (8)$$

is of fundamental importance. A unique theory is not guaranteed by the simultaneous smallness of σ and ϵ . Instead, the magnitude of U (the Ursell parameter) must also be specified. Only when U is of order unity do finite-amplitude permanent forms arise.

In order, then, to obtain the wanted solution Peregrine adopts the assumption that $U = 1$, replacing σ by ϵ in his development. It might be noted that in the similar work of Fenton (1973) U is also assumed to be of order unity but both σ and ϵ are retained in the expansions, greatly clarifying their roles and the order of approximation at each stage. While we follow Peregrine here for simplicity, future work would more likely be based on the approach of Fenton.

The independent variables are first scaled as

$$x_1 = x/\epsilon \quad t_1 = t/\epsilon \quad (9)$$

which are simply x^*/L^* and t^*/T , where T is a characteristic time scale such as the characteristic length L^* divided by the speed of longwave propagation. The variables η and u vanish in the absence of waves (neglecting a mean current) and so are expanded in the form

$$\epsilon f_1 + \epsilon^2 f_2 + \dots$$

The cross-sectional velocities are expanded as

$$\sqrt{\epsilon} (\epsilon f_1 + \epsilon^2 f_2 + \dots)$$

and the variables p and A , not vanishing, are taken to be of the form

$$f_0 + \epsilon f_1 + \epsilon^2 f_2 + \dots$$

The expansion solution is now straightforward. The expanded forms are substituted into the governing equations, terms of the same order are grouped and equated to zero, giving successive approximations to the dependent variables.

It is easy to see that the only zero'th order solutions are

$$p_0 = -z \quad \text{and} \quad A_0 = \text{constant}$$

That is, the pressure is hydrostatic and the cross-sectional area is constant (assuming a uniform channel) to this approximation.

Peregrine obtains the first order approximation by defining a two-dimensional velocity potential function $\phi_1(x_1, y, z, t_1)$ such that

$$v_1 = \phi_{1y} \quad \text{and} \quad w_1 = \phi_{1z} \quad (10)$$

which is permitted by the irrotationality condition to the first order (Eq 5)

$$v_{1z} - w_{1y} = 0 \quad (11)$$

Equation 5 also shows that to first order u is independent of y and z so that

$$u_1 = u_1(x_1, t_1)$$

Using Peregrine's two-dimensional gradient operator defined as

$$\nabla_1 = (0, \partial/\partial y, \partial/\partial z)$$

the first order y and z momentum equations yield

$$\nabla_1 p_1 = 0$$

Expanding the pressure condition on the free surface gives the first order condition

$$p_0 + \epsilon p_1 = 0 \quad \text{on} \quad z = \epsilon \eta_1$$

so that the first order expression for p is found to be

$$p_1(x_1, t_1) = \eta_1(x_1, t_1)$$

The x momentum equation at first order is found to be

$$(u_1)_{t_1} + (\eta_1)_{x_1} = 0 \quad (12)$$

and the integrated form of the continuity equation is, similarly,

$$(A_1)_{t_1} + (Q_1)_{x_1} = 0$$

Letting the width of the channel be denoted by $B(z)$, it is clear that the first correction to channel cross-sectional area is

$$A_1 = B(0)\eta_1 = B_0\eta_1$$

Furthermore, we must have $Q_1 = A_0 u_1$ so that the continuity equation can be rewritten as

$$B_0(\eta_1)_{t_1} + A_0(u_1)_{x_1} = 0 \quad (13)$$

Now, u_1 is eliminated from Equations 12 and 13 giving

$$(\eta_1)_{t_1 t_1} = A_0/B_0 (\eta_1)_{x_1 x_1} \quad (14)$$

This is just the wave equation from which we can identify the first approximation to the wave celerity, c_0 , to be given by

$$c_0^2 = A_0/B_0 \quad (15)$$

which is just the mean depth of the channel.

Now we introduce the cross-sectional velocity potential into the continuity equation (Eq 4), finding

$$(u_1)_{x_1} + \nabla_1^2 \phi_1 = 0$$

On all solid boundaries we must satisfy $(\phi_1)_n = 0$ and on the surface the first order condition

$$(\phi_1)_z = -c_0^2 (u_1)_{x_1} \text{ at } z = 0$$

where an η -derivative has been replaced by a u -derivative using Equation 13.

Guided by inspection of this last expression, Peregrine introduces a new function, ψ , defined by

$$\phi(x_1, y, z, t_1) = - (u_1)_{x_1} \psi(y, z)$$

Comparison with the foregoing equations shows that ψ must satisfy

$$\begin{aligned} \nabla_1^2 \psi &= 1 \quad \text{everywhere} \\ \psi_n &= 0 \quad \text{on solid boundaries} \\ \psi_z &= c_0^2 \quad \text{on } z = 0 \end{aligned} \quad (16)$$

Clearly, this is a well-posed Neumann problem which we solve numerically in a subsequent section.

To obtain the transverse variations, it is necessary to proceed to the next approximation. Collecting terms through the second order in ϵ in the momentum equation gives

$$(\nabla_1 \phi_1)_t + \nabla_1 p_2 = 0 \quad (17)$$

which can be integrated to yield

$$p_2 = (u_1)_{x_1} t_1 \psi(y, z) + D(x_1, t_1)$$

in which D is an arbitrary function. The free surface pressure condition at this order is $p_2 = \eta_2$ so that the expression above immediately gives the transverse wave amplitude variation as

$$\eta_2 = (u_1)_{x_1} t_1 \psi(y, 0) + D \quad (18)$$

In other words, the variation of the free surface is like $\psi(y, 0)$ which is obtained as discussed above.

From the irrotationality condition, taking the y and z components to $O(\epsilon^2)$, Peregrine shows the next approximation for u to be

$$u_2 = -(u_1)_{x_1} x_1 \psi(y, z) + E(x_1, t_1) \quad (19)$$

in which E is arbitrary (obtained by an integration as in Equation 18).

Proceeding, the next order in the x-momentum equation (to ϵ^2) is found to be

$$(u_2)_{t_1} + u_1(u_1)_{x_1} + (p_2)_{x_1} = 0$$

Neglecting the cross-sectional variations in both u_2 and p_2 this becomes an equation relating D and E

$$E_{t_1} + u_1(u_1)_{x_1} + D_{x_1} = 0 \quad (20)$$

Now, assuming that over the small range from the still water surface to the instantaneous surface, the top width is given by

$$B(z) = B_0 + zB_1$$

and incorporating the transverse variation of Equation 18, the second order term in the expansion of flow area is

$$A_2 = B_1 \eta_1^2 / 2 + B_0 D + B_0 \psi_B (u_1)_{x_1} t_1 \quad (21)$$

Here, B_1 denotes the slope of the bank at $z = 0$, and ψ_B is the mean value of ψ on the surface given by

$$\psi_B = 1/B_0 \int_B \psi(y, 0) dy \quad (22)$$

Similarly, the second order term in the flux, Q, is shown to be

$$Q_2 = B_0 u_1 \eta_1 + A_0 E - A_0 \psi_A (u_1)_{x_1} x_1 \quad (23)$$

in which ψ_A is the mean value of ψ over the entire cross-section given by

$$\psi_A = 1/A_0 \iint_A \psi(y, z) dy dz \quad (24)$$

Peregrine now introduces another transformation of the dependent variables, introducing quantities which are correct to the second order, but neglecting the cross-sectional variations. That is, for the free surface, define

$$\zeta = \epsilon \eta_1 + \epsilon^2 D$$

while for the longitudinal flow define

$$u' = \epsilon u_1 + \epsilon^2 E$$

With these definitions, one now combines ϵ times Equation 12 with ϵ^2 times Equation 20, reverts to un-scaled x and t coordinates, and finds for the momentum equation

$$u_t' + u'u_x' + \zeta_x = 0 \quad (25)$$

The continuity equation is not as simple, being

$$(\zeta + k\zeta^2/2)_t + (c_0^2 u' + \zeta u')_x + (\psi_B - \psi_A)(u')_{xtt} = 0 \quad (26)$$

in which k is B_1/B_0 .

A solution of these equations which is extremely similar to the familiar solitary wave is

$$\zeta = a \operatorname{sech}^2 \frac{x - ct}{2} \left\{ \frac{a(1 - kc_0^2/3)}{c_0^2(\psi_B - \psi_A)} \right\}^{1/2} \quad (27)$$

in which the wave celerity is given by

$$c = c_0[1 + (1 - kc_0^2/3)a/2c_0^2] \quad (28)$$

Peregrine (1968) concludes at this point without presenting an explicit expression for the transverse amplitude variation. The missing steps are easy to supply, however. In Equation 18 we replace the time-derivative of velocity by the x -derivative of η using Equation 12. This second derivative of η is then evaluated using Equation 27. Since we are interested only in the crests, we then set the phase position to zero and find the transverse variation of amplitude, a , to be

$$a = a_0 + \frac{a_0^2 B_0 (1 - B_1 A_0 / 3B_0^2) \psi(y, 0)}{2A_0 (\psi_B - \psi_A)} \quad (29)$$

This result is given both by Fenton (1973) and in a second paper by Peregrine (1969), the latter without derivation. In this expression, a_0 is the wave amplitude at the minimum of $\psi(y, 0)$ which we shall later construe to be at the center of a simple, symmetric cross-section (in fact, at $y = 0$).

We should note before concluding this section that two limitations are inherent in the theoretical development (beyond the requirement of small σ and ϵ). First, it was tacitly assumed that the bank slope is not too small. This arises in Equation 21: if B_1 is large owing to an extremely gentle slope, its contribution is no longer second order, violating the assumption.

The second limitation is that the channel should not be too wide compared with the depth. Peregrine (1969) shows that contrary to expectation, increasing the channel width eventually causes such a large transverse amplitude variation that the assumption of small amplitude must be violated.

This completes the theoretical development of the topic to the extent needed for this preliminary Phase I effort. We shall

suggest that in Phase II we pursue this theory along three major lines:

- *) Investigation of particle velocities in the bank area for the determination of forces on bank structures .
- *) Investigation of both velocities and accelerations at the crest in the bank area in order to define wave-breaking criteria (both kinematic and dynamic)
- *) Generalization to remove or mitigate the errors associated with increasing channel width and decreasing bank slope

This copy made at U.S. Government expense.

3.1.2 Analytical Solutions

Analytical solutions of the foregoing equations have been obtained only in a small number of simple geometries. For example, in a rectangular channel (physically equivalent to the unbounded constant depth case) we have

$$\begin{aligned}\psi(y, z) &= \psi(z) \\ \psi_z &= c_0^2 = 1 \quad \text{at } z = 0 \\ \psi_z &= 0 \quad \text{at } z = -1\end{aligned}$$

with which (guessing a polynomial solution) we immediately find

$$\psi = z + z^2/2$$

Isolevels of ψ are horizontal and consequently all cross-sectional flow is vertical (perpendicular to the isolevels). Equation 29 shows that the surface is level since ψ is not a function of y (and we have tacitly taken the arbitrary constant in the solution for ψ to be such that ψ is zero on the free surface). This is, of course, a trivial case.

Somewhat more interesting is the result found by Peters (1966) for a semi-circular cross-section. The expression for ψ is moderately complex, and gives the following approximation for bank amplification of wave amplitude

$$a_b/a_0 \approx 1 + a_0/6r$$

In this expression, a_b is the amplitude at the shore and r is the circular channel radius. It is noted that the amplification is quite small. Even for near limit wave amplitude, the ratio is only about 1.1, or a 10% increase near the banks. Physically, this seems to be due to the fact that the banks are vertical at the still water level, and nearly vertical over a substantial depth.

A third analytical solution of more practical interest can be found for channels of triangular cross-section. Guessing a polynomial expression and noting that c_0^2 is $1/2$ for a triangle, it is easy to find

$$\psi = z/2 + (y^2 + z^2)/4$$

Again, the arbitrary constant is chosen so that ψ is zero at the origin. We have $A_0 = B_0/2$ in this case and $B_1 = B_0$. The sloping bank is defined by

$$y = (1 + z)B_0$$

which becomes the upper limit on the inner integral for ψ_A (Equation 24). We find, after some algebra

$$\psi_B = B_0^2 / 12$$

$$\psi_A = (B_0^2 - 3)/24$$

so that Equation 29 reduces to

$$a = a_0 + a_0^2 \left\{ 5y^2 / (3 + B_0^2) \right\}$$

Of greatest interest is the amplitude at the bank ($y = B_0$) which, when normalized by the central amplitude, is the amplification factor given by

$$R = a_b/a_0 = 1 + a_0 \left\{ 5B_0^2 / (3 + B_0^2) \right\}$$

Note that B_0 is just $\tan(\alpha)$ where α is the angle between the bank and the vertical. We shall denote the angle between the bank and the horizontal by θ .

The following Table shows the variation of R with both side slope and center-channel amplitude for triangular channels.

θ , degrees	R			
	$a_0 = 0.1$	0.2	0.4	0.6
15	1.41	1.82	2.64	3.47
22.5	1.33	1.66	2.32	2.98
30	1.25	1.50	2.00	2.50
45	1.12	1.25	1.50	1.75
60	1.05	1.10	1.20	1.30

It is seen that the amplification of wave height on the banks is sensitive to both bank slope and center-channel wave amplitude. The amplification rises sharply with increasing amplitude.

It is of interest that Peregrine (1968) notes the triangular solution in a particularly elegant form, although he does not go on to provide the development for amplitude variation given here. In his expression for ψ , he takes the origin at the channel vertex for which

$$\psi(y,z) = (y^2 + z^2) / 4$$

This shows clearly that the isolines of ψ are segments of circles. Since in a triangle the banks are simply radii of these circles, the solid wall boundary condition is satisfied by inspection. Surprisingly, all cross-sectional motion must be radial from the channel invert. This also helps to make clear why all triangular sections have the same form for ψ .

No other analytical solutions have been found.

3.1.3 Numerical Solutions

We have implemented a numerical model based on the foregoing theoretical development for the case of trapezoidal channels. The model at this time is limited to determination of the wave crest profile across the channel to investigate bank amplification effects, as described above for the known analytical solutions.

It is first necessary to solve numerically for ψ throughout the domain, satisfying the Poisson equation and boundary conditions of Equations 16. Then we apply Equation 29 to determine the surface transverse profile.

We have adopted a simple Simultaneous Over-Relaxation scheme, based in part on the methods described in Press, et al (1986). Since we are restricting attention to trapezoids in this Phase I numerical effort, we need model only half the channel, from the center to either bank. Then, by symmetry, the appropriate boundary condition on $y = 0$ is the same as for a solid wall running down the center of the channel:

$$\psi_y = 0 \quad \text{at } y = 0 \quad (30)$$

Letting j and k denote indices in the y - and z -directions, respectively, the Gauss-Seidel difference expression for an interior point is simply

$$\psi_{j,k}^* = 1/4 \left\{ \psi_{j+1,k}^n + \psi_{j-1,k}^{n+1} + \psi_{j,k+1}^n + \psi_{j,k-1}^{n+1} - \Delta x^2 \right\} \quad (31)$$

in which we assume a square mesh. Letting the over-relaxation weighting factor be ω , the updated quantity is

$$\psi_{j,k}^{n+1} = \omega \psi_{j,k}^* + (1 - \omega) \psi_{j,k}^n \quad (32)$$

It is not clear what the optimum choice of ω might be for our geometry. But in view of the speed and economy of desktop PC's, expenditure of effort to determine an optimum value is not worthwhile. Instead, we have simply adopted values appropriate for the bounding rectangular domain, assuming these to be a reasonable guess for our somewhat truncated region.

Therefore, we take

$$\omega = 2 / [1 + \sqrt{(1 - \rho_J^2)}] \quad (33)$$

in which ρ_J is the Jacobian spectral radius given by

$$\rho_J = 1/2 [\cos(\pi/J) + \cos(\pi/K)] \quad (34)$$

with J and K being the (integer) dimensions of the grid. Again, this expression assumes a square mesh.

The domain is sketched in Figure 10a. On the left boundary, we set ψ equal to the old values one column to the right. On the bottom boundary, similarly, we set ψ equal to the values just above. For most of the top boundary, we set ψ equal to the values just below plus a constant equal to the space step times c_0' .

On the right (sloping) boundary, we construct a perpendicular from the boundary cutting either a vertical or horizontal side of an adjacent cell (depending upon bank slope). The value assigned to the boundary point is the value interpolated from the endpoints of the intercepted side.

Difficulty comes for the free-surface condition in the vicinity of the bank for gentle bank slopes (small θ). In this case, there may be several surface points for which there does not exist a valid adjacent point on the second row (points on the second row lying below the slope, outside the domain) on which to construct the surface gradient. This case is sketched in Figure 10b.

After some experimentation, we have adopted the following artifice which has appeared to work adequately. From the surface point of interest, point A for example, drop vertically to the bank (point B). Then from this point, construct a perpendicular to the bank intersecting the free surface at point C. By the zero gradient condition on the bank, approximate ψ at B by the interpolated value of ψ at C using the most recent values on the first row. Then, by the surface gradient condition, add the quantity $c_0^2 \delta z$ in which δz is the distance between points A and B.

Finally, at the conclusion of each iteration, the value of $\psi(0,0)$ is subtracted from every grid point, thereby fixing the arbitrary constant in ψ appropriately. A convergence test is made on the trace of the matrix, with termination upon achieving a relative change of less than 10^{-6} (with a minimum of 100 iterations, however).

With these conditions, we have successfully simulated a range of trapezoid geometries and wave heights. The source code for the model is included as Appendix A of this report (written in Pascal suitable for PC applications). Results obtained with the model will be shown in Section 4.

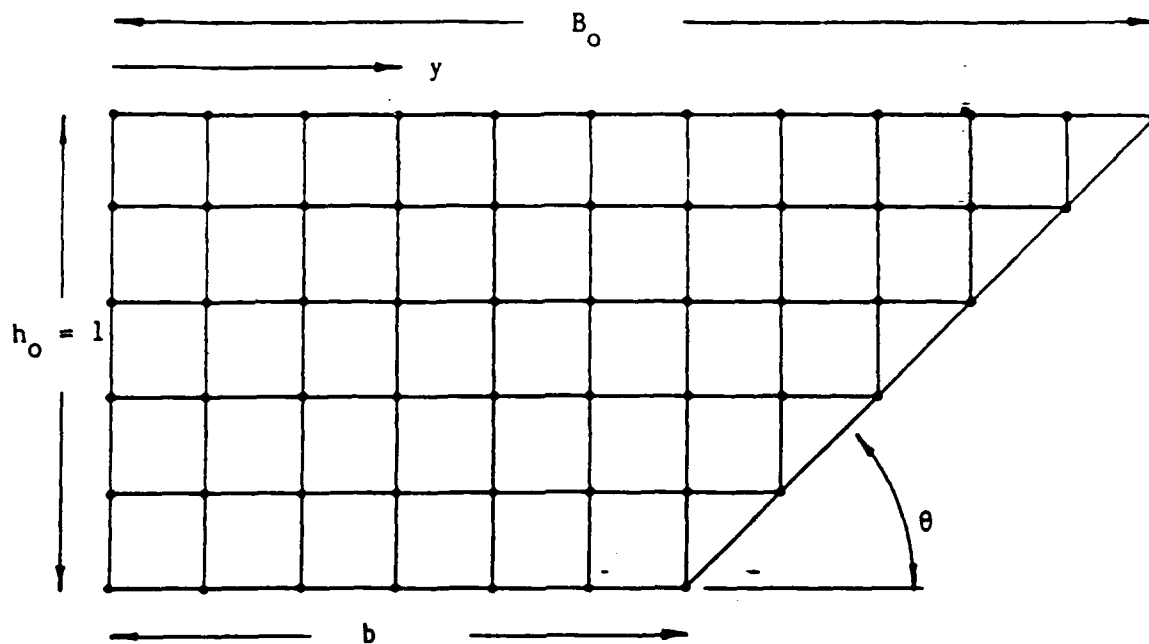


Figure 10a: Numerical Mesh

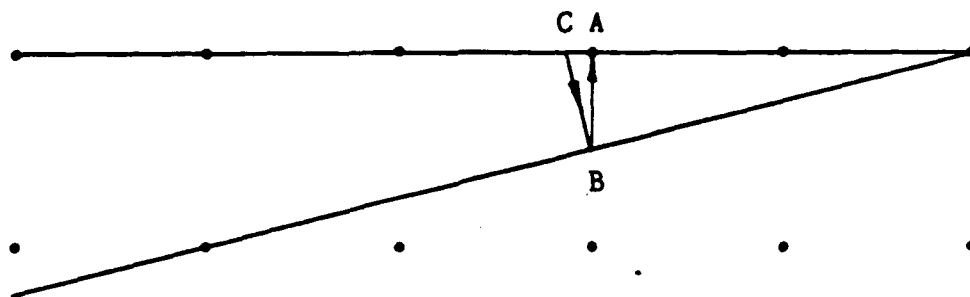


Figure 10b: Sketch Illustrating Approximate Surface Boundary Condition (see text).

3.2 Damping

3.2.1 Frictional Damping

Frictional damping is not usually much of a consideration for explosion wave propagation. In open water, radial spreading causes a rapid drop in height; this loss is compounded by frequency dispersion if the depth is not too small. Breaking may also be encountered. However, in the case of the surf-zone effect (the so-called 'Van Dorn effect'), LeMehaute (1985) has shown that friction may play an important role owing to the long distances of propagation over a gentle slope and the reduction of radial spreading by refraction. Whether shoaling is adequate to maintain a destructive breaker or whether friction may be just large enough to keep the waves sub-breaking, could be a critical question.

For waves in channels it is possible that friction may be of moderate importance since radial spreading is eliminated, depths may be small, and breaking is restricted to limited zones at the banks. Of course, depending upon the geometry, other decay mechanisms such as channel branching and irregularity are likely to be much more important than friction in causing the eventual demise of a wave. Overall, friction is probably a secondary consideration, although still of interest.

The long waves of interest here may be approximately cnoidal in form, or, in the limit, solitary. This indicates that the rate of loss under crests will be much greater than under troughs owing to the concentration of velocity near the crests and to the fact that the dependence on velocity is quadratic.

Consequently, it is of interest to assess the magnitude of frictional damping from the standpoint of cnoidal or solitary waves rather than sinusoidal waves. In this Phase I effort we have gone part of the way toward that goal, while avoiding unnecessary complexity, by starting from the 'hyperbolic wave theory' of Iwagaki (1967).

Hyperbolic waves are simply a practical approximation to cnoidal waves of sufficient length. Cnoidal wave theory is expressed in terms of the elliptic integrals $E(k)$ and $K(k)$, and the Jacobian elliptic function $cn(\theta; k)$. For waves with sufficient amplitude and length, the parameter k is very nearly unity and $E(k)$ is negligibly greater than unity. $K(k)$, however, remains finite, becoming large (the solitary wave limit) only for k extremely near unity; departures as small as 10^{-40} are not insignificant.

Iwagaki (1967) noted that a useful approximation would result if we simply set k and $E(k)$ to unity, and determine $K(k)$ as a function of water depth, wave height, and wave period. The Jacobian elliptic functions reduce to their hyperbolic-function limits (hence, the name 'hyperbolic waves'), greatly simplifying engineering computations at little sacrifice of accuracy. In

particular, the function $\text{cn}(\theta; k)$ becomes $\text{sech}(\theta)$ and $\text{sech}(\theta)$ is not periodic. This poses no real problem. We simply imagine a succession of waves patched together where the troughs should be. At these patches, the wave description is not at all accurate (the direction of flow is wrong, for example) but since effects are concentrated at the crests we proceed on the hope that the net error will be small. In this Phase I effort we further simplify matters (greatly) by truncating all expressions for hyperbolic wave features (particle velocities, energy density, and so forth) at the leading, dominant terms, neglecting in particular powers of H/h .

Given these assumptions, we proceed as follows. Let E denote the wave energy density per unit area averaged over the length of the wave. Assume that the rate of energy dissipation per unit area is given by

$$E_t = \dot{E} = k_f \rho u_b^3 \quad (35)$$

Averaging this over the wavelength we write the energy conservation equation as

$$(\bar{E} V_g)_x + \bar{\dot{E}} = 0 \quad (36)$$

in which V_g is the group velocity and u_b is the fluid velocity at the bed; k_f is a friction coefficient equal to $f/8$ in which f is the Darcy-Weisbach friction coefficient.

From hyperbolic theory we use the approximation

$$u_b = \sqrt{(gh)} H/h \text{sech}^2(2Kx/L)$$

in which K is approximated by

$$K = T\sqrt{(3gH)}/4h \quad (37)$$

The reader will note that this is essentially the solitary wave approximation, again neglecting H/h . The advantage is just that we retain L explicitly for purposes of defining wavelength averages (the average energy density over a solitary wave being zero).

Substituting into

$$\bar{\dot{E}} = 1/L \int_L \dot{E} dx$$

we find

$$\bar{\dot{E}} = k_f \rho H^3 (g/h)^{3/2} \tanh K (8/3 + 4/3 \text{sech}^2 K + \text{sech}^4 K)/5K$$

On the other hand, the total energy density is

$$E = 2/3 \rho g H^2 [1 - 3/(2K)]/K$$

THIS COPY MADE BY U.S. GOVERNMENT

from which we can evaluate \bar{E}_x as

$$\bar{E}_x = \rho g H_x / A^2 (A\sqrt{H} - 1)$$

in which A is the constant $T\sqrt{(3g)}/4h$.

Substituting these expressions for \bar{E}_x and \bar{E}_t into the energy conservation equation gives an expression for H_x which can be integrated analytically to give an expression relating H_1 , H_2 , and X (the subscripts denoting wave height at the beginning and end of an interval X). This expression is a cubic in $\sqrt{H_2}$ which can be solved in the form

$$\theta_2^3 + p\theta_2 + q = 0$$

$$\theta_2 = \sqrt{H_2}$$

$$p = -K_2\theta_1^3 / (x\theta_1^3 + K_2\theta_1 - K_1)$$

$$\theta_1 = \sqrt{H_1}$$

$$K_1 = 20h^3 / [k_f T\sqrt{(3g)}]$$

$$K_2 = 15 h^2 / 2k_f$$

$$q = K_1\theta_1^3 / (x\theta_1^3 + K_2\theta_1 - K_1)$$

Graphs showing attenuation computed in this manner are shown in Figures 11 - 13 for initial wave amplitudes (dimensionless) of 0.2, 0.4, and 0.6, respectively. In each case, H_2 is shown versus reduced propagation distance (X/L) with relative wave length as a parameter. The Darcy-Weisbach coefficient was taken as 0.02 giving a value for k_f of 0.0025. This corresponds to a Manning coefficient of about 0.028 in a water depth of 100 feet.

Despite the appearance of these curves, it will be seen that in practice we will generally encounter dimensionless propagation distances on the order of 10 to 20 so that typical height reductions will be on the order of only 10%.

3.2.2 Breaking Dissipation

We have found no information directly pertinent to defining the breaking zone on the banks and the associated energy losses. This remains an important item for future research including several lines of approach. For example, the three-dimensional solitary wave theory should be pursued for particle velocities and accelerations in order to define a breaking criterion analogous to the familiar $H/h = 0.78$. This condition is obtained from the McCowan solitary wave theory under the kinematic assumption that particle velocity at the crest equals wave celerity.

Phenomenological models of wave breaking should also be inves-

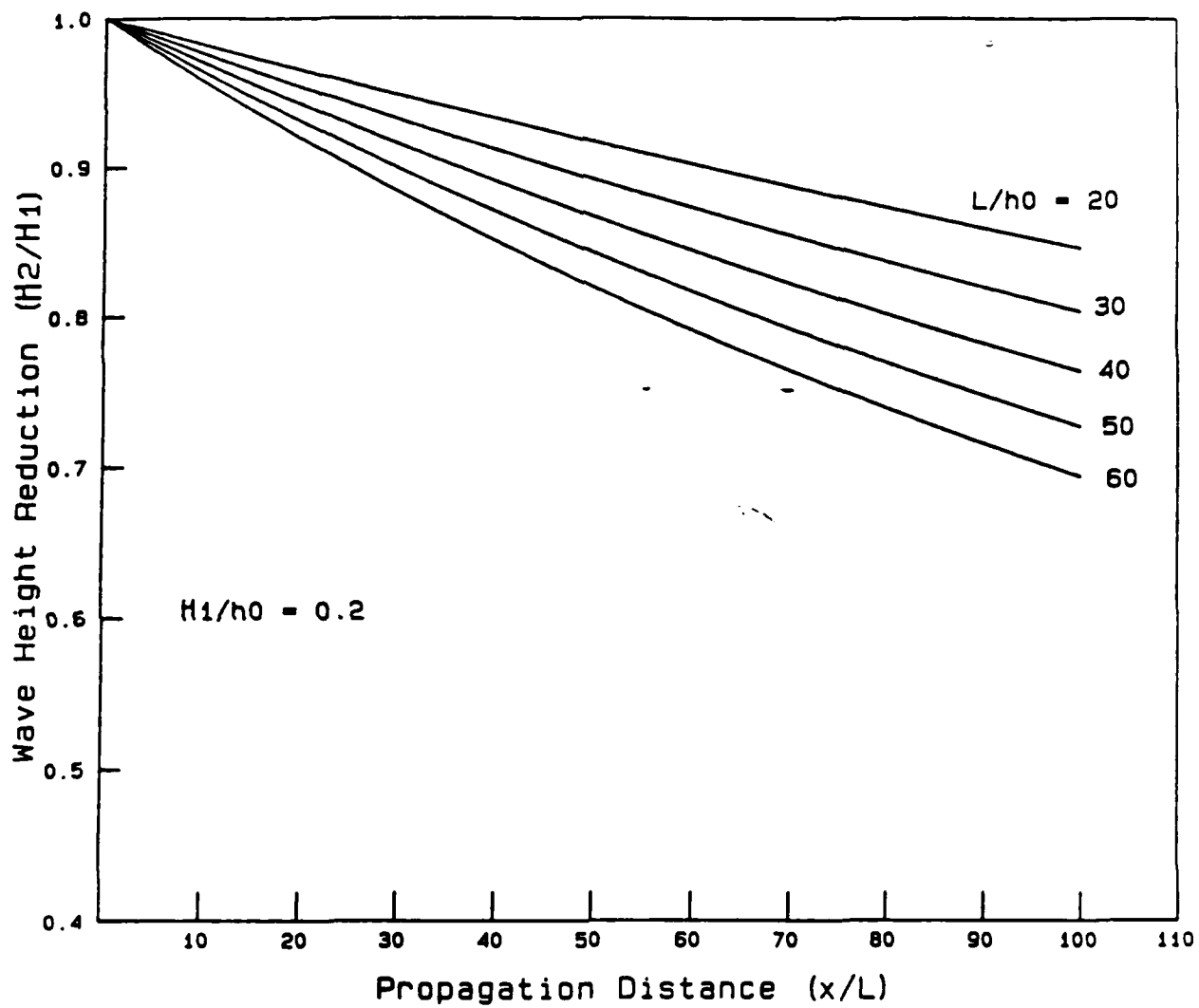


Figure 11: Frictional Height Reduction for Initial Height of 0.2.

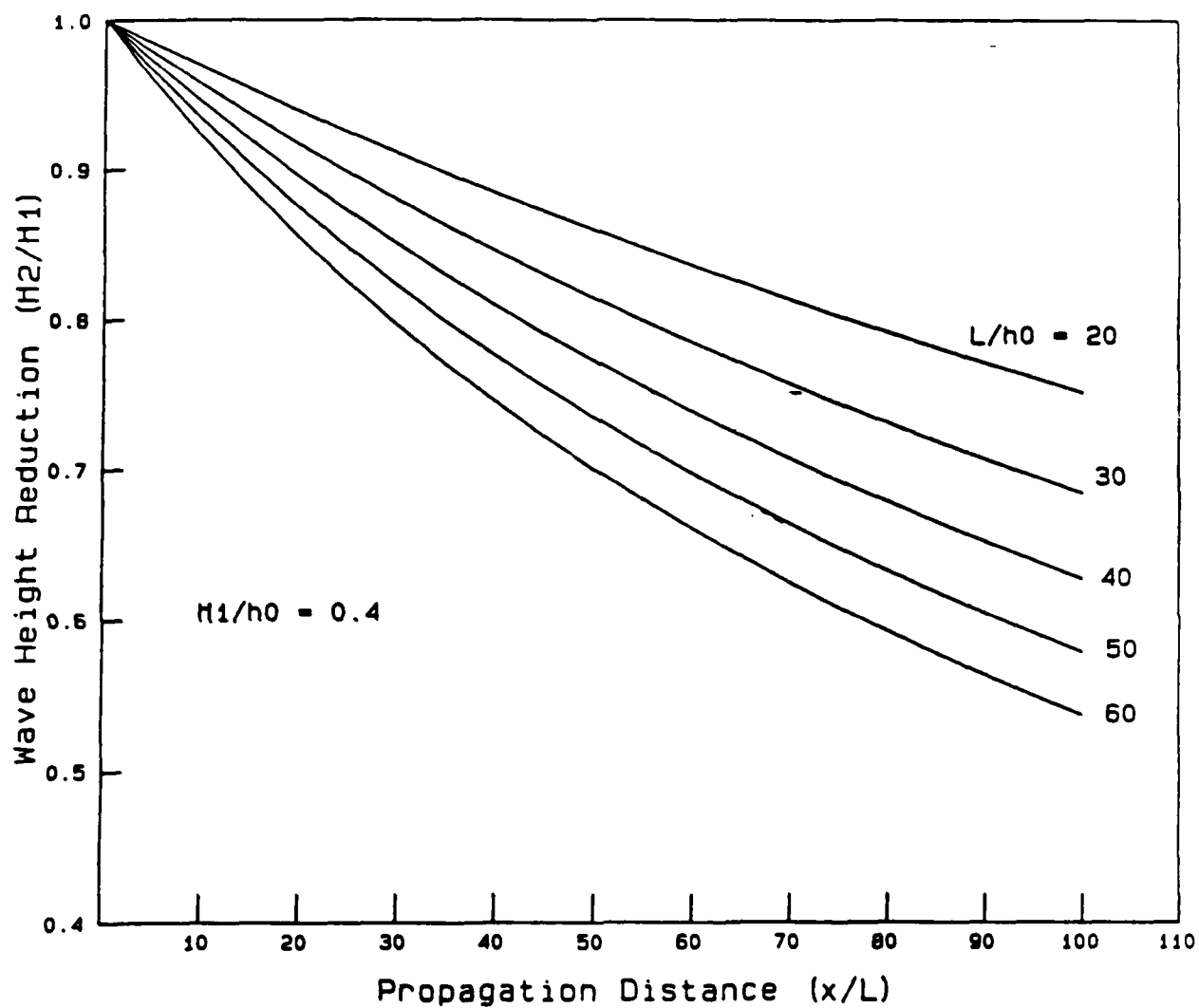


Figure 12: Frictional Height Reduction for Initial Height of 0.4.

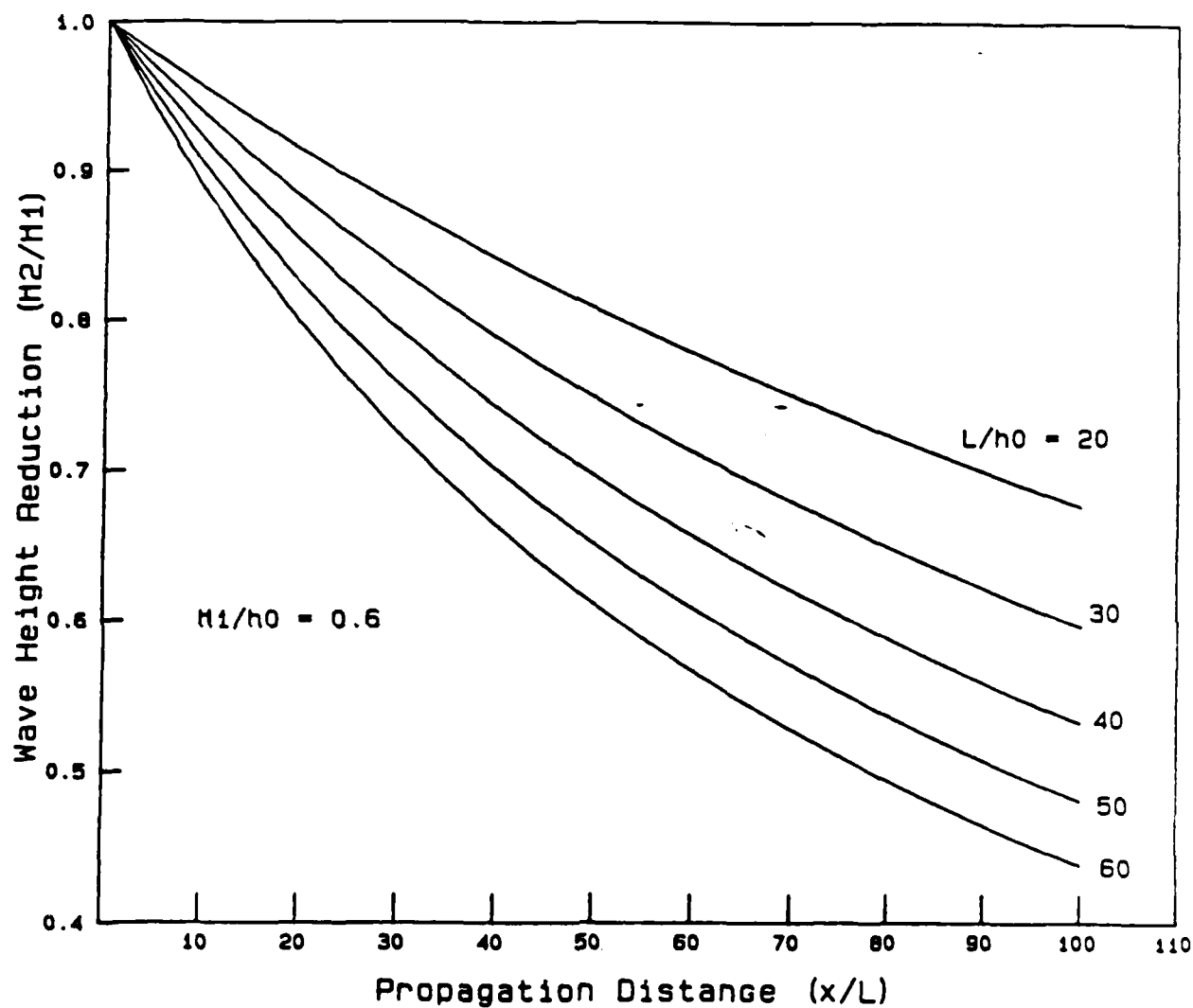


Figure 13: Frictional Height Reduction for Initial Height of 0.6.

tigated. The non-saturated breaker theory of LeMehaute (1962) is an example of such a theory which attempts to relate breaking energy dissipation to simpler, underlying concepts such as rate of energy loss in an analogous hydraulic jump.

It is important, however, that at least a limited experimental series be undertaken to give empirical guidance in this area. Without this, any theoretical kinematic or dynamic breaking criterion must be considered speculative.

3.3 Channel Branching Effects

The final topic of general interest is the height loss associated with splitting of the channel into branches. This can be an extremely complex problem -- every site being unique -- if the channel junction is not smaller than the length of the wave. For short waves, the methods of coastal engineering must be invoked, following the waves by ray-tracing or some other method accounting for refraction, diffraction, reflection, and so forth. No simple general rules would suffice.

But in the event that the waves are reasonably long with respect to the size of the junction, it is possible to make a very great simplification in the analysis. In this approximation -- the compact junction assumption -- we introduce the notions of channel admittance and impedance (here following Lighthill, 1978).

If the junction is compact, then it is reasonable to assume that each branch is subject to much the same surface elevation, or pressure excess. The admittance of a channel is defined as the ratio of volume flow to pressure excess and is named by analogy with the electrical admittance function which is the ratio of current to voltage difference. In the case of a channel of arbitrary cross-section, Lighthill shows that the admittance, Y , is given by

$$Y = A / (\rho c)$$

in which A is the channel cross-sectional area, ρ is density, and c is wave celerity. The impedance, Z , is defined as the reciprocal of the admittance.

Now consider a multiple junction -- assuming continuity of pressure and volume flux -- with an incident wave, f , in one branch. Lighthill shows that the ratio of the transmitted wave height, h (which is the same in all secondary branches), to the incident height is

$$h/f = 2Y_1 / (Y_1 + \sum Y_i)$$

in which the summations are taken over the secondary channels. Similarly, the reflected wave amplitude ratio, g/f , is given by

$$g/f = (Y_1 - \Sigma Y_i) / (Y_1 + \Sigma Y_i)$$

In these expressions we assume that we are dealing with a single wave and we ignore the possibility that with multiple waves the waves reflected from one branch would arrive as incident waves at another branch so that superposition would have to be considered.

Lighthill treats the case of periodic waves through multiple branches by a straight-forward extension of the above ideas. In our case, however, we will be content to consider each wave as a separate entity.

Despite the approximate nature of this treatment, it is felt adequate for our purposes. Its primary limitation is the assumption that junctions are compact. But even in the case that this is not strictly true, the above expressions still give a useful first order estimate which can only be improved with considerable effort.

4. PREDICTIONS AND COMPARISONS WITH OBSERVATIONS

4.1. Parametric Presentation of Numerical Results

We have exercised the numerical model described in the previous chapter for a range of trapezoidal channel sizes and shapes, and for a range of center wave amplitudes.

The basic results are shown in the following five four-part figures, Figures 14-18, showing results for bank slopes of 15, 22.5, 30, 45, and 60 degrees, respectively. In each figure we show four curves, corresponding to relative wave amplitudes at the centers of the channels of 0.1, 0.2, 0.4, and 0.6. The four parts of each figure, designated a-d, present data for bottom half-widths of 1.0, 1.5, 2.0, and 5.0, respectively.

These figures clearly show the expected trends. Amplification increases with increasing channel width, with increasing central wave height, and with decreasing bank slope. Amplifications of 2 to 3 appear typical.

In order to demonstrate the dependence on bottom width, holding other factors constant, we present Figure 19. This figure shows the amplification at the shoreline only, as a function of bottom width, holding bank slope constant at 15 degrees. The result is clearly that within the range of widths considered here, amplification is not sensitive to width.

This finding is very comforting in view of the limitation of the theory to channels which are not too wide. The indication is that for widths as great as five, or so, spurious amplification associated with excessive width is not a problem.

In Figure 20, we fix the bottom width at 1.5 and show amplification at the banks versus bank slope. Here we see a strong dependence on slope, as expected. We also see a deficiency of the free-surface boundary condition treatment in the case of a very gentle slope. As already discussed, in our simple square mesh scheme, several surface points are estimated using an approximate technique when the slope is 15 degrees. While that technique gives a reasonable estimate and does not destroy convergence, it does appear to underestimate the bank amplification by about 10% in this case.

In order to see this, we have plotted the values corresponding to the analytical solution for a 15 degree triangle; these points give the dashed extensions of the curves to 15 degree slope. Noting from Figure 19 that bottom width is not a sensitive parameter, it is reasonable to think that this analytical solution will be close to the desired trapezoidal value for this width.

Indeed, Figure 20 shows that the points corresponding to the triangle solution do appear to fall at about the expected values.

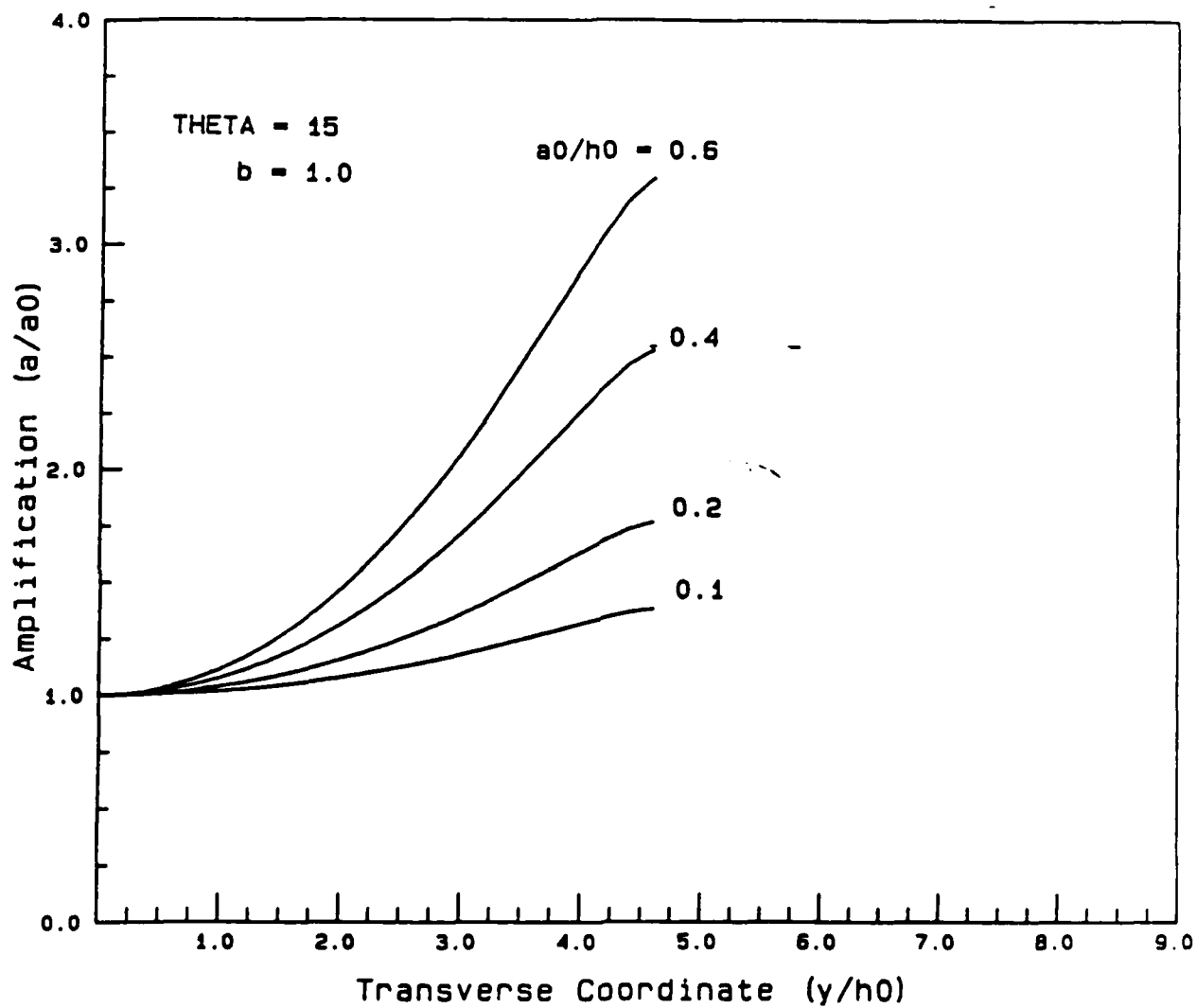


Figure 14a: Amplitude Variation for Indicated Condition.

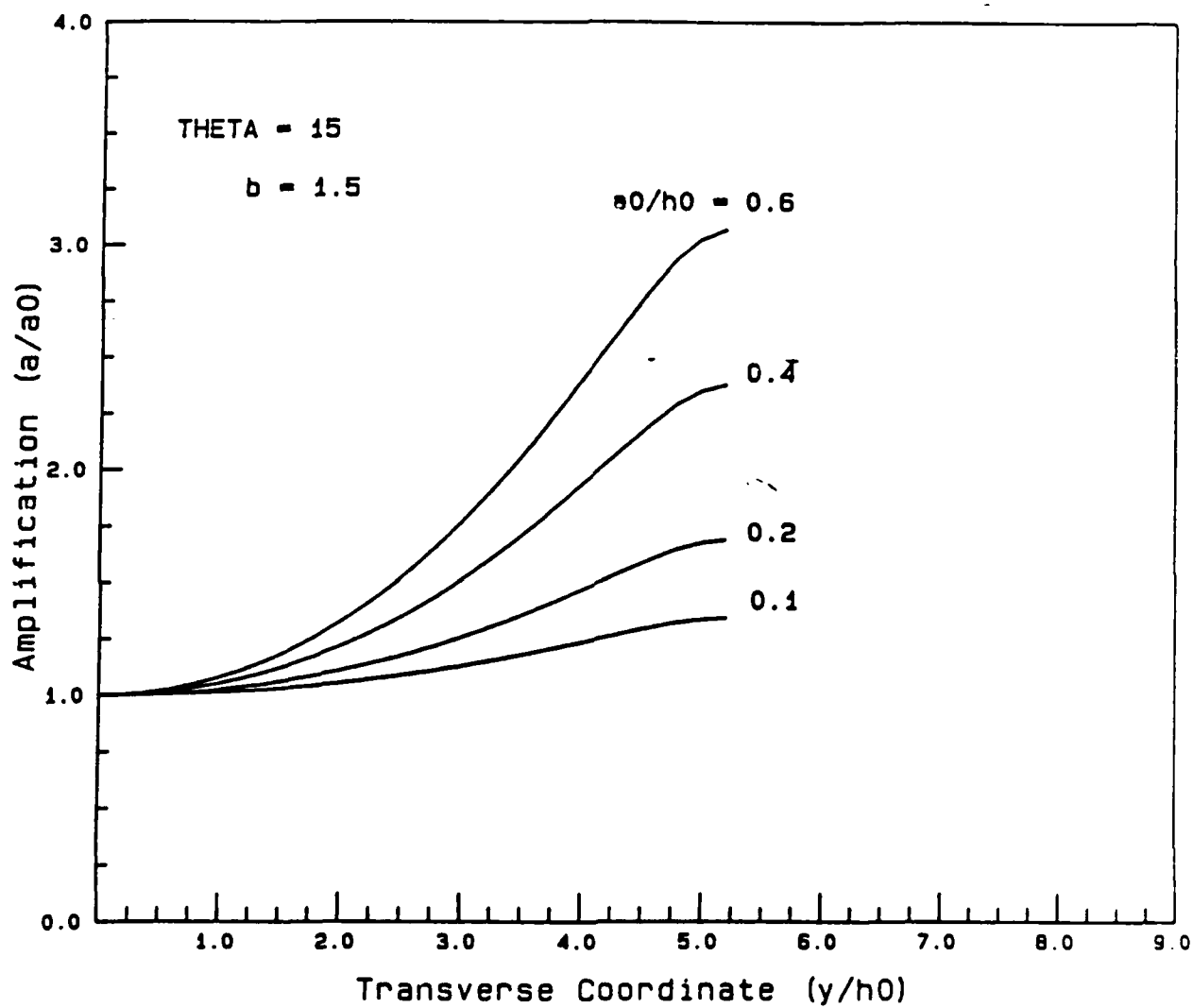


Figure 14b: Amplitude Variation for Indicated Condition.

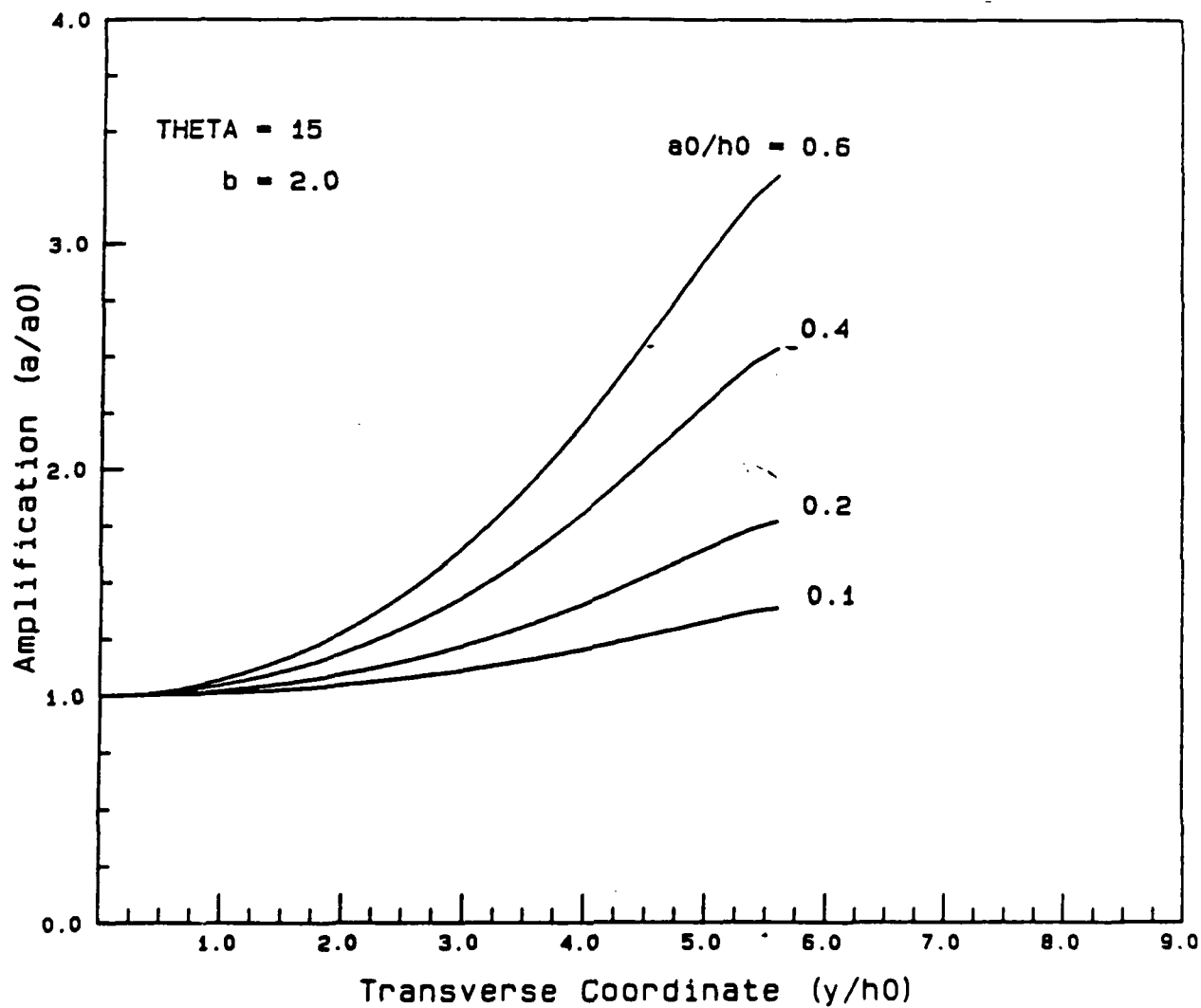


Figure 14c: Amplitude Variation for Indicated Condition.

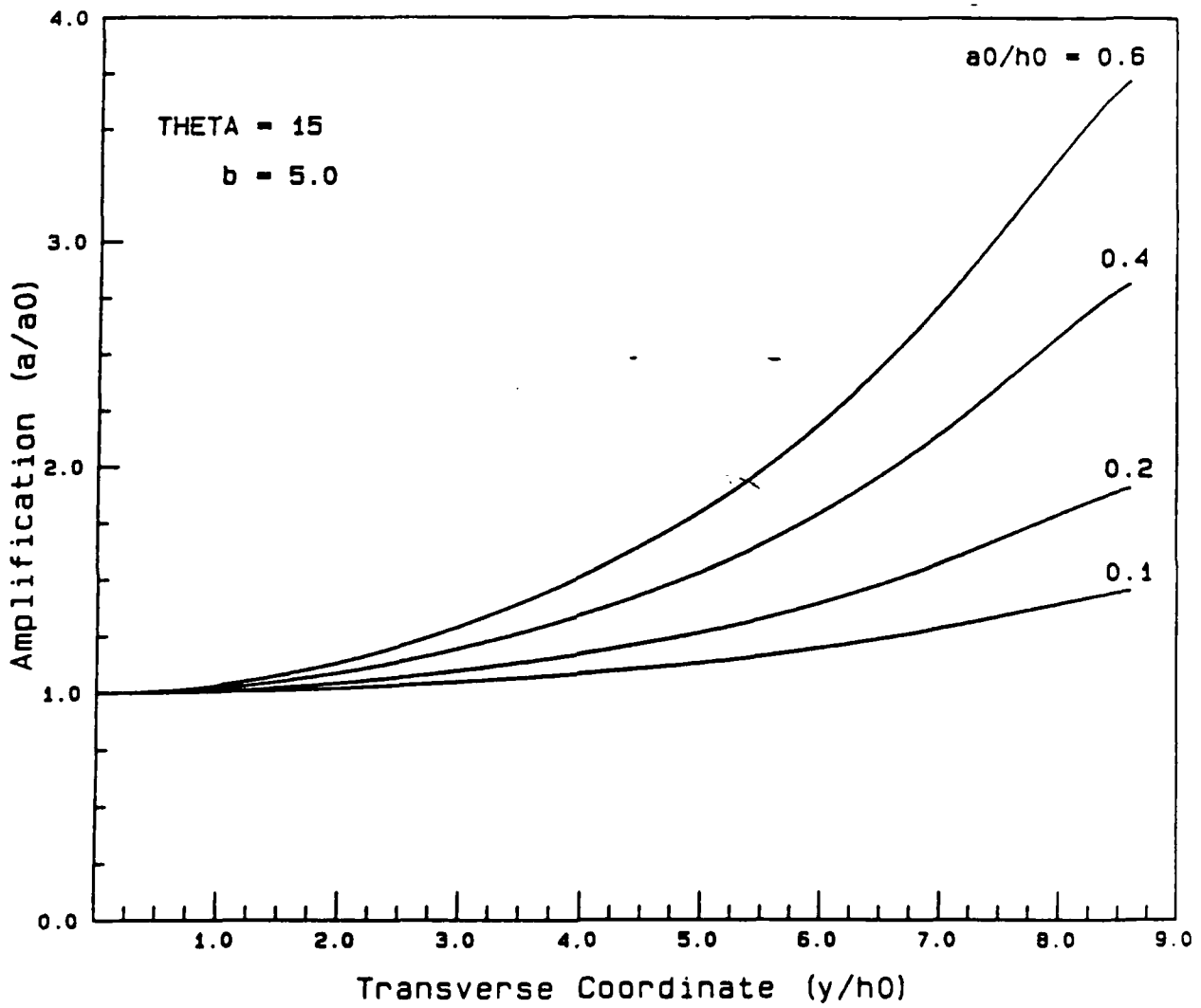


Figure 14d: Amplitude Variation for Indicated Condition.

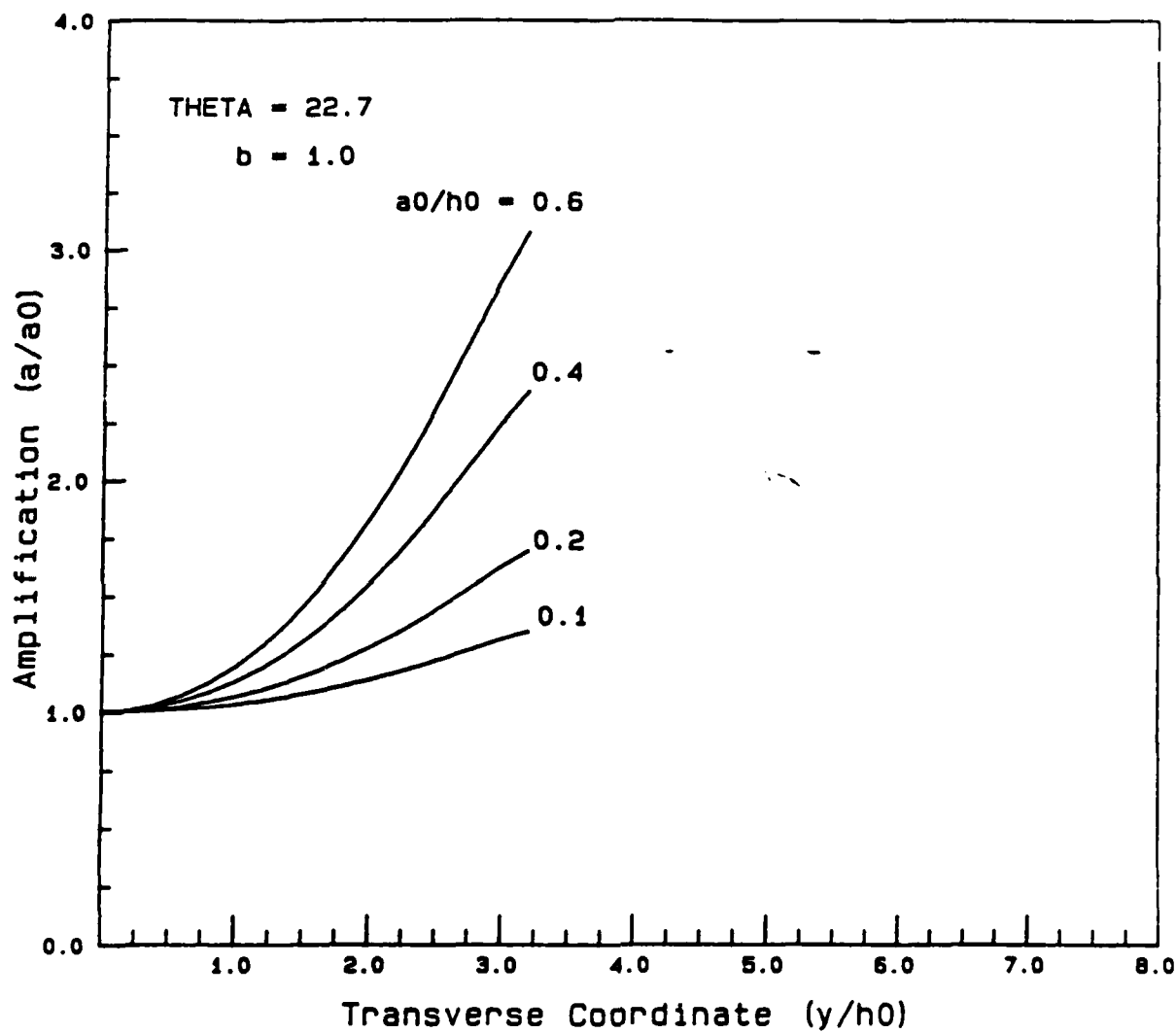


Figure 15a: Amplitude Variation for Indicated Condition.

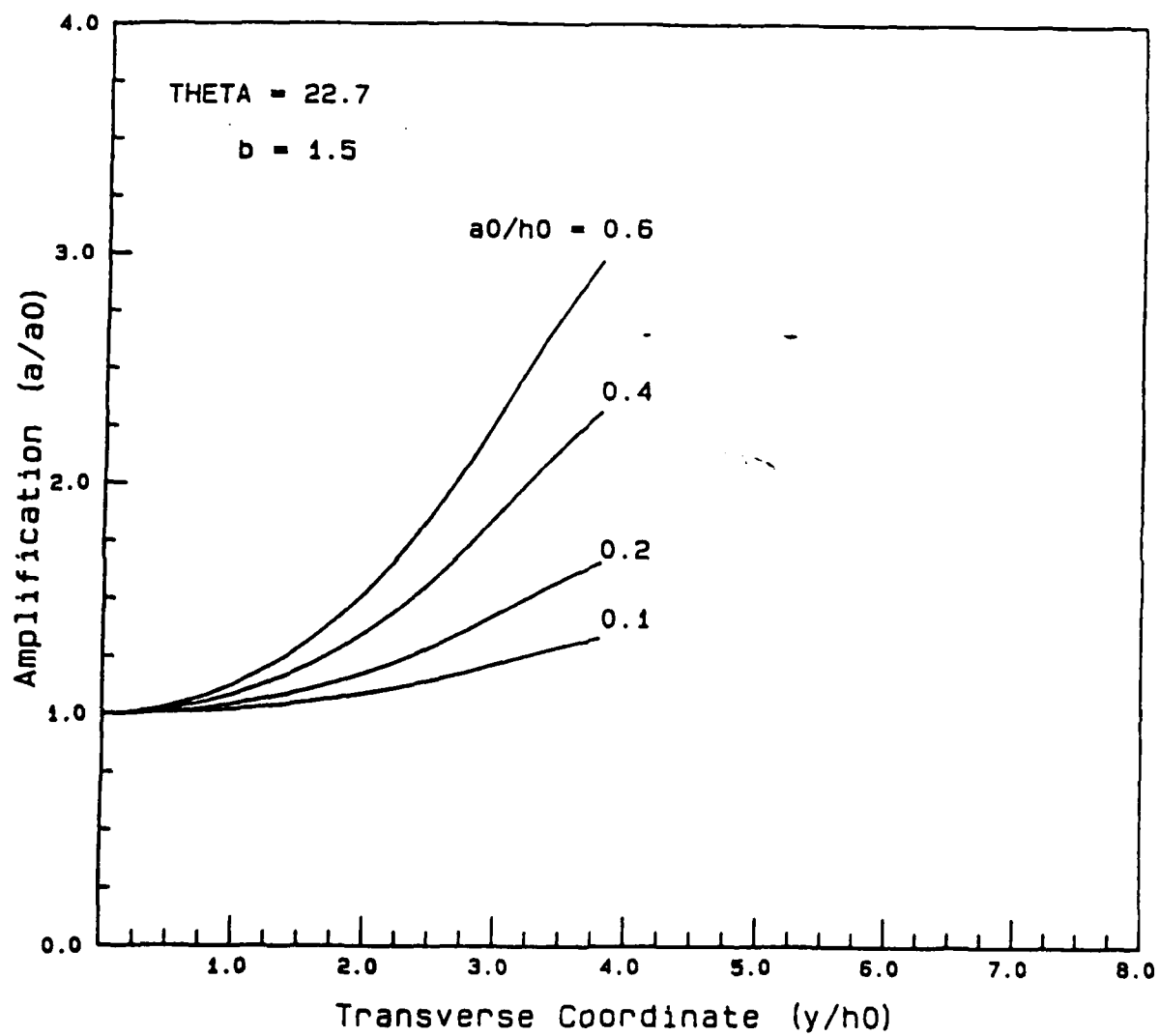


Figure 15b: Amplitude Variation for Indicated Condition.

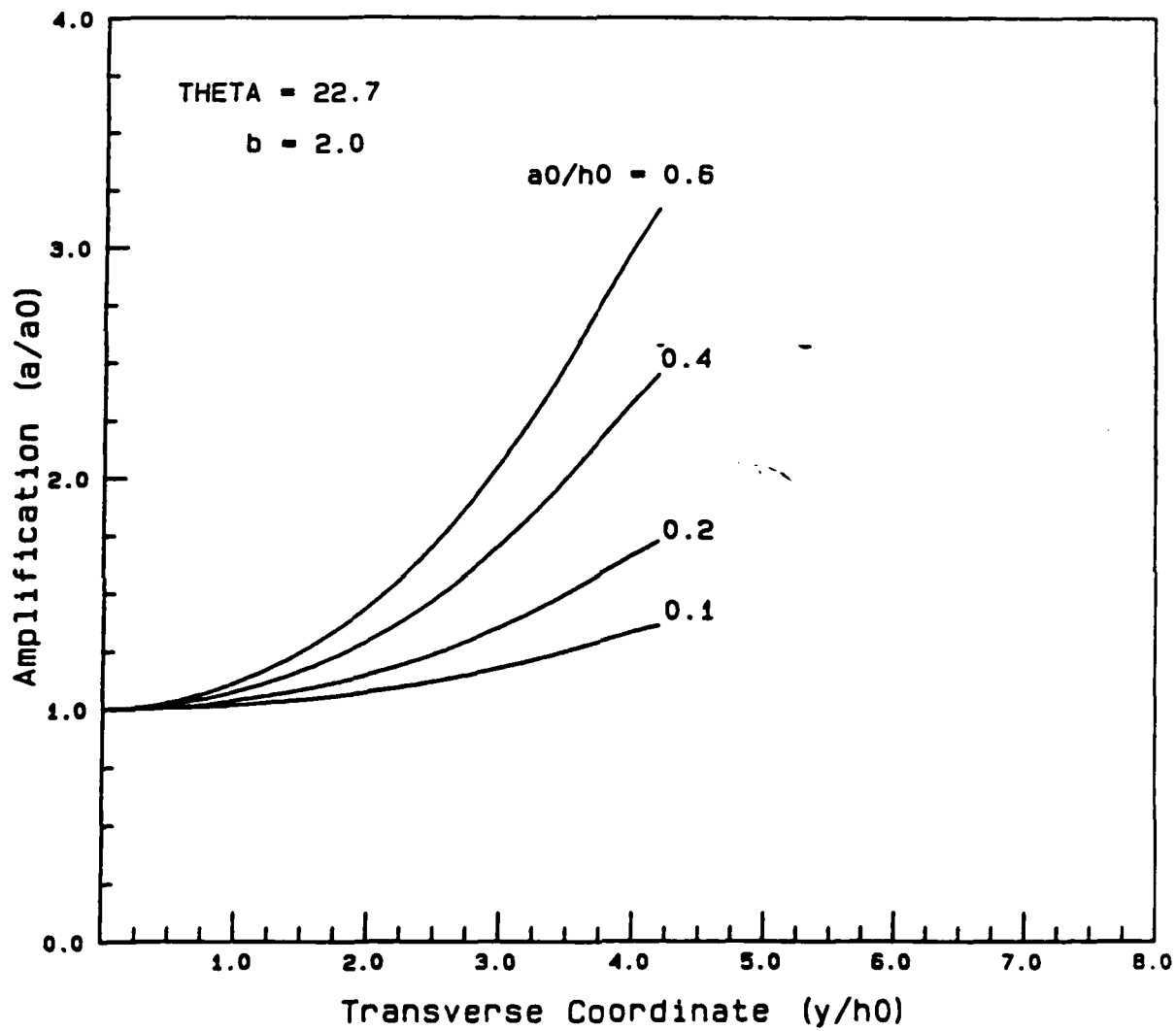


Figure 15c: Amplitude Variation for Indicated Condition.

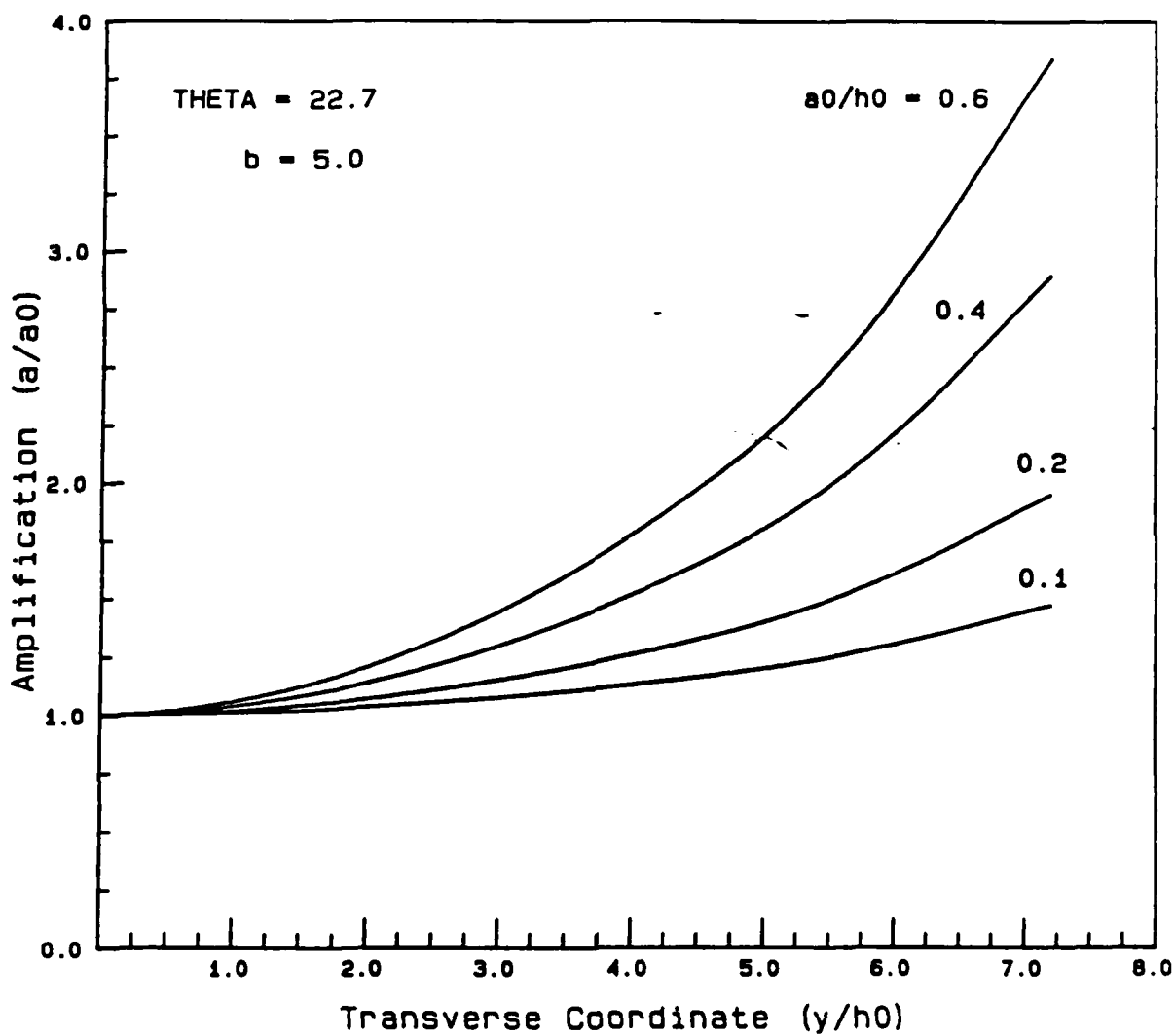


Figure 15d: Amplitude Variation for Indicated Condition.

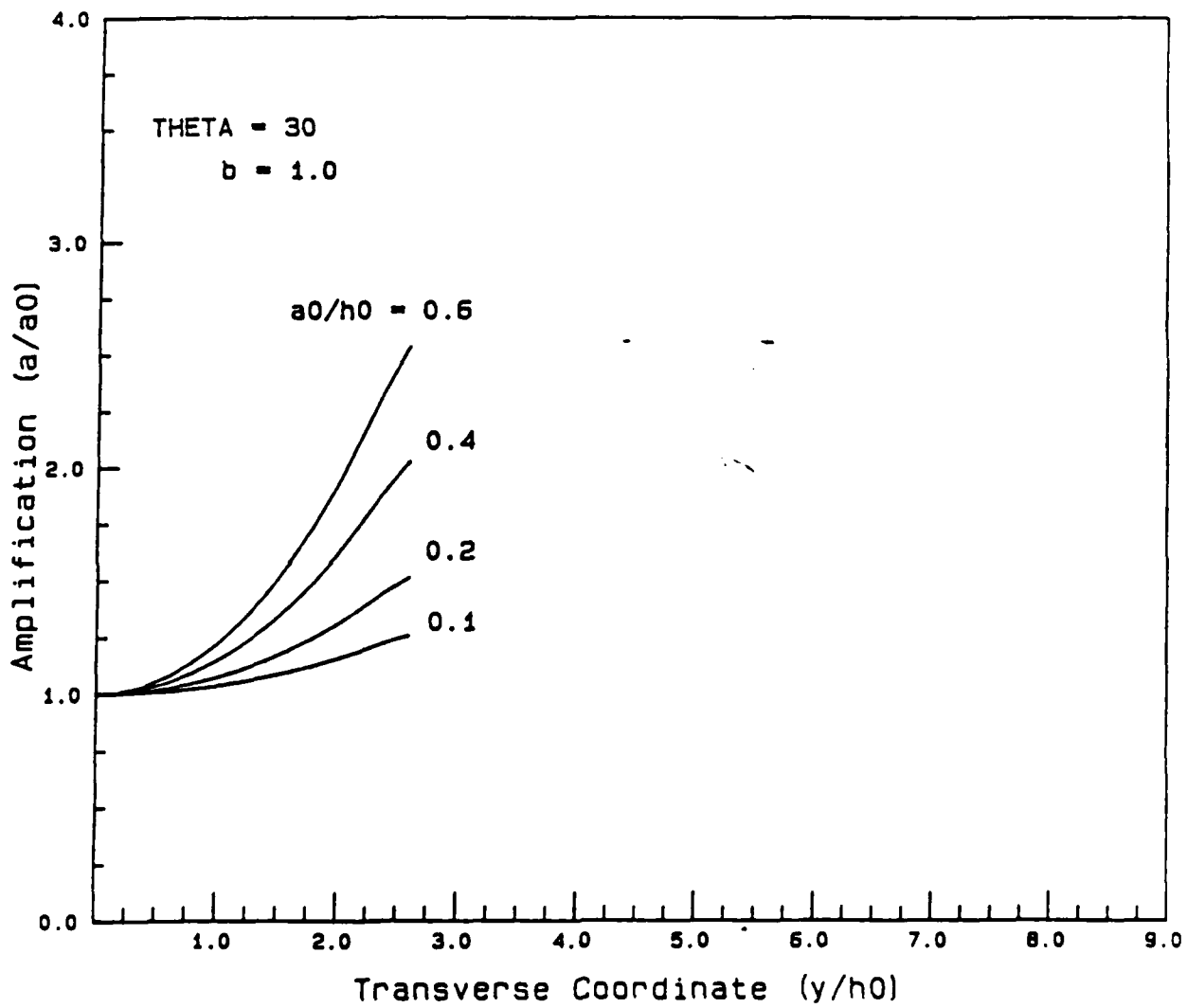


Figure 16a: Amplitude Variation for Indicated Condition.

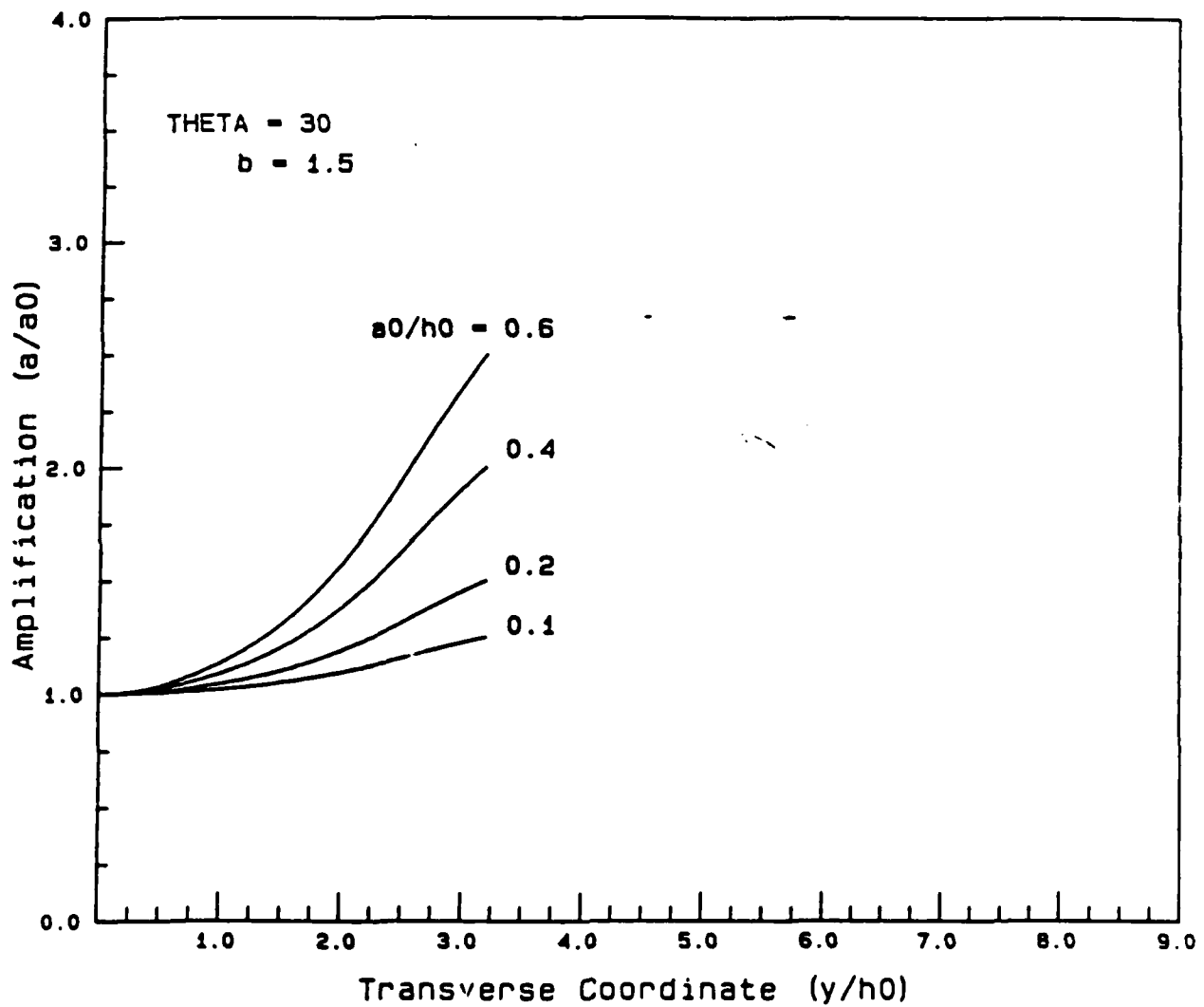


Figure 16b: Amplitude Variation for Indicated Condition.

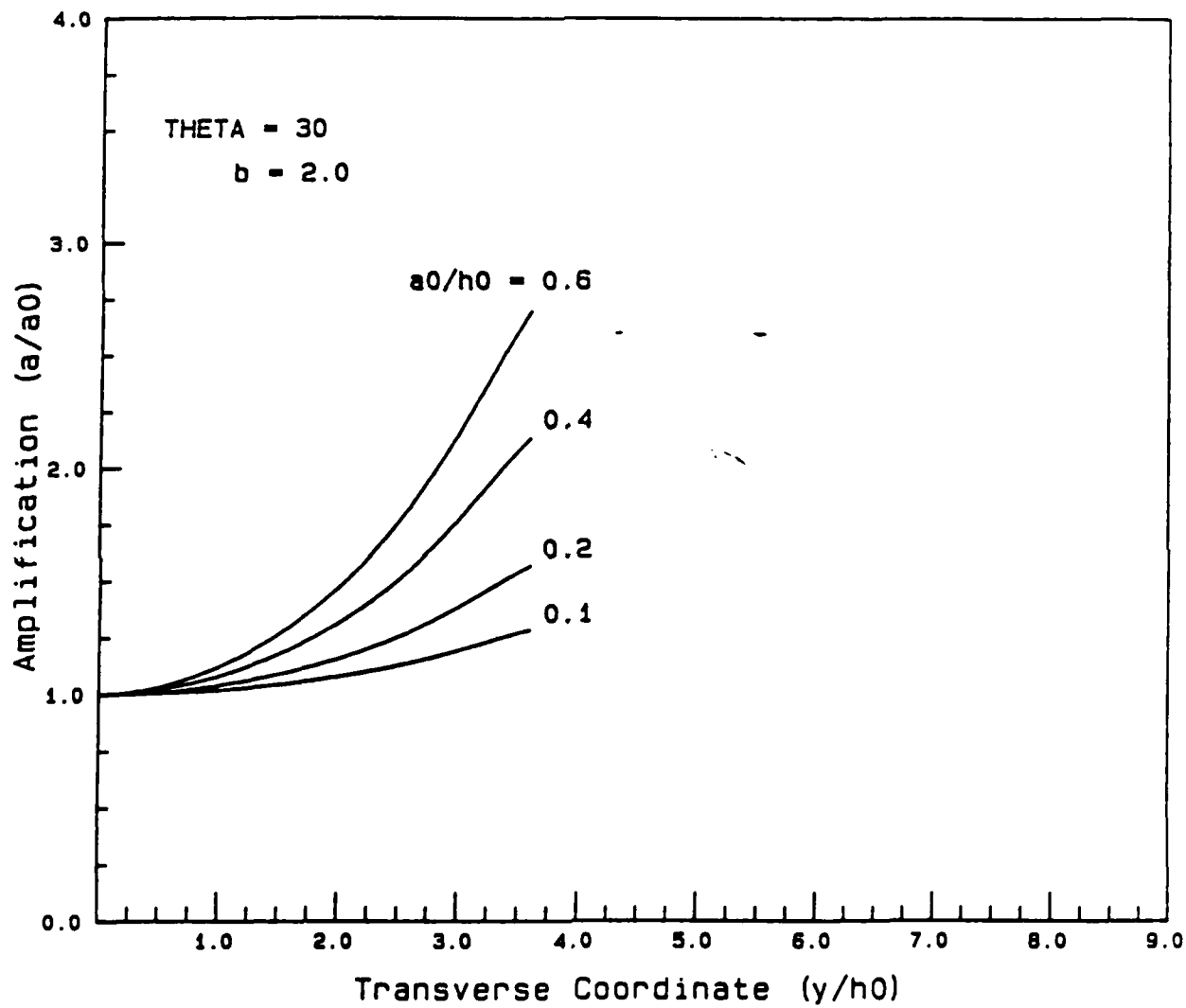


Figure 16c: Amplitude Variation for Indicated Condition.

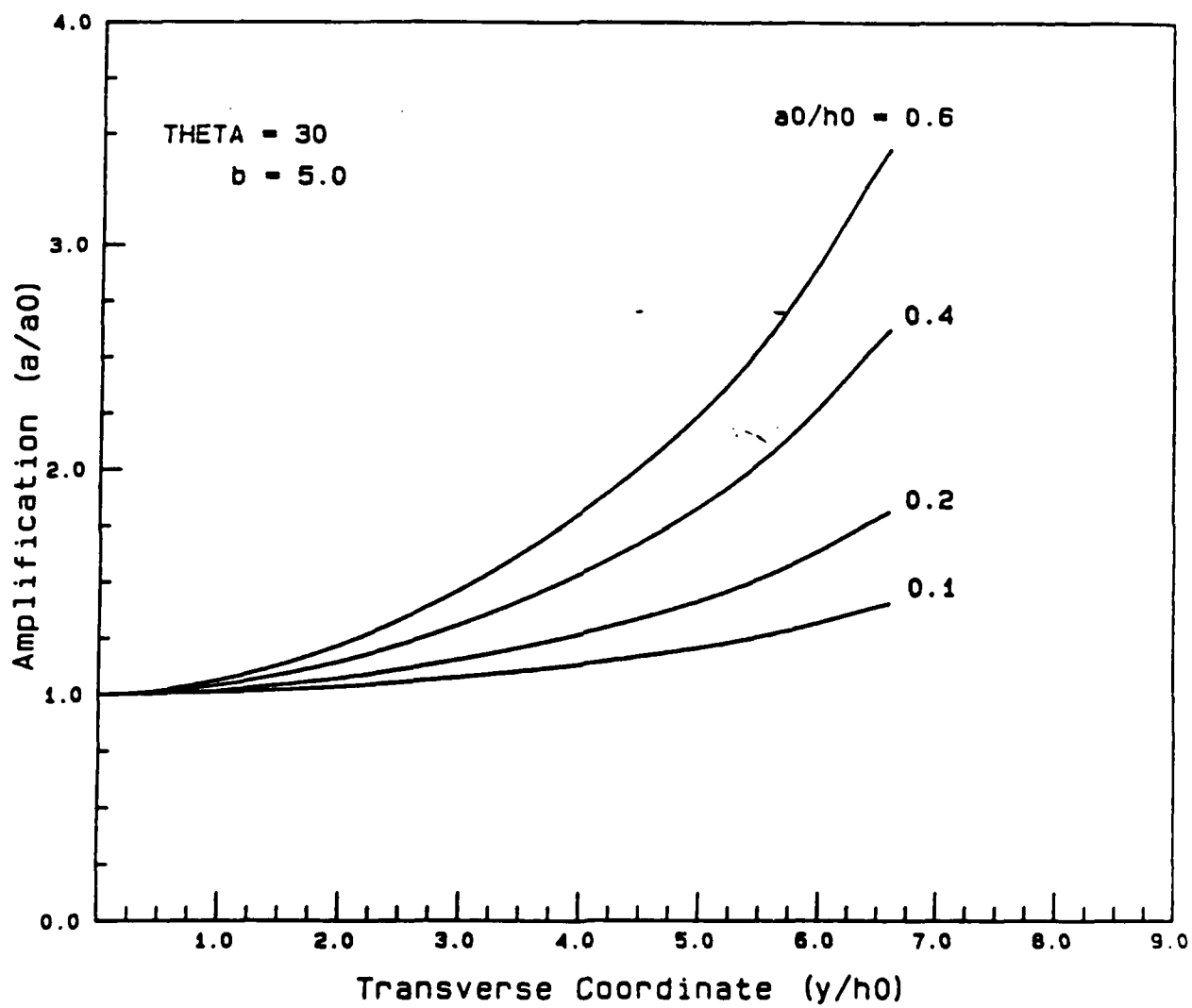


Figure 16d: Amplitude Variation for Indicated Condition.

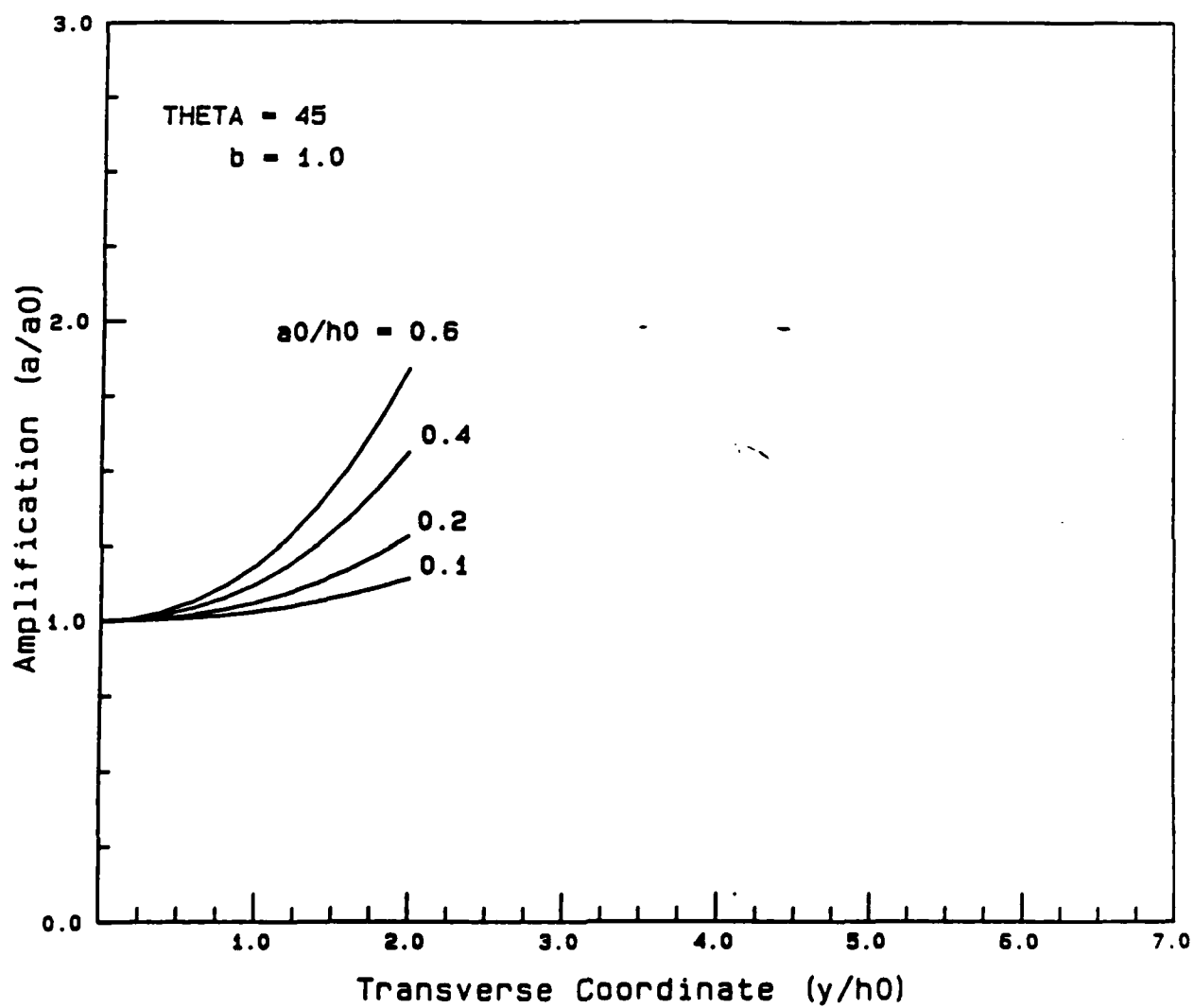


Figure 17a: Amplitude Variation for Indicated Condition.

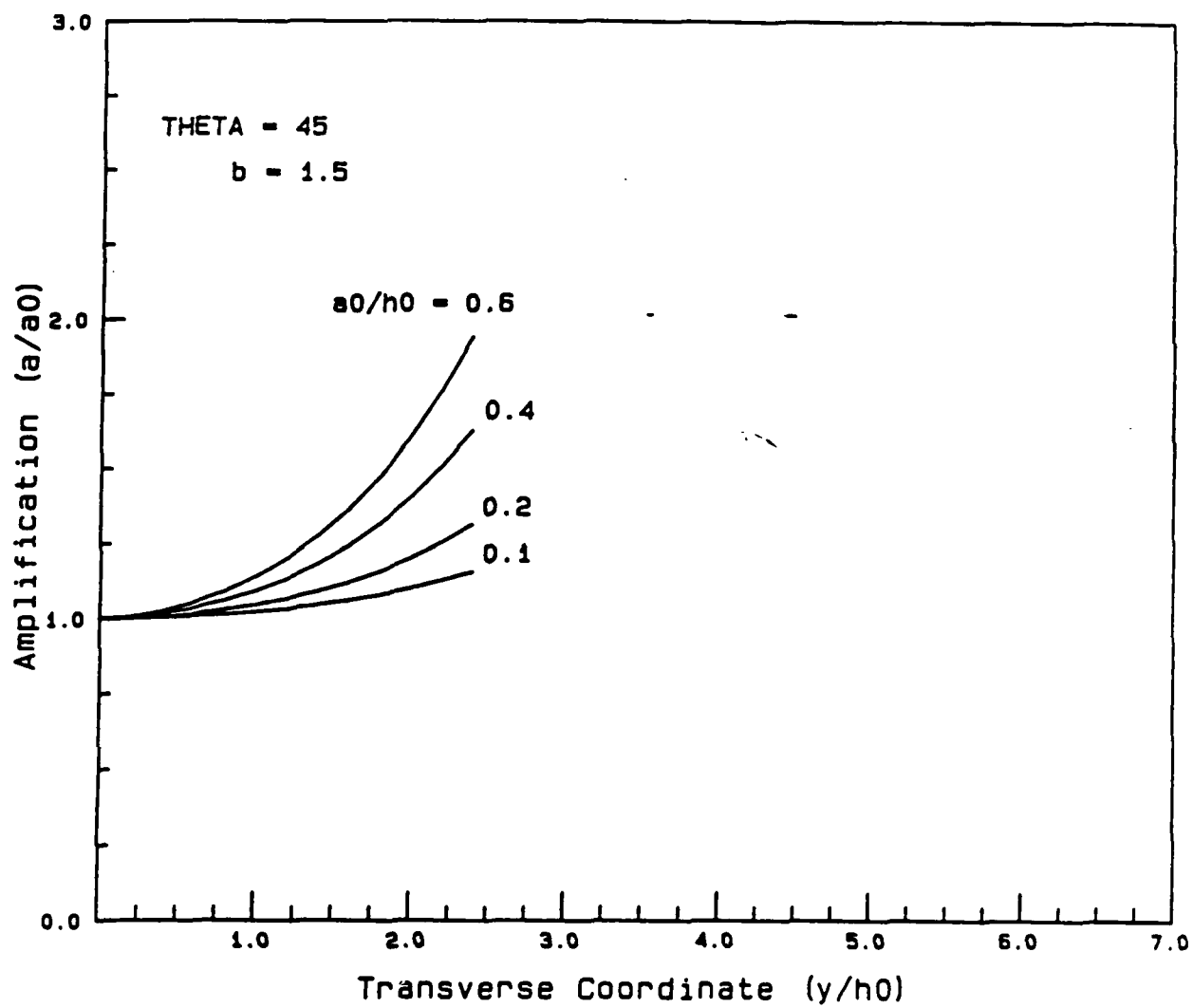


Figure 17b: Amplitude Variation for Indicated Condition.

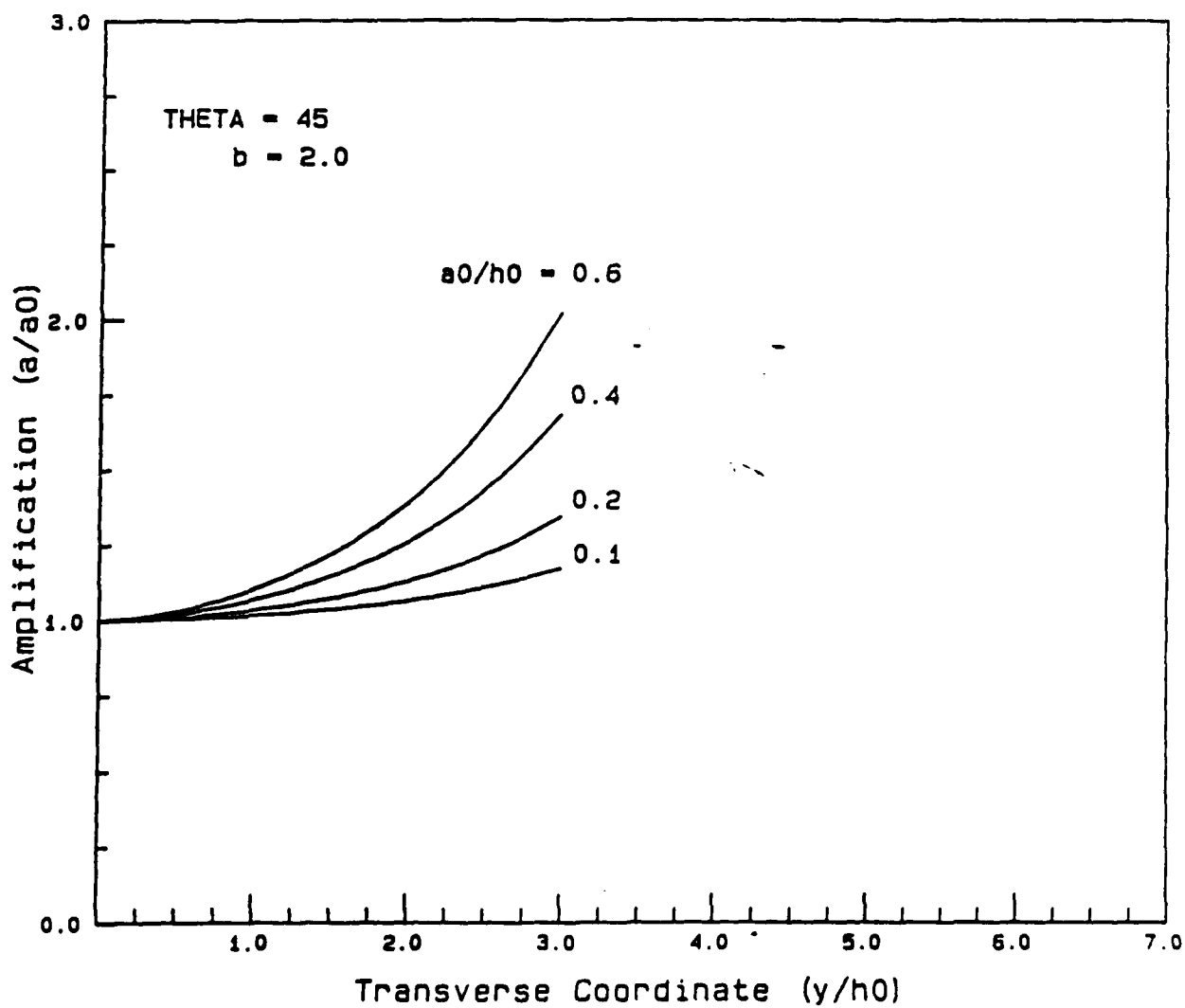


Figure 17c: Amplitude Variation for Indicated Condition.

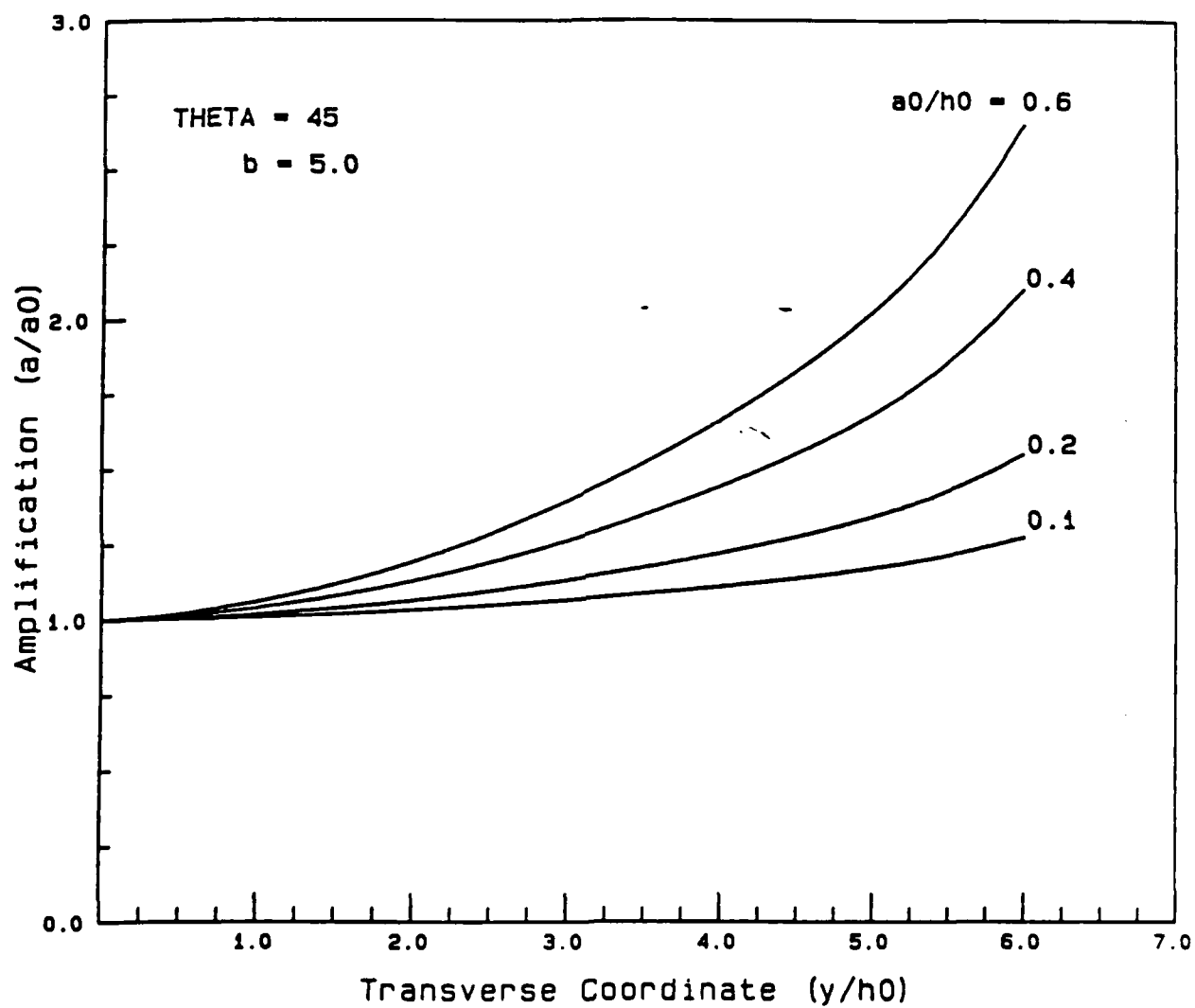


Figure 17d: Amplitude Variation for Indicated Condition.

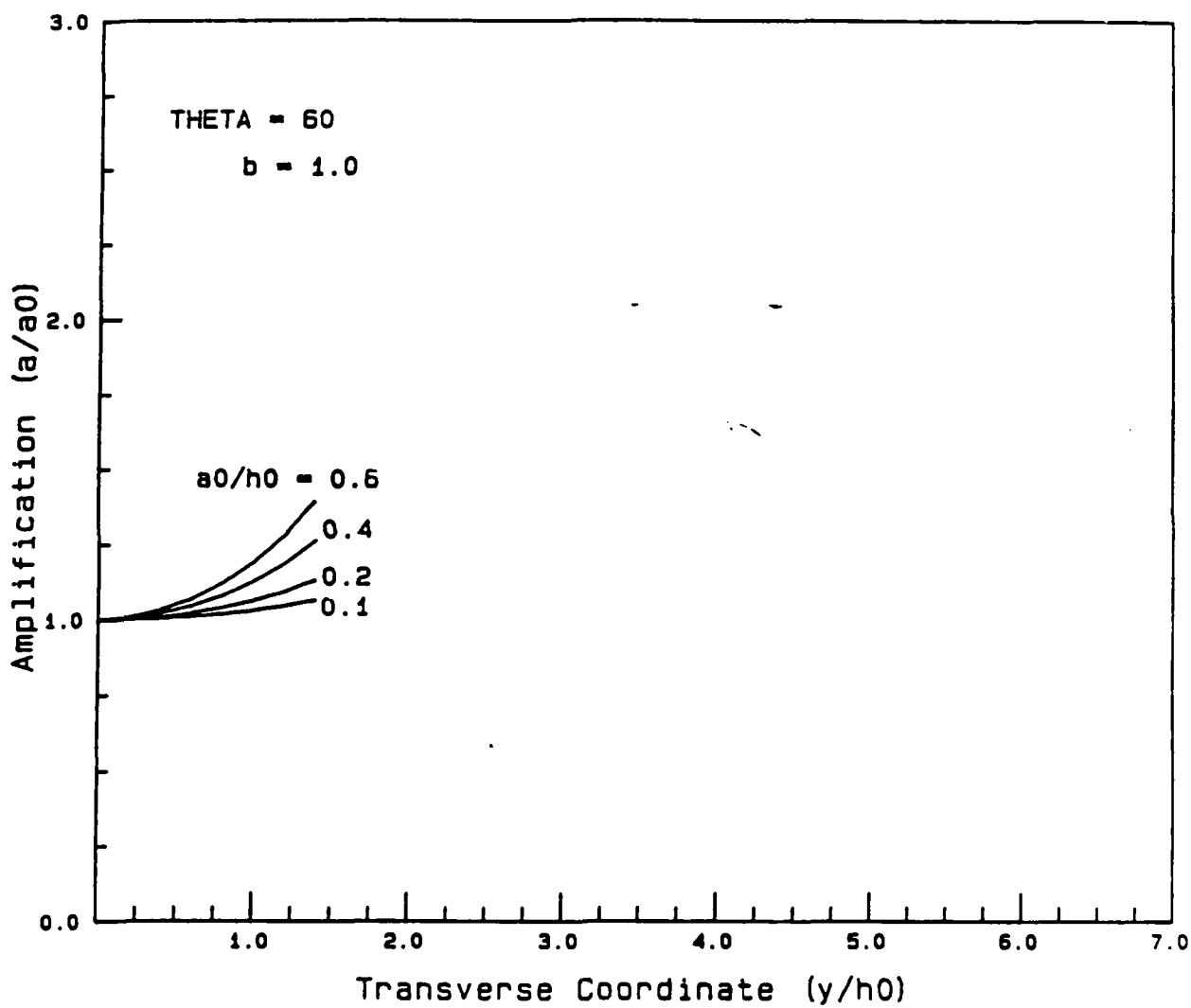


Figure 18a: Amplitude Variation for Indicated Condition.

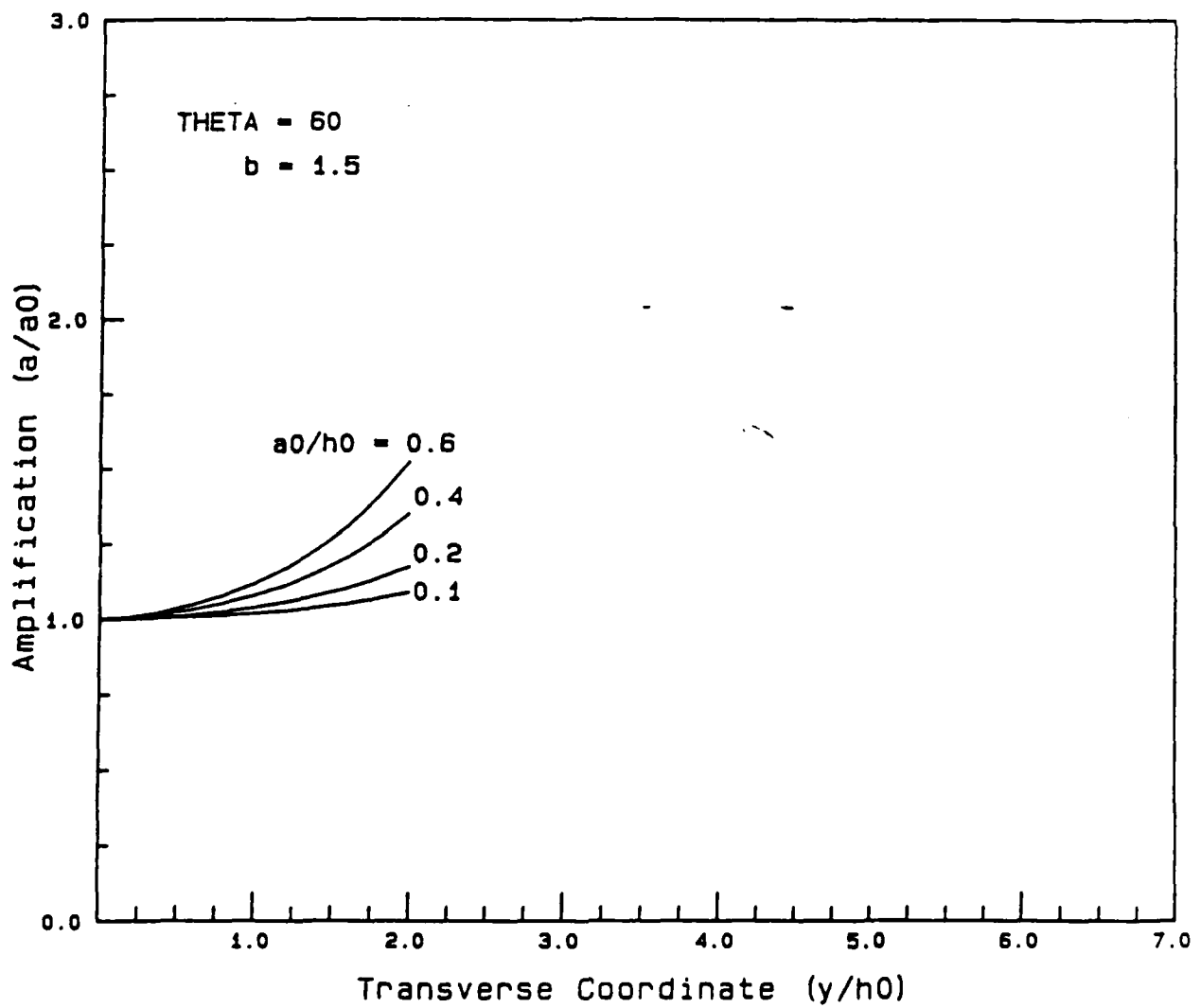


Figure 18b: Amplitude Variation for Indicated Condition.

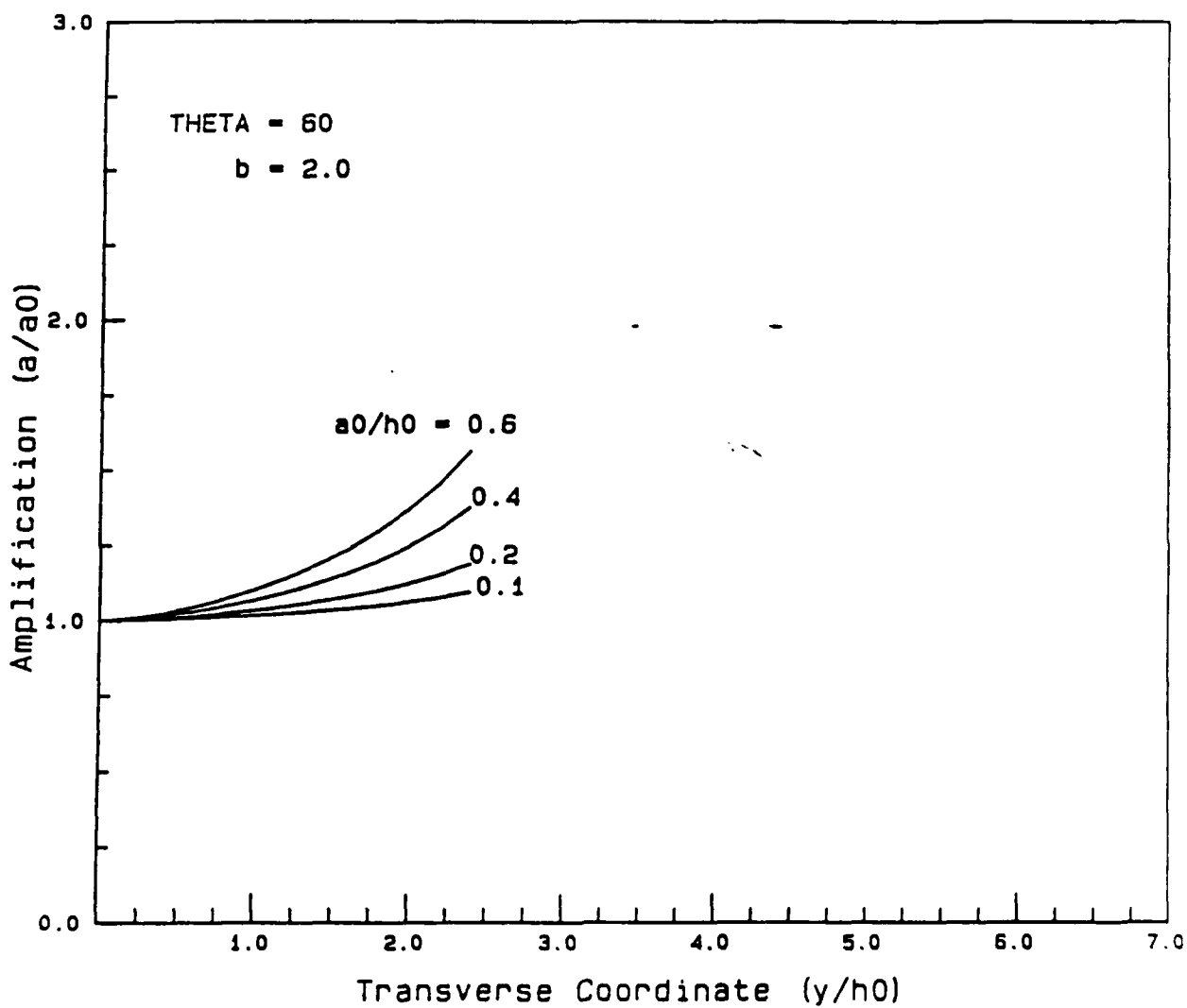


Figure 18c: Amplitude Variation for Indicated Condition.

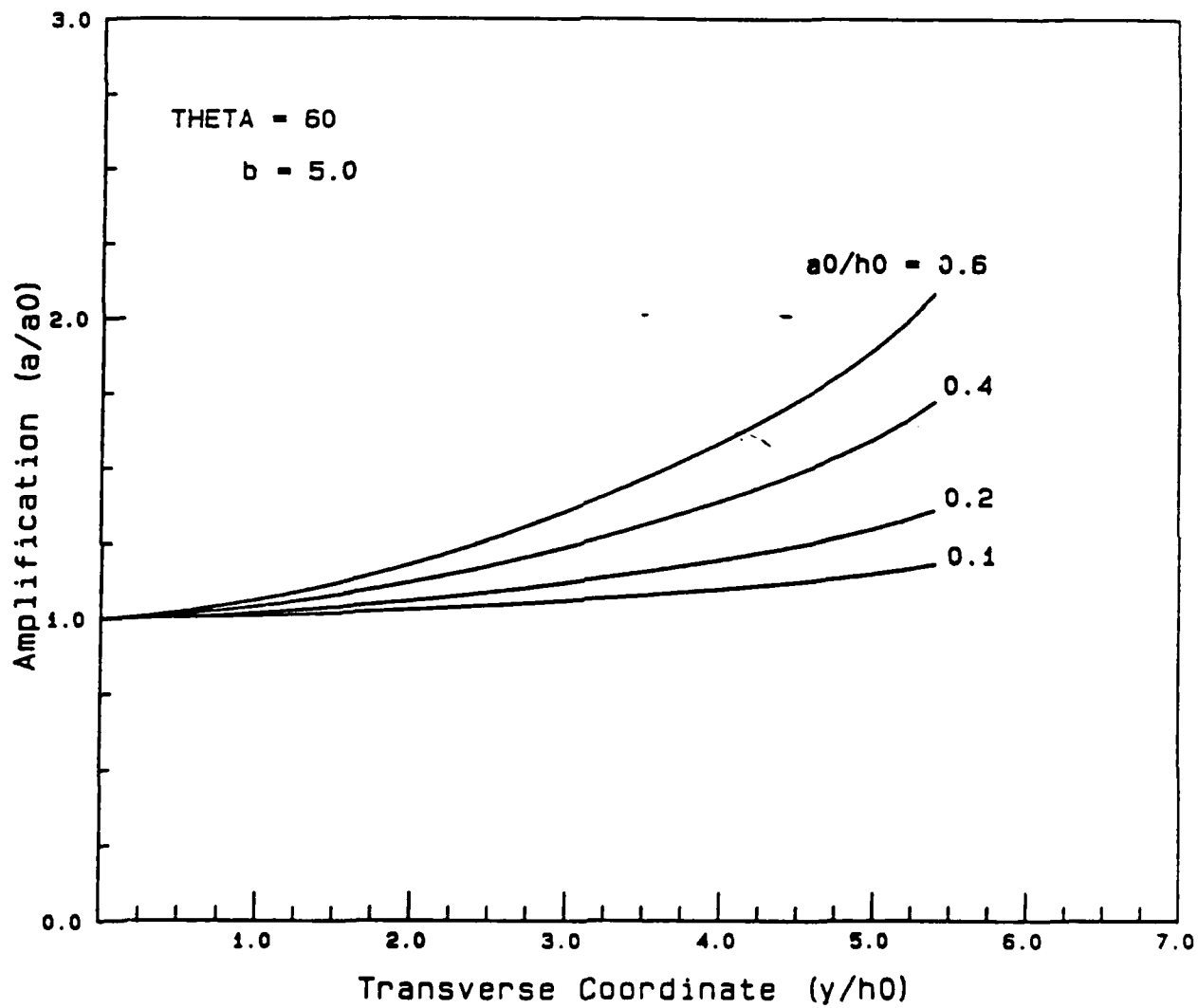


Figure 18d: Amplitude Variation for Indicated Condition.

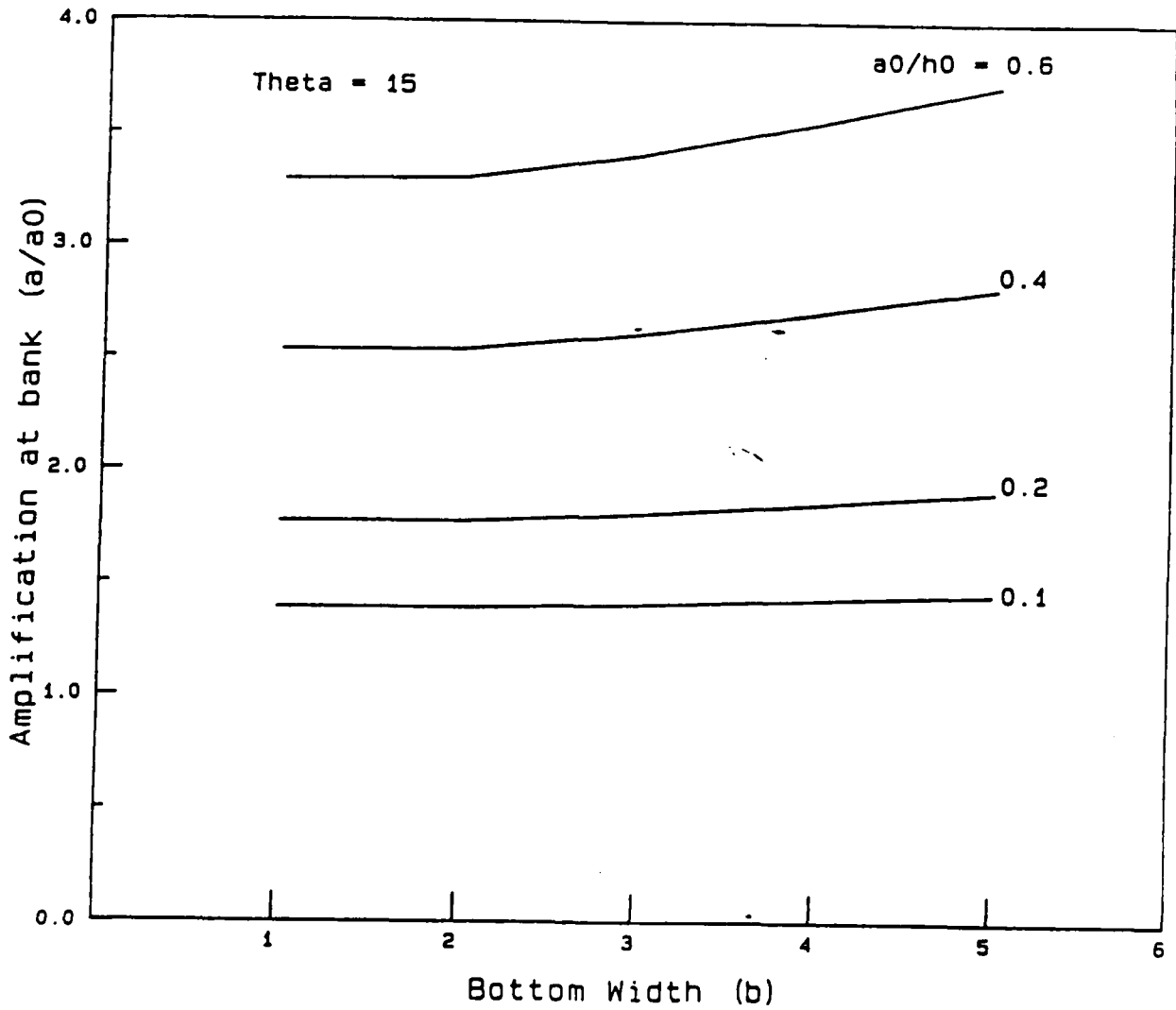


Figure 19: Variation of Amplitude at Bank with Bottom Width.

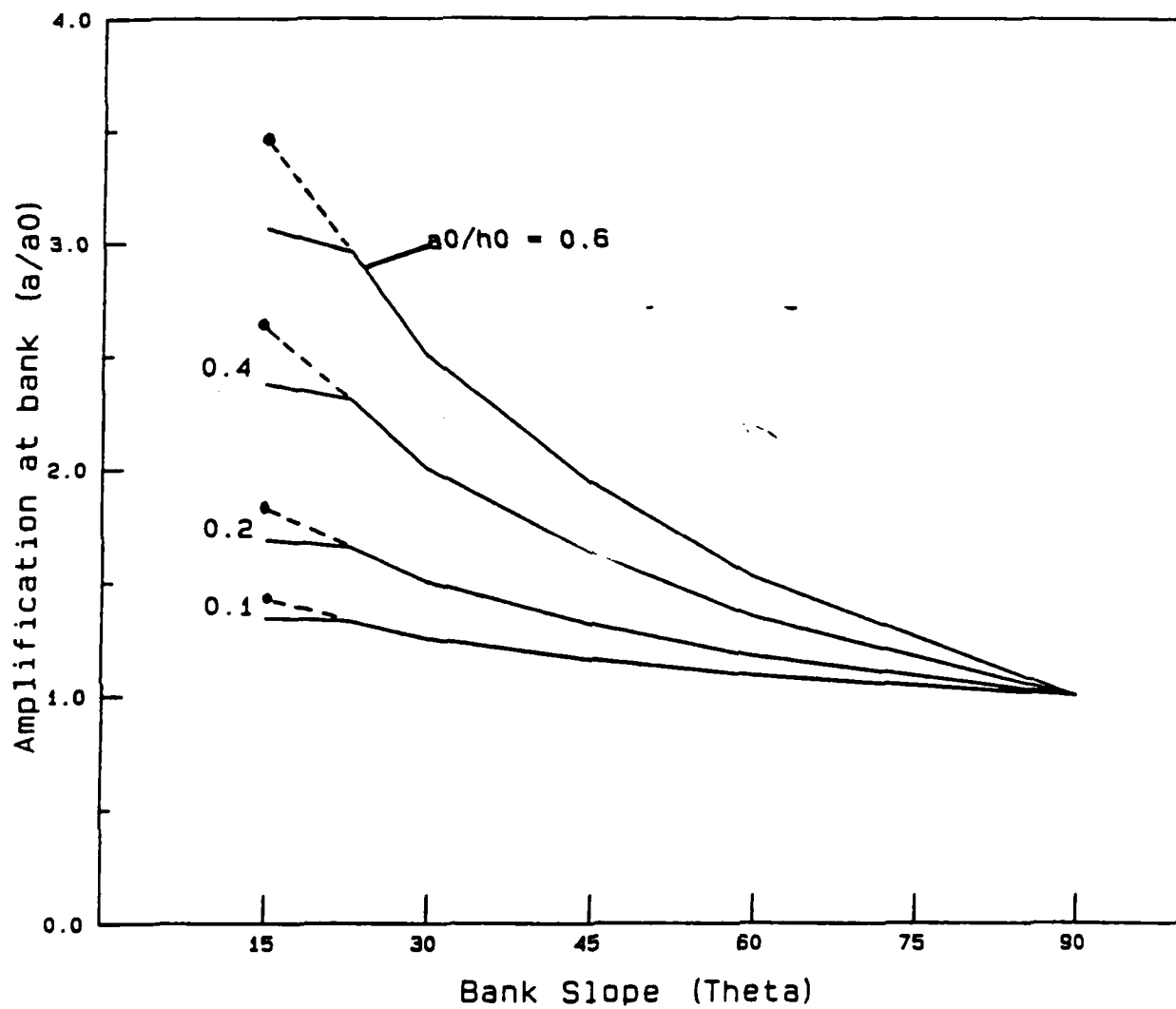


Figure 20: Variation of Amplitude at Bank with Bank Slope.

4.2. Comparisons with Observations

4.2.1. Data of Peregrine

We have already discussed Peregrine's (1969) data in connection with Figure 8. Suffice it to say here that we have carefully scaled the surface profiles of his two figures to determine his observed bank amplifications, and have then compared the results of our numerical model with those values. In every case, our model agrees as well with the data or better than does Peregrine's own computed points.

4.2.2. Lituya Bay Landslide Wave

Comparisons here are really speculative but nevertheless of interest. While we have some idea of the peak water levels from Figure 1, we do not have observations of the waves at the center of the Bay. However, we can borrow the numerical estimates of Chiang, et al (1981) who simulated this case.

The basic results of Chiang, et al, are summarized in the following table where the nine station locations are as indicated in Figure 1a.

<u>Station #</u>	<u>Model Peak Height</u>	<u>Nearby Observed</u>
1	200 ft	> 1000
2	120	350
3	80	130
4	60	100
5	30	100
6	50	90
7	20	--
8	40	85
9	25	30

Clearly, at Stations 1 and 4, the comparisons are not appropriate since what is actually occurring is a normal sort of runup in those areas. Station 7 is in the shadow of the island and is difficult to interpret. But for all other points where we might expect some sort of bank amplification we do, in fact, find one. If the model values are assumed to be reasonable estimates, then the apparent amplification is about 2 to 3 typically.

It does appear reasonable to think the computed values are valid. To be greatly off, it would be necessary to have mis-estimated the slide mass by a considerable amount. Since the slide energy goes like the mass and since wave height goes like the square root of energy, a 100% error in slide mass estimation would correspond to about a 40% error in computed heights. It is doubtful that the indicated values are that much in error.

Although this example is very indirect and somewhat speculative, it is nevertheless welcome in view of the general lack of data of any other sort. It does appear to be consistent with the general idea that amplifications on the order of a factor of two are typical.

THIS COPY MADE AT U.S. GOVERNMENT EXPENSE

5. EXAMPLES

In this section we give one detailed example of the foregoing methods in estimating explosion wave vulnerability, and one more speculative example.

[REDACTED]

[REDACTED]

[REDACTED]


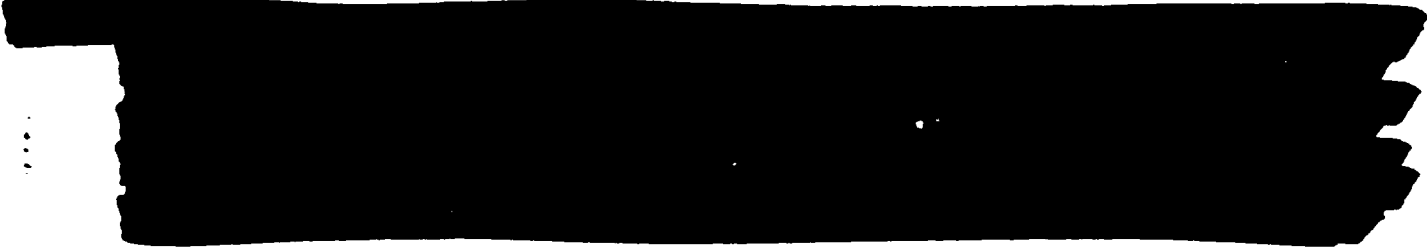

[REDACTED]

[REDACTED]

[REDACTED]



[REDACTED]

Assume the incident channel has a depth of about 500 feet and a cross-sectional area of about 3×10^6 ft². Let the left branch have a depth of about 500 feet also, with an area of about 7×10^6 ; let the right branch have a depth of about 300 feet and an area of about 2×10^6 .



The second example is a rough illustration only. Figure 23 is reproduced from Jane's Defence Weekly, Sept 6, 1986, and shows a satellite photo of a supposed Soviet submarine base. According to the accompanying article, the facility is for 'Typhoon' class submarines. The article further suggests that the quays visible in the photo (within the box) are on the order of 200 meters in length.

Taking this as a rough guide, we estimate the total width of the channelized geometry to be about 2400 feet. Assuming a slope of about 15 degrees and a depth of, say, 250 feet, we arrive at an estimate of bottom half-width (dimensionless) of about 1.5.



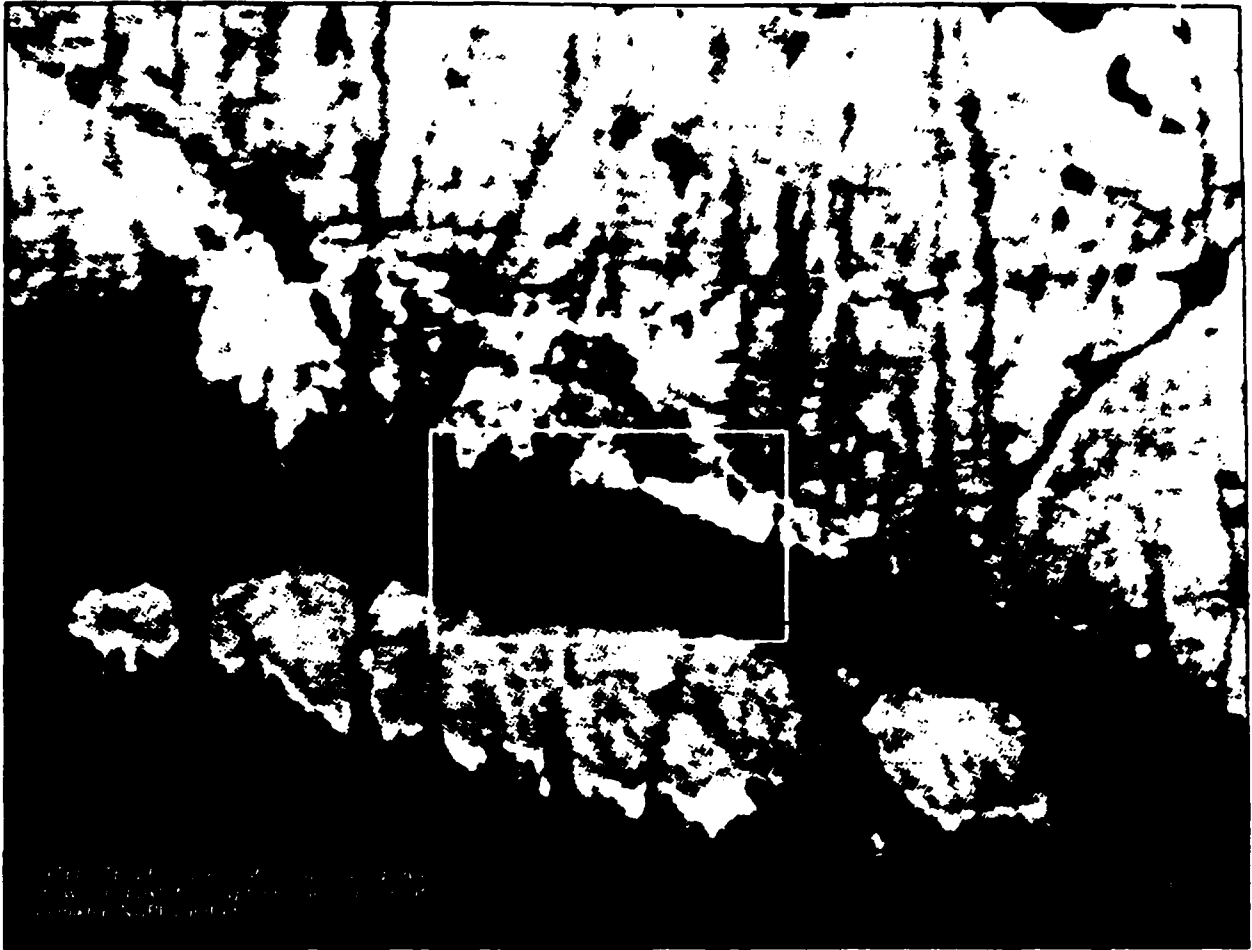


Figure 23: Aerial Photo of a Soviet Submarine Base in a Channelized Geometry (Kola Peninsula; Photo Reproduced from Jane's Defence Weekly, Sept. 6, 1986).

6. CONCLUSIONS AND RECOMMENDATIONS

This Phase I effort has summarized the major known features of large amplitude cnoidal or solitary waves in channels, and has provided simple formulas to estimate wave generation by both explosions and landslides. The salient points are:

In a uniform channel, waves may propagate long distances with little loss owing to the smallness of the friction effect and the confinement afforded by a channel.

Opposing influences include wave diminution by channel branching, channel irregularity, and breaking in the shallow wedge-like segment of the crest propagating along the dry bank.

In the case of sufficiently long waves, channel branching effects are reasonably easily estimated, and channel irregularities become secondary.

Breaking losses are still unknown. In wide channels with moderate slopes the losses will be small since the breaking zone is expected to be very limited. In any case, the breaking zone coincides with the target zone so that this form of dissipation is not, in a sense, 'wasted.'

There may be significant enhancement of wave height on the banks, a sort of 'lateral shoaling' in the shallower regions on the slope (although the effect extends even beyond the bank into the flat-bottom region of a trapezoidal channel).

Figure 24 shows the approximate upper limit of the amplification factor as a function of bank slope and center channel amplitude. The more extreme portions of this figure would be greatly modified by breaking effects.

Additional effects, not specifically discussed earlier, may also play a significant role in the wave description. For example, a channel with gradually changing depth or width may amplify (or attenuate) the wave owing to familiar mechanisms of shoaling and compression of wave orthogonals (coincident with the banks). In particular, there may exist important sites for which wave generation could occur in relatively deeper water (say, offshore or in an embayment) and then propagate into the channel (upstream). In this way, the center channel wave amplitude might be much greater than could be achieved by a detonation within the channel itself. This would have the double effect of increasing the bank amplification factor as well (moving up to a higher curve in Figure 24).

This Phase I effort was primarily intended to be a problem review and discussion. In Phase II we recommend that a research

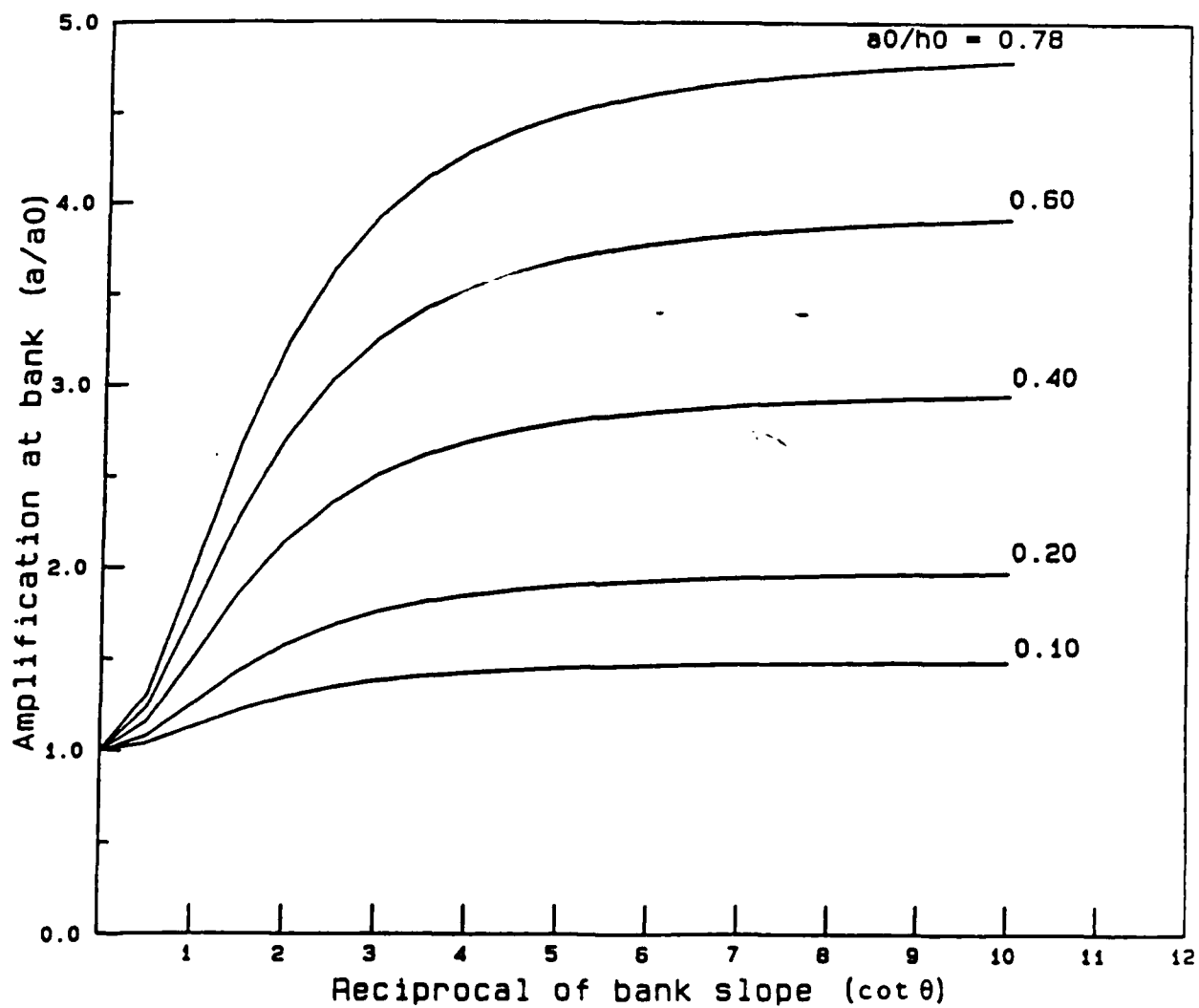


Figure 24: Approximate limit of bank amplification as a function of bank slope. These curves represent the triangular cross-section analytical solution, neglecting the additional enhancement obtained in wider channels.

effort be undertaken to extend our understanding of these questions. In particular, we suggest the following.

The three-dimensional wave theory should be further pursued to eliminate the limitations discussed earlier. That is, it should be extended to handle both wide channels (single banks in the limit) and gentle slopes.

The numerical implementation given here should be extended to handle irregular channel geometry and to improve the treatment of the boundary conditions.

The numerical model should be exercised for a variety of channels of interest.

The three-dimensional theory should be pursued to derive expressions for fluid particle velocities and accelerations.

Using these results, breaking criteria should be sought. For example, particle velocities and accelerations along the portion of the crest lying on the dry bank should reveal the occurrence of a critical condition indicating incipient disintegration of the wave (either kinematic or dynamic).

A supplementary, small experimental program should be performed to guide and verify analytical work, especially in the matter of breaking criteria.

Based on all the above, improved methods of estimating bank heights should be developed.

Similarly, expressions should be derived relating gross wave and channel characteristics to over-bank dynamic effects (wave forces on bank structures).

The implications of these results should be assessed for wave behavior in non-channelized geometries. For example, a solitary-like waveform in a complex three-dimensional geometry may at some points interact with slopes in a manner giving rise to amplification. This might be ultimately related to the problem of behavior in a Mach-stem zone.

The developed methods should be implemented to assess the vulnerability of selected sites (worldwide) to both explosion and landslide effects using the most appropriate generation descriptions available.

7. REFERENCES

- Benet, F. and J.A. Cunge, 1971, "Analysis of Experiments on Secondary Undulations Caused by Surge Waves in Trapezoidal Channels," *Journal of Hydraulic Research*, v9.
- Benjamin, T.B. and M.J. Lighthill, 1954, "On Cnoidal Waves and Bores," *Proceedings of the Royal Society*, A224.
- Chiang, W.L., Divoky, D., Parnicky, P., and W. Wier (1981), "Numerical Model of Landslide-generated Waves," Bureau of Reclamation O-07-81-S0134.
- Divoky, D. and John Lane, 1973, "Edge Bores," Office of Naval Research. 00014-72-C-0366, Tetra Tech Rept TT-P-282-73-1.
- Fenton, J.D., 1973, "Cnoidal Waves and Bores in Uniform Channels of Arbitrary Cross-Section," *Journal of Fluid Mechanics*, v58, part 3, pp 417-434.
- Iida, K., D. Cox, and G. Pararas-Carayannis, 1967, "Preliminary Catalog of Tsunamis Occurring in the Pacific Ocean," Hawaii Institute of Geophysics, HIG-67-10.
- Iwagaki, Y., 1968, "Hyperbolic Waves and their Shoaling," *Proceedings, 11th Conference on Coastal Engineering*.
- Korteweg, D.J. and G. de Vries, 1895, "On the Change of Form of Long Waves Advancing in a Rectangular Canal and on a New Type of Long Stationary Wave," *Philosophical Magazine*, v39, n5.
- Kranzer, H. and J. Keller, 1959, "Water Waves Produced by Explosions," *Journal of Applied Physics*, v30, n3.
- LeMehaute, B., 1962, "On the Nonsaturated Breaker Theory and the Wave Runup," *Proceedings, 8th Conference on Coastal Engineering*.
- LeMehaute, B., Divoky, D., and A. Lin 1968, "Internal Characteristics of Explosion-generated Waves on the Continental Shelf," Defense Atomic Support Agency, DASA 01-67-C-0099.
- LeMehaute, B., 1971, "Theory of Explosion-generated Water Waves," in Advances in Hydrosience, v7, Academic Press, N.Y.
- LeMehaute, B., 1985, "Explosion Generated Waves and Submarine Response, Volume 1," DNA, Contract DNA-001-84-0053, February.
- Lighthill, J., 1978, Waves in Fluids, Cambridge University Press, Cambridge.
- Miller, D.J., 1960, "Giant Waves in Lituya Bay, Alaska," USGS Professional Paper 354-C.

Noda, E.K., 1969, "Theory of Water Waves Generated by a Time-Dependent Boundary Displacement," Technical Rept. HEL 16-5, University of Calif., Berkeley.

Peregrine, D.H., 1968, "Long Waves in a Uniform Channel of Arbitrary Cross-Section," Journal of Fluid Mechanics, v32, part 2, pp 353-365.

Peregrine, D.H., 1969, "Solitary Waves in Trapezoidal Channels," Journal of Fluid Mechanics, v35, part 1, pp 1-6.

Peters, A.S., 1966, "Rotational and Irrotational Solitary Waves in a Channel with Arbitrary Cross-Section," Communications on Pure and Applied Mathematics, v19, pp 445-471.

Press, W.H., B.P. Flannery, S.A. Teukolsky, and W.T. Vetterling, 1986, Numerical Recipes, The Art of Scientific Computing, Cambridge University Press, Cambridge.

Raney, D., and H.L. Butler, 1975, "A Numerical Model for Predicting the Effects of Landslide-Generated Water Waves," US Army Corps of Engineers, Waterways Experiment Station, Report H-75-1.

Slingerland, R., and B. Voight, 1982, "Evaluating Hazard of Landslide-Induced Water Waves," ASCE Journal WW4, November.

Strange, J.N., 1955, data contained in "Effects of Explosions in Shallow Water," US Army Corps of Engineers Waterways Experiment Station, Technical Memorandum 2-406.

Ursell, F., 1953, "The Long-Wave Paradox in the Theory of Gravity Waves," Proceedings of the Cambridge Philosophical Society, v49.

Wang, S., R. Wade, and W. Wier, 1977, "Vulnerability of Surface Effect Vehicles to EGWW," prepared for Office of Naval Research, Tetra Tech Rept. TC-645.

Wiegel, R. 1964, Oceanographical Engineering, Prentice-Hall, N.J.

A P P E N D I X A

This copy made at U.S. Government expense.

```

{$V-} {$R+} {$U-} {$C+} {$K-}

Program bankWaves;

Procedure Pause;
var
    junk : char;
Begin
    write(' .. Press Any Key To Continue .. ':45);
    read(kbd, junk);
    writeln;
end;

(===== TIMER MODULE =====)

const
    nTimers = 5;

var
    beginTime: array[1..nTimers] of real;

procedure initializeTimers;
var
    i: byte;
const
    infinity = 1.0E30;
begin
    for i := 1 to nTimers do beginTime[i] := infinity
end;

function currentTime: real;
type
    regPack = record
        ax, bx, cx, dx, bp, si, di, ds, es, flags: integer;
    end;
var
    regs: regPack;
begin
    with regs do
        begin
            ax := $2C00;
            msdos(regs);
            currentTime := lo(dx)/100 + hi(dx) + 60 * (lo(cx) + 60 * hi(cx))
        end
    end;

procedure beginTimer(n: byte);
begin
    if n in [1..nTimers] then beginTime[n] := currentTime
end;

function elapsedTime(n:byte): real;
const
    infinity = 1.0E30;
begin
    if n in [1..nTimers] then elapsedTime := currentTime - beginTime[n]
    else elapsedTime := infinity
end;

(===== END OF TIMER MODULE =====)

```

```

type
  anyStr = string[255];
  str2 = string[2];
  str3 = string[3];

const
  omegaFactor = 1.0;
  minIterations = 100;
  maxIterations = 2000;
  maxRows = 21;
  maxCols = 151;
  epsilon = 1.0E-7;
  infinity = 1.0E30;
  tolerance = 1.0E-6;

var
  response: char;

  index, row, col, nRows, nCols, iterCount,
  showSteps, zSteps, baseCol, midCol, col14, col34, triCol: integer;

  midMax, lastCol: array[1..maxRows] of integer;

  depth, width, alpha, oldSum, newSum, topWidth, height0,
  delY, delZ, beta, betaSqr, betaSqInv, spectralRadius, omega,
  aZero, bZero, delySqr, delSurf, factor1, factor2,
  tanAlpha, cotAlpha, surfGrad, bZeroPrime, uNew, theta, omegaOpt,
  coeff1, coeff2, duration, oldCorner, newCorner, convergeTest: real;

  u: array[1..maxRows, 1..maxCols] of real;

  height: array[1..maxCols] of real;

  OK, showResults, converged, save: boolean;

  onBoundary: array[1..maxRows] of boolean;

function tan(theta: real): real;
begin
  tan := sin(theta)/cos(theta)
end;

procedure bell(freq, time: integer);
begin
  sound(freq);
  delay(time);
  noSound;
end;

procedure wait(message: anyStr);
var
  ch: char;
begin
  write(message);
  repeat until keypressed;
  read(kbd, ch)
end;

procedure getInput;

```

```

begin
  clrscr;
  write('Enter depth of the channel: ':55);
  readln(depth);
  write('Enter number of steps in depth direction: ':55);
  readln(zSteps);
  write('Enter bottom width of channel: ':55);
  readln(width);
  write('Enter bank inclination (degrees from horizontal): ':55);
  readln(theta);
  alpha := 90 - theta;
  if (theta <= 0) or (theta > 90) then
  begin
    bell(500, 500);
    writeln('Bank slope out of legal range...exiting...');
    wait('...press any key...');
    halt
  end;
  write('Enter wave amplitude at left boundary: ':55);
  readln(height0);
  showResults := false;
  write('...Want to see intermediate results... Y/N ? ':55);
  repeat
    read(kbd, response);
    response := upcase(response)
  until response in ['Y', 'N'];
  writeln(response);
  if response = 'Y' then
  begin
    showResults := true;
    write('...After every how many iterations ? ':55);
    readln(showSteps);
  end;
  write('Save results to a text file... Y/N ? ':55);
  repeat
    read(kbd, response);
    response := upcase(response)
  until response in ['Y', 'N'];
  writeln(response);
  save := response = 'Y';
end;

procedure initialize;
var
  zRow, widthRow, zPtBelow, yPtBelow, zPtRight, yPtRight: real;
begin
  converged := false;
  iterCount := 0;
  oldSum := 0;
  newSum := 0;
  oldCorner := 0;
  newCorner := 0;
  convergeTest := 1.0;
  delZ := depth / zSteps;
  delY := delZ;
  beta := delY/delZ;
  delySqr := delY * delY;
  nRows := zSteps + 1;
  alpha := alpha * pi / 180;
  tanAlpha := tan(alpha);

```

Listing of Channel Wave Program CHANWAVE.PAS, page 4

```

if theta = 90 then cotAlpha := infinity else cotAlpha := 1 / tanAlpha;
factor1 := cotAlpha / beta;
factor2 := beta * tanAlpha;
topWidth := width + depth * tanAlpha;
nCols := trunc(topWidth / delY + epsilon) + 1;
for col := 1 to nCols do height[col] := 0;
for row := 1 to nRows do for col := 1 to nCols do u[row,col] := 0;
for row := 1 to nRows do
begin
  zRow := delZ * (nRows - row);
  widthRow := width + zRow * tanAlpha;
  lastCol[row] := trunc(widthRow / delY + epsilon) + 1;
  onBoundary[row] := ((widthRow - (lastCol[row] - 1) * delY) < epsilon);
end;
for row := 1 to nRows do
for col := 1 to lastCol[row] do
  u[row,col] := tanAlpha * sqrt(topWidth) *
    (1 - sqrt(1 - (col - 1) * delY / topWidth)) - 0.4 * (row - 1) * delZ;
baseCol := trunc(width / delY + epsilon);
midCol := baseCol div 2;
col14 := baseCol div 4;
col34 := 3 * col14;
triCol := (baseCol + nCols) div 2;
for row := 1 to (nRows - 1) do
begin
  col := baseCol;
  repeat
    yPtBelow := delY * (col - 1);
    zPtBelow := delZ * (nRows - row - 1);
    OK := ((width + zPtBelow * tanAlpha - yPtBelow) >= -epsilon);
    zPtRight := delZ * (nRows - row);
    yPtRight := delY * col;
    if OK then OK := ((width + zPtRight * tanAlpha - yPtRight) >= -epsilon);
    col := col + 1
  until not OK;
  midMax[row] := col - 2
end;
midMax[nRows] := baseCol;
writeln;
writeln(nRows, ' rows, ', nCols, ' columns. ');
writeln;
for row := 1 to nRows do
  writeln(row:5, midMax[row]:10, lastCol[row]:10, onBoundary[row]:10);
writeln;
wait('...press any key...');
writeln;
betaSqr := beta * beta;
betaSqInv := 1 / betaSqr;
aZero := width + 0.5 * tanAlpha;
bZero := topWidth;
surfGrad := aZero / bZero;
delSurf := surfGrad * delZ;
bZeroPrime := tanAlpha;
spectralRadius :=
  (cos(pi/(nRows-1)) + betaSqInv * cos(pi/(nCols-1))) / (1 + betaSqInv);
omegaOpt := omegaFactor * 2 / (1 + sqrt(1 - sqr(spectralRadius)));
omega := omegaOpt;
writeln('Columns printed: ', '1':5, col14:5, midCol:5,
  col34:5, baseCol:5, triCol:5, ' plus points on slope. ');
writeln;

```



```

coeff1 := omega / (2 * (1 + betaSqr));
coeff2 := 1 - omega;
end;

procedure topRow;
  procedure upperLeftCorner;
    begin
      u[1,1] := u[1,2]
    end;
  procedure midTop;
    begin
      for col := 2 to midMax[1] do u[1,col] := u[2,col] + delSurf
    end;
  procedure upperRightWedge;
    var
      delHeight, factor: real;
      function useTop(col: integer): boolean;
        begin
          delHeight := 1 - delY * (col - baseCol - 1) * cotAlpha;
          factor := delHeight * cotAlpha / delY;
          useTop := factor <= 1;
        end;
    begin
      for col := (midMax[1] + 1) to lastCol[1] do
        if useTop(col) then
          u[1,col] := u[1,col] + factor * (u[1,col-1] - u[1,col]) +
            surfGrad * delHeight
        else
          u[1,col] := u[1,col-1] + (delHeight/delZ - factor2) *
            (u[2,col-1] - u[1,col-1]) + surfGrad * delHeight;
          if delHeight < epsilon then
            u[1,col] := 3 * (u[1,col-1] - u[1,col-2]) + u[1,col-3]
          end;
        end;
      begin
        upperLeftCorner;
        midTop;
        upperRightWedge
      end;
    end;

  procedure midRow(row: integer);
    procedure leftPoint;
      begin
        u[row,1] := u[row,2]
      end;
    procedure midPoints;
      begin
        for col := 2 to midMax[row] do
          begin
            uNew := u[row,col+1] + u[row,col-1]
              + betaSqr * (u[row+1,col] + u[row-1,col]) - delYsqr;
            u[row,col] := coeff1 * uNew + coeff2 * u[row,col];
          end;
        end;
    procedure rightPoints;
      begin
        for col := (midMax[row] + 1) to lastCol[row] do
          u[row,col] := u[row,col-1] +
            (1 / (1 + cotAlpha / beta)) * (u[row-1,col] - u[row,col-1])
        end;
      begin

```

```

leftPoint;
midPoints;
rightPoints
end;

procedure bottomRow;
  procedure lowerLeftCorner;
  begin
    u[nRows,1] := u[nRows,2]
  end;
  procedure midBottom;
  begin
    for col := 2 to midMax[nRows] do u[nRows,col] := u[nRows-1,col]
  end;
  procedure lowerRightCorner;
  var
    uAsIfBottom, uAsIfSide: real;
  begin
    uAsIfBottom := u[nRows-1,lastCol[nRows]];
    if theta < 45 then
      uAsIfSide := u[nRows-1,lastCol[nRows]] +
        factor1 * (u[nRows-1,lastCol[nRows]-1] - u[nRows-1,lastCol[nRows]])
    else
      uAsIfSide := u[nRows,lastCol[nRows]-1] +
        factor2 * (u[nRows-1,lastCol[nRows]-1] - u[nRows,lastCol[nRows]]);
    u[nRows,lastCol[nRows]] := 0.5 * (uAsIfBottom + uAsIfSide)
  end;
begin
  lowerLeftCorner;
  midBottom;
  lowerRightCorner
end;

procedure normalize;
var
  uZero: real;
begin
  uZero := u[1,1];
  oldSum := newSum;
  newSum := 0;
  oldCorner := newCorner;
  for row := 1 to nRows do
    for col := 1 to lastCol[row] do
      begin
        u[row,col] := u[row,col] - uZero;
        newSum := newSum + abs(u[row,col])
      end;
    newCorner := u[nRows,lastCol[nRows]]
  end;
end;

function psiA: real;
var
  sum: real;
  row, col: integer;
begin
  sum := 0;
  for row := 1 to (nRows - 1) do
    for col := 1 to (nCols - 1) do
      sum := sum + u[row,col] + u[row,col+1] + u[row+1,col] + u[row+1,col+1];
    psiA := (dely * delz / aZero) * (sum / 4);
  end;
end;

```

```

and;

function psiB: real;
var
  topSum : real;
  row, col: integer;
begin
  topSum := 0;
  row := 1;
  for col := 1 to (nCols - 1) do
    topSum := topSum + u[row,col] + u[row,col+1];
  psiB := (dely / bZero) * topSum / 2
end;

function heightVar(height: real; col: integer): real;
var
  numerator, denominator : real;
begin
  numerator := height * height * bZero *
    (1 - (bZeroPrime * aZero) / (bZero * bZero * 3));
  numerator := numerator * u[1,col];
  denominator := 2 * aZero * (psiB - psiA);
  heightVar := numerator / denominator
end;

procedure surfaceVariation;
begin
  for col := 1 to nCols do
    begin
      height[col] := (height0 +
        heightVar(height0,col))/height0;
      writeln(col:10, height[col]:10:3)
    end
  end;

procedure compute;
begin
  iterCount := iterCount + 1;
  topRow;
  for row := 2 to (nRows-1) do midRow(row);
  bottomRow;
  normalize;
  writeln(iterCount:10, newSum:20:4, newCorner:10:3,
    convergeTest:15:6, omega:10:3)
end;

function finished: boolean;
begin
  convergeTest := abs((newSum - oldSum)/newSum);
  converged := convergeTest < tolerance;
  finished := (converged and (iterCount >= minIterations))
    or (iterCount >= maxIterations)
end;

procedure saveResults;
var
  widthStr: str3;
  thetaStr: str2;
  stepStr: str3;
  heightStr: str3;

```

```

fileName: string[12];
saveFile: text;
  procedure fill2(var xStr: str2);
  begin
    while length(xStr) < 2 do xStr := '0' + xStr
  end;
  procedure fill3(var xStr: str3);
  begin
    while length(xStr) < 3 do xStr := '0' + xStr
  end;
begin
  str(width*10:0:0, widthStr);
  str(theta:0:0, thetaStr);
  str(zSteps:0, stepStr);
  str(height0*1000:0:0, heightStr);
  fill2(thetaStr);
  fill3(widthStr);
  fill3(stepStr);
  fill3(heightStr);
  fileName := thetaStr + widthStr + stepStr + '.' + heightStr;
  assign(saveFile, fileName);
  rewrite(saveFile);
  for index := 1 to 5 do writeln(saveFile);
  writeln(saveFile, 'Data file: ', fileName);
  writeln(saveFile);
  writeln(saveFile, 'Depth = ', depth:0:1, ' Bottom width = ', width:0:1,
    ' Theta = ', theta:0:1, ' Top width = ', topWidth:0:1);
  writeln(saveFile, 'delta Z = ', delZ:0:2, ' delta Y = ', delY:0:2,
    ' # Rows = ', nRows:0, ' # Columns = ', nCols:0);
  writeln(saveFile, 'Omega = ', omega:0:3,
    ' Convergence tolerance = ', tolerance);
  writeln(saveFile, 'Sum over matrix = ', newSum:0:4,
    ' psiA = ', psiA:0:4, ' psiB = ', psiB:0:4);
  writeln(saveFile);
  write(saveFile, iterCount:0, ' iterations completed; computations ');
  if converged then writeln(saveFile, 'converged.')
  else writeln(saveFile, 'did not converge. ');
  writeln(saveFile, 'Relative error in matrix sum = ', convergeTest);
  writeln(saveFile, duration:0:0, ' seconds for iterations. ');
  writeln(saveFile);
  writeln(saveFile);
  writeln(saveFile, 'Transverse surface profile: ');
  writeln(saveFile);
  writeln(saveFile, 'Column':12, 'Y':7, 'Amplitude':13);
  writeln(saveFile);
  for col := 1 to nCols do writeln(saveFile, col:10,
    delY * (col - 1):10:2, height[col]:10:3);
  writeln(saveFile);
  writeln(saveFile);
  writeln(saveFile, 'Solution matrix (rotated -- 1,1 is at upper right): ');
  writeln(saveFile);
  writeln(saveFile);
  write(saveFile, 'ROW');
  for row := nRows downto 1 do write(saveFile, row:8);
  writeln(saveFile);
  writeln(saveFile, 'COL');
  writeln(saveFile);
  for col := 1 to nCols do
  begin
    write(saveFile, col:2, ' ');
  end;

```